Master of Science Thesis

Bayesian Identification of Thermodynamic Parameters from Shock Tube Data

Jacob Butler

February 2, 2018

Aerodynamics

Faculty of Aerospace Engineering

TU Delft

Delft University of Technology

Bayesian Identification of Thermodynamic Parameters from Shock Tube Data

Master of Science Thesis

For obtaining the degree of Master of Science in Aerospace Engineering
at Delft University of Technology

Jacob Butler

February 2, 2018

Faculty of Aerospace Engineering · Delft University of Technology

Delft University of Technology

DELFT UNIVERSITY OF TECHNOLOGY
DEPARTMENT OF AERODYNAMICS

The undersigned hereby certify that they have read and recommend to the Faculty of Aerospace Engineering for acceptance the thesis entitled **"Bayesian Identification of Thermodynamic Parameters from Shock Tube Data"** by **Jacob Butler** in fulfillment of the requirements for the degree of **Master of Science**.

Dated: February 2, 2018

Supervisors:

_____
Reader 1

_____
Reader 2

_____
Reader 3

_____
Reader 4

Preface

This report concerns a project on the subject of Bayesian identification of thermodynamic parameters of an equation of state of a dense gas, from shock tube data from the Flexible Asymmetric Shock Tube (FAST) experiment.

I would like to thank my supervisors Richard Dwight and Matteo Pini for their invaluable guidance and input. I would also like to thank Mauro Gallo for his crucial insight and assistance regarding the experimental aspects.

I would also like to thank my family for their steadfast support and encouragement.

Summary

The objective of this project is to reduce the uncertainty on parameters of a thermodynamic equation of state for a dense gas. The dense gas considered is the D_6 siloxane and the equation of state used is the polytropic van der Waals equation. The reduction of the uncertainty is attempted by applying a Bayesian inference technique. A statistical model is chosen that associates the results from a shock tube experiment with the output of a computer model. The shock tube data comes from the flexible asymmetric shock tube experiment Mathijssen et al. (2015) and the computer model is a Roe solver which solves quasi-one-dimensional Euler equations with a source term that depends on time. A surrogate model based on sparse grids and a sensitivity analysis using Sobol' indices are both applied. The Markov chain Monte Carlo technique is applied to arrive at the posterior probability distribution on the chosen parameters of the computer model. The resulting probability distributions indicated that some of the thermodynamic parameters were identified, but that those that were showed a disagreement between the mean values that were found and the true values in the literature. It is recommended that the approach be applied to a more complex equation of state.

Table of Contents

List of Figures

List of Tables

Chapter 1

Introduction

This introduction will present the context of the current project, explaining the need for the uncertainty reduction in the specific field. First, the necessity of accurate thermodynamic models for dense gases will be outlined. Next, the literature review will be presented. Finally, the layout of the report will be described.

1.1 Accuracy of Dense Gas Thermodynamic Models

Siloxanes are a type of dense gas useful as a working fluid in organic Rankine cycle (ORC) systems (Colonna et al. (2007)). There is a need for improving the accuracy of thermodynamic models for these dense gases (e.g. Mathijssen et al. (2015)). Specifically, it is desirable to specify in which thermodynamic states these gases will display certain nonclassical behaviour. These special properties have application in improving the use of these gases in ORC systems.

Bayesian calibration is a statistical technique that permits the prior probability distribution regarding the true value of a parameter to be updated using data collected about a measured quantity thought to be a function of the parameters. In this situation, the procedure can allow some prior knowledge about the value of some true parameters of the thermodynamic model to be updated using the measured pressure data from the Flexible Asymmetric Shock Tube (FAST) experiment, and a computer model that takes these parameters as input values.

The objective in this project is to apply the Bayesian calibration technique to an adjusted version of the computer code thought to be appropriate to model the fluid in the experimental setup, in order to determine if the uncertainty on the input parameters of the model (including thermodynamic parameters) can be reduced.

1.2 Literature Review

1.2.1 Dense Gases

Dense gases, also known as Bethe-Zeldovich-Thompson (BZT) fluids, are a class of fluids which theoretically display certain nonclassical behaviour in certain thermodynamic states, examples of which are the siloxanes, discussed in Colonna et al. (2007). The authors point out that the nonclassical region for these fluids, i.e. where the fundamental derivative of thermodynamics is negative, occurs in the vapour region not the two-phase region. The fundamental derivative,

$$\Gamma = \frac{v^3}{2c^2}\left(\frac{\partial^2 P}{\partial v^2}\right)_s = 1 + \frac{c}{v}\left(\frac{\partial c}{\partial P}\right)_s, \tag{1.1}$$

was defined by Thompson (1971), and c is the fluid's speed of sound, the subscript s implies constant entropy, ν is the specific volume and P is the pressure. Colonna et al. (2007) obtain evidence for the presence of the region via calculations using the highly accurate Span-Wagner thermodynamic model. Further, it is shown that the nonclassical region is sensitive to the thermodynamic parameters, whose uncertainty is high due to lack of relevant data. Additionally, a computational fluid dynamics calculation is made for a rarefaction shock wave in the siloxane D_6.

1.2.2 Equations of State

Several equations of state have been applied in the investigation of dense gases. In Colonna and Guardone (2006), the authors use the van der Waals equation of state to gain insight into how the molecular characteristics of the gas influence the change in the speed of sound in the nonclassical region. The equation of state and the Euler equations are used to compute the changing wave propagation behaviour for gases of different molecular complexity.

The Span-Wagner equation of state is a 12-parameter equation of state, and is used in Colonna et al. (2006) to construct highly accurate thermodynamic models for several siloxanes, using experimental data. Information on the value of the saturated vapor density was produced by the Peng-Robinson equation of state with the Stryjeck and Vera modification (PRSV), to be used where little experimental data was available. The problem of optimising the parameters for minimum error is a non-linear regression problem, solved using existing software, and each data point is weighted according to the uncertainty associated with it. The resulting equations of state are checked against existing models and found to perform favourably.

1.2.3 Analytical and Numerical Investigation of Ducts and Shock Tubes

In Gottlieb and Igra (1983), the authors analyse the effect of a rarefaction wave incident on an area reduction using a perfect gas model. Four possible quasi-steady wave patterns are

identified as resulting from the starting condition. All four result in the incident rarefaction wave producing a rarefaction wave transmitted by the duct and also a reflected rarefaction wave. The patterns differ in that while the first pattern involves only the aforementioned features, the second pattern also includes a stationary shock in the duct and a contact surface traveling away from the duct. In the third pattern, there is a shock wave that faces upstream towards the duct but cannot reach the duct because the flow from the duct is supersonic. This pattern also features the contact surface. Finally, the fourth pattern involves no shock or contact surface but rather a rarefaction wave emanating from the duct facing the same direction as the incident wave but unable to travel towards the duct because the flow from the duct is supersonic. The area reduction ratio of the convergent duct and the strength of the incident rarefaction determine which pattern emerges. The non-stationary evolution from the starting incident wave to the quasi-steady patterns described is investigated using a random choice method to numerically solve the quasi-one-dimensional Euler equations.

The work in Igra et al. (1984) considers the counterpart case of the interaction of a rarefaction wave with an area enlargement for a perfect gas and identifies two possible quasi-steady states to which the flow will evolve over time. The first possibility is that a reflected shock wave is produced traveling away from the divergent duct in the opposite direction to the incident rarefaction wave, followed by a contact surface also traveling away from the duct in the opposite direction to the incident rarefaction wave, and also a transmitted rarefaction wave. The second possibility is as the first, except for the presence of an additional rarefaction wave facing upstream but between the contact surface and the transmitted wave. This is due to the flow through the area enlargement becoming supersonic, preventing the passage of the entire rarefaction wave upstream. The authors determine that the emergence of one or the other wave patterns depends on both the strength of the incident rarefaction and also on the area ratio of the duct enlargement, using a quasi-steady analysis. This analysis also informs how the strength of the transmitted wave depends on the duct ratio and incident wave strength, and how the relatively weak reflected shock strength also changes with the incident wave strength. Further, a non-stationary analysis is performed, which provides insight into the precise evolution from the starting incident rarefaction wave to the described structures of the steady flow state.

A computational study of a dense gas shock tube with constant cross section area is performed in Argrow (1996). One-dimensional Euler equations are used, with real gas thermodynamic states being captured by use of the van der Waals equation of state. Various initial conditions allow for the production of nonclassical phenomena in the simulations. The equations are solved using a Total Variation Diminishing (TVD) predictor-corrector scheme. This method uses two steps: a forward differencing step to approximate the next solution in time, which is used to calculate the flux function, and then a backward differencing step, combined with the flux function to determine the actual solution at the next time step (LeVeque and Yee (1990)). Solid boundary conditions are applied at the ends of the tube and the results include periods of the simulation in which waves reflected by these boundaries interact with the flow in the domain. Simulations at the limit of the van der Waals parameters that correspond to a perfect gas are performed to check they correspond with perfect gas results. Three cases of wave fields featuring nonclassical phenomena are described, all of which emerge from results to some extent containing thermodynamic states in the region where $\Gamma < 0$. Expansion shocks and compression fans occur where $\Gamma < 0$ and if Γ changes sign between thermodynamic states

in a single wave pattern, then so-called composite or split waves occur. Complex behaviour is observed for nonclassical wave reflections. The authors advise an approximate Riemann solver might be used in further analysis, as the adopted TVD MacCormack method is merely adequate for capturing the waves in the field and suggest a more accurate equation of state might be used. Furthermore, validation with experiments is suggested.

During the design of the Flexible Asymmetric Shock Tube facility, the designers undertook a numerical simulation of the designed experiment, in Zamfirescu et al. (2006). Use is made of a real gas equation of state, specifically, the PRSV equation of state, to calculate thermodynamic states of the working fluid, the siloxane D_6. An outline of the preliminary design summarises how the design aims to record data about a phenomenon (rarefaction shock waves in dense gases) that is highly sensitive to the initial conditions of the experiment. The numerical simulation then performed involves numerical solution of the quasi-one-dimensional Euler equations, where the intended experimental setup's geometry is simplified and adapted to the requirements of this computer model. There is further investigation of off-design conditions, using different nozzle dimensions and the potential viability of different working fluids with the chosen setup. Furthermore, the question of how thermodynamic model uncertainty affects the simulation output is considered. It is found that the results are highly sensitive to the accuracy of the thermodynamic model.

1.2.4 Dense Gas Shock Tube Experiments

Results using nitrogen as the working fluid from a shock tube designed for dense gases are reported in Fergason et al. (2003). The design of the facility, including how the temperature of the high pressure state is maintained and the pressure data recording setup is described. Two static pressure sensors are present, one in each section of the shock tube. Two dynamic pressure sensors are placed in the high pressure region. The high pressure and low pressure states are separated using a copper diaphragm. An estimate is made of diaphragm opening time using the method of characteristics and the estimate is checked by performing a one-dimensional simulation of the shock tube. The finite opening time of the diaphragm is accounted for by replacing the initial discontinuity data with initial data containing a linear variation of pressure between the high and low pressure states. An investigation into the potential incomplete bursting of the diaphragm, using a three-dimensional Euler flow simulation showed that a partial diaphragm burst resulted in a slightly weaker rarefaction wave. This was because the final rarefaction wave evolved through a different process, involving the coalescing of a reflected, curved expansion front into the final primary wave.

The data used in the current project is produced by the TU Delft (FAST) Facility. This is a Ludwieg tube designed to be used with D_6. Data from the experiment are presented and discussed in Mathijssen et al. (2015). The intention is to obtain data demonstrating nonclassical behaviour in the D_6 gas.

1.2.5 Riemann Solvers

This project will apply an approximate Riemann solver to solve the quasi-one-dimensional Euler equations. The equations feature sources term which capture the cross section area varying along the length of the shock tube.

In LeVeque and Yee (1990), problems arising when solving equations with stiff source terms due to coupling of conservation laws with source terms related to chemical reactions, were studied. They apply two different implicit techniques to an advection equation with a source term. They find splitting the conservation law and the chemical reaction laws into separate steps is preferable.

An application of an approach to balance the flux gradients and the source terms when using Roe's approximate Riemann solver is shown in Hubbard and Garcia-Navarro (2000). They discretise the governing equations in such a way as to better represent the balancing of source terms and flux derivatives that is present in the mathematical model, and extend the technique to slope and flux limited schemes, and in multiple dimensions.

A problem can arise when applying the Roe scheme (and other conservative schemes) to certain flows, in which the method will not ensure that the density remains positive (Einfeldt et al. (1991)). Certain types of initial data provided to the scheme are shown to result in negative density or internal energy and the scheme fails. The authors show certain conditions in which the Harten-Lax-van Leer scheme will be so-called "positively conservative". An approach is described in Pelanti et al. (2001) which involves applying a new entropy fix to achieve a Roe scheme which is postively conservative with low dissipation. The authors apply the entropy fix to check it achieves the original goal in the case of two rarefaction waves moving away from each other.

1.2.6 Surrogate Modeling

The problem is expected to involve a computer model with some number of input parameters, without knowing beforehand which parameter is the most important. The approach of Gerstner and Griebel (2003) is to apply a sparse grid method, with some additional features. The sparse grid method approximates the underlying function using a sum of individual approximations with each dimension treated the same. The authors then apply an adaptive technique to improve the grid approximation by refining it for specific important dimensions. Importance is quantified by adding index locations in such a way that the integration error on the sparse grid is reduced, while still achieving an admissible index set. The index set is the set of integer values, where each index represents the position of a grid point, and admissible index sets include a variety of possible index sets including classical sparse grids. The authors detail an efficient algorithm to determine an admissible set with low estimation error for a particular application, show how the grid data can make efficient use of computer memory and apply the approach to several applications.

1.2.7 Sensitivity Analysis

Sobol' devised a method of assessing global variance of a function output with uncertain inputs (Sobol' (2001)). This system of global sensitivity indices uses properties of functions which can be subject to a so-called ANOVA decomposition. It is then possible to estimate variances for combinations of parameters to assess how much of the variance of the function is due to that combination of parameters. The advantage of this method is that it captures the variation in the entire domain, not just at a single point. The sparse grid and Sobol' index code implements the previously described sparse grid quadrature and also the computation of the global sensitivity indices (Dwight and Resmini (n.d.)).

1.2.8 Statistical Model and Bayesian Calibration

A statistical model can be used to treat the measured outputs as the result of some process and such a model can incorporate uncertainty from the beginning. Bayesian calibration techniques can be applied to reduce uncertainty on parameters of computer models that simulate the true process. Certain issues arise when applying these techniques to particular problems, such as when the model output is multivariate and high dimensional.

Sources of Error and Statistical Models

A framework for incorporating uncertainty in a statistical model of a process was introduced in Kennedy and O'Hagan (2001). They suggest one possible structure in which the measurement output is constructed as:

$$z_i = \zeta(\mathbf{x}_i) + e_i = \rho\eta(\mathbf{x}_i, \boldsymbol{\theta}) + \delta(\mathbf{x}_i) + e_i, \tag{1.2}$$

where $\zeta(\mathbf{x}_i)$ is the true process and e_i is the measurement error. They also define a vector of experimental observations and computer simulation outputs, d, and set the goal of determining the posterior probability, which can be written:

$$p(\boldsymbol{\theta}|\boldsymbol{d}) \propto p(\boldsymbol{\theta})p(\boldsymbol{d}|\boldsymbol{\theta}), \tag{1.3}$$

where $p(\boldsymbol{\theta})$ is the prior probability about the true value of the calibration parameters, and $p(\boldsymbol{d}|\boldsymbol{\theta})$ expresses the likelihood function. Amongst other derivations and manipulations, the authors indicate that Markov chain Monte Carlo (MCMC) sampling is an appropriate technique to achieve the posterior for higher dimensioned (number of parameters) problems.

Bayesian Calibration Techniques and Algorithms

As mentioned, a numerical approach can be used to approximate the posterior distribution. An algorithm that can be used to sample from the posterior distribution is the Metropolis-Hastings algorithm (Hastings (1970)). This algorithm is a particular kind of MCMC sampling method, involving a proposal step and an acceptance/rejection step. The form of the acceptance/rejection step is what is characteristic of this algorithm. Other sampling methods can also be applied, as implemented in the PyMC3 software (Salvatier et al. (2016)).

Multivariate Output and High Dimension Output

The current application involves many pressure values located in time. Care is needed when applying these calibration techniques to multivariate output. McFarland et al. (2008) investigate an application in which the model output is "highly multivariate", i.e. consists of output at many spatial or temporal points. The use of a Gaussian Process (GP) model becomes problematic due to the need to express the covariance of the output locations. The authors propose a method using an algorithm to choose a subset of the points to construct a GP model. A different method is used by Higdon et al. (2012) who construct a GP model that makes use of "Principal Component" basis vectors for a problem involving multi-dimensional output (an image) across several experimental scenarios. Conti and O'Hagan (2010) look at the use of surrogate models for time-varying output of computer models, suggesting several approaches for accounting for the time variable.

Identifiability of the Model Inadequacy Term

Some statistical models make use of a so-called model inadequacy term in equation 1.2. This, as described in Kennedy and O'Hagan (2001), is an additive or multiplicative term, itself a Gaussian Process, that can be tuned to account for the difference between the true process and the model output. The problem is whether the calibration process can distinguish between errors due to uncertain parameters and errors due to model inadequacy. Arendt et al. (2012) show how choices in the model structure affect the identifiability of the model inadequacy and that sometimes inadequacy is identifiable but, in other situations, increasing the amount of data does not improve identifiability.

1.2.9 Applications of Bayesian Calibration

Merle and Cinnella (2015) use a model of dense gas flow and a thermodynamic model in an application of Bayesian calibration. They use a two-dimensional inviscid flow model and several different complex thermodynamic models to calibrate on reference data. The computer model is replaced with a surrogate model, and Sobol' indices are computed to determine sensitivity of the model output to parameters. Using a Markov chain simulation, they calibrate two different statistical model structures. They conclude that the parameters of the model are not working to give information about the real thermodynamic behaviour, but rather have, in the author's words, "become tuning parameters".

Robinson et al. (2013) perform a calibration of a thermodynamic model directly and use experimental thermodynamic data for the procedure. The experimental data are shock speeds in aluminium 6061, and a computer model is used that computes shock speeds. There are two calibration parameters. Their model has no model inadequacy terms and variance of the observation error is not assumed to have a value but is rather treated as a calibration parameter. The posterior distribution is approximated using a Markov chain simulation. The authors go on to use the thermodynamic model with a hydrodynamic code. Boon et al. (2012) use Bayesian calibration in a final step to investigate the results from a panel method analysis of an airfoil that has uncertain geometry. This is related to experimental measurements of

a wing with uncertain geometry. Model inadequacy is not incorporated, yielding a similar statistical model to that of Robinson et al. (2013).

1.3 Structure

The objective of the project described in this report is to attempt to reduce the uncertainty on thermodynamic parameters of an equation of state of a dense gas using shock tube data and a computer model. The data used is pressure-time data from the FAST experiment for the gas D_6. The computer model used will be a Roe-type solver for the compressible quasi-one-dimensional Euler equations, which is modified to approximately model the flow of the gas in the experiment. Input parameters for the model will be selected and the approach of Sobol' indices will be applied for sensitivity analysis of the computer output. The sparse grid interpolation technique will be used to replace the actual computer code with a surrogate model. This surrogate model will be used to compute the Sobol' indices. A statistical model will provide the framework for a Bayesian inference approach in order to determine if the experimental data informs about the parameters of the model.

Chapter 2 provides an overview of the experimental setup from which the already existing data originated and also what the experimental data consists of. This is necessary in order to explain certain features of the data and also in choosing how to model the process. Chapter 3 details the working of and changes made to the computer model used to simulate the gas flow in the shock tube. Additionally, the qualitative aspects of the computer model output are discussed. Chapter 4 presents the surrogate model and sensitivity analysis approach, and also justifies the statistical model structure choice. Chapter 5 outlines the results of the investigation and a discussion of the surrogate model, sensitivity analysis and Bayesian inference results is undertaken. The conclusions and recommendations are contained in Chapter 6.

Chapter 2

Experimental Data

This chapter gives an overview of the experimental data that was obtained by Mathijssen et al. (2015). An overview of the experimental setup is given. This is followed by presentation of the data that will be used in the calibration.

2.1 Overview of the Experiment

The flexible asymmetric shock tube (FAST) experiment consists of a high pressure charge tube, a nozzle, a fast-opening valve (FOV) and a low pressure plenum (LPP). Figure 2.1, taken from Mathijssen et al. (2015), shows the overview of the experiment.

The areas of particular relevance to this project are the six segments of the charge tube, and the LPP, within which resides the FOV. Before the experiment starts, the charge tube contains the high pressure gas, maintained in a desired thermodynamic state. During the experiment, the FOV opens, allowing gas to flow from the charge tube, into the LPP, which is maintained as close to vacuum as possible. Figure 2.2, based on Mathijssen et al. (2015), shows a simplified view of the experimental setup. Here, the nozzle and valve, which make up the FOV are assumed to precede the LPP. This assumption is necessary because, later, a quasi-one-dimensional model is used.

The nozzle and valve that make up the FOV are shown in Figure 2.3, taken from Mathijssen et al. (2015), which shows a drawing of the cross section of the valve and the inlet nozzle which precedes it. The important aspects are the inlet valve, the minimum throat area set by the green adjustable element, and the venting holes which allow the air to outlet into the LPP. The operation of the valve is described in Mathijssen et al. (2015). A number of important issues from that work that arise in its practical employment are now highlighted, as they are relevant in the later modeling decisions.

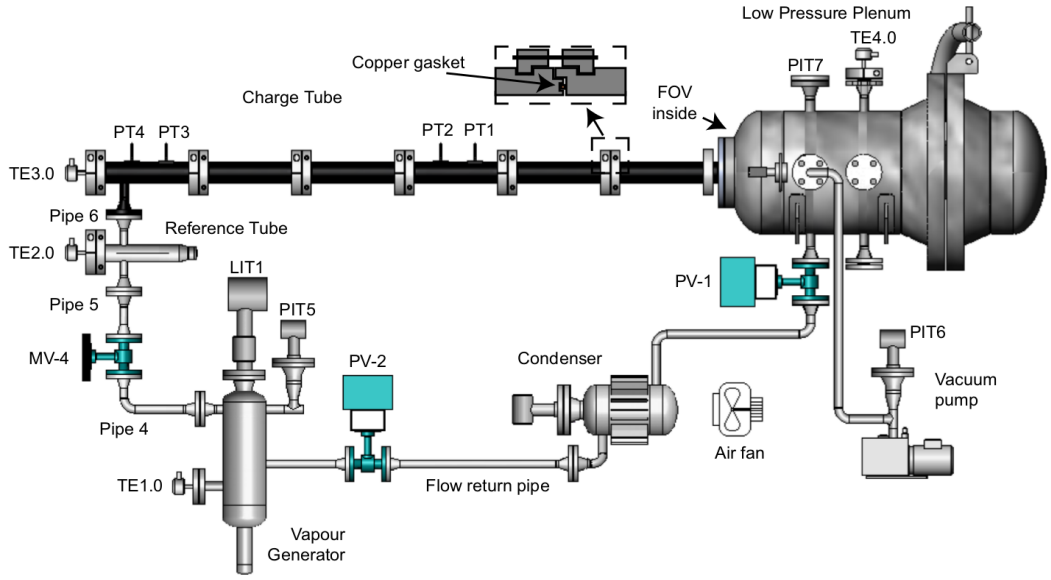

Figure 2.1: Overview of the experimental setup. Source: T. Mathijssen, M. Gallo, E. Casati, N. Nannan, C. Zamfirescu, A. Guardone, and P. Colonna. The flexible asymmetric shock tube (FAST): a ludwieg tube facility for wave propagation measurements in high-temperature vapours of organic fluids. *Experiments in Fluids*, 56 (10):112, 2015.

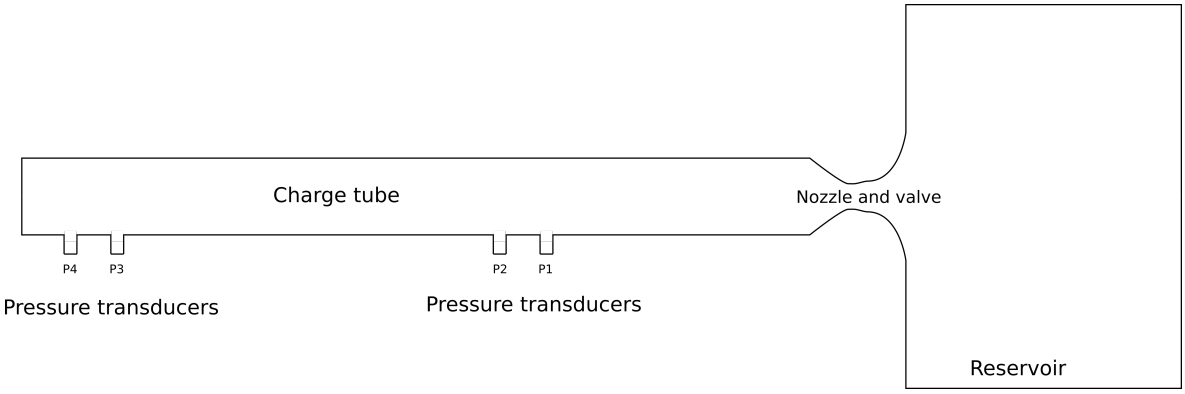

Figure 2.2: Simplified view of the experimental setup. Based on: C. Zamfirescu, A. Guardone, and P. Colonna. Numerical simulation of the fast dense gas experiment. In *Proceedings of the European conference on computational fluid dynamics, ECCOMAS CFD*, volume 2006, 2006.

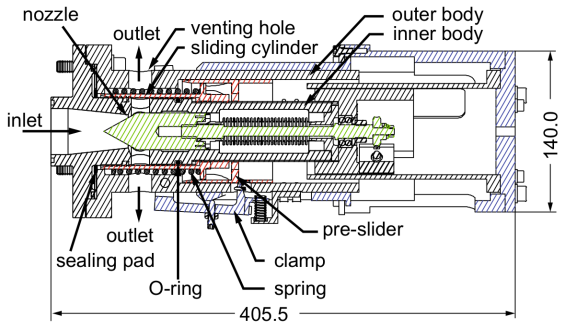

Figure 2.3: Drawing showing the FOV components. Source: T. Mathijssen, M. Gallo, E. Casati, N. Nannan, C. Zamfirescu, A. Guardone, and P. Colonna. The flexible asymmetric shock tube (fast): a ludwieg tube facility for wave propagation measurements in high-temperature vapours of organic fluids. *Experiments in Fluids*, 56 (10):112, 2015.

- The valve is unheated in the actual experiments, meaning that condensible gases (such as the dense gases) may condense in the valve and nozzle.

- The sliding cylinder, which moves to allow the gas to leave via the venting holes, does not always move smoothly during the opening procedure. This is particularly the case for non-condensible gases. The result is that the flow is choked at various minimum areas, at each moment that the sliding cylinder pauses. This results in a stepped expansion profile, rather than the usual smooth pressure drop. This behaviour is not predictable in the current project.

- In the event that the sliding cylinder moves smoothly, there are always two very small pressure drops that precede the main pressure drop. These occur because when the cylinder is unclamped, the gas begins to escape through small pathways that unavoidably exist in the mechanism, resulting in the flow being initially choked by those very small throat areas, before the cylinder clears the vents and the main pressure drop occurs.

- The opening that results at the nozzle throat is ring, not a circle.

2.2 Pressure Data From Experiment 28

This analysis makes use of data already collected and analysed by Mathijssen et al. (2015). First, the gas state in the experiment is described. Afterwards, the pressure-time data is presented.

Table 2.1: Parameters used to plot the thermodynamic state P-v diagram for the polytropic van der Waals gas. P_{cr} is the critical pressure, T_{cr} is the critical temperature, c_v is the specific heat at constant volume, and R is the specific gas constant.

Parameter	Value
$P_{cr}[Pa]$	961000
T_{cr} [K]	645.8
$\frac{c_v}{R}[-]$	90.9

2.2.1 High Pressure Initial State

The initial high pressure state in the charge tube (CT) in Experiment 28 was defined in Mathijssen et al. (2015) as $P_{CT} = 1.27 \times 10^5$ Pa and $T_{CT} = 571.15$ K. To show where this thermodynamic state is located, the P-v diagram for a polytropic van der Waals gas with a set of nominal parameters is shown. The nominal parameters used will be elaborated in Chapter 3. For now, the parameters used are shown in Table 2.1.

The van der Waals equation of state's pressure equation is

$$P(v,T) = \frac{RT}{v-b} - \frac{a}{v^2}, \tag{2.1}$$

where R is the specific gas constant, T is the temperature, $v = V/m$ is the specific volume, and a and b are material specific constants defined as:

$$a = \frac{27}{64}\frac{R^2T_{cr}^2}{P_{cr}}, \tag{2.2}$$

$$b = \frac{1}{8}\frac{RT_{cr}}{P_{cr}}. \tag{2.3}$$

The objective is to plot the initial high pressure state along with the critical isotherm line (isotherm where $T = T_{cr}$), an approximation of the saturation curve, and the line $\Gamma = 0$, where Γ is the fundamental derivative of equation 1.1. The idea, explained by Thompson (1971), is that for values where $\Gamma < 0$, the isentropes on a P-v have increasing negative gradient, and that unusual fluid behaviour is expected in this "inversion" region.

To derive the expression for Γ for a van der Waals gas, the isentropic constraint on the partial derivative terms is noted. If the volume and temperature are both allowed to change then

$$ds = \frac{\partial s}{\partial v}dv + \frac{\partial s}{\partial T}dT = 0, \tag{2.4}$$

along the isentropes. Using Maxwell's relations (Bejan (2016)),

$$\left(\frac{\partial s}{\partial v}\right)_T = \left(\frac{\partial P}{\partial T}\right)_v, \tag{2.5}$$

which can be found from the van der Waals pressure equation, so

$$\left(\frac{\partial s}{\partial v}\right)_T = \frac{R}{v-b}. \tag{2.6}$$

Using the definition of change in entropy, and assuming constant volume, it can be shown that

$$(\delta Q^{\text{rev}})_v = (ds)_v T = c_v dT, \tag{2.7}$$

where $(\delta Q^{\text{rev}})_v$ is an infinitesimal increment of heat energy. Therefore:

$$\left(\frac{\partial s}{\partial T}\right)_v = \frac{c_v}{T}, \tag{2.8}$$

and substituting these terms into equation 2.4, and rearranging, it is found that

$$dT = -\frac{RT}{c_v\,(v-b)}dv, \tag{2.9}$$

along the isentropes. To arrive at the expression for the fundamental derivative, first the speed of sound for a general equation of state is given as

$$c = \sqrt{-v^2\left(\frac{\partial P}{\partial v}\right)_s}. \tag{2.10}$$

By deriving the total differential of P and substituting in the value of dT under constant entropy as found above, the speed of sound in a polytropic van der Waals fluid is found to be

$$c(v,T) = \sqrt{-v^2\left(-\frac{R^2T}{c_v(v-b)^2} - \frac{RT}{(v-b)^2} + \frac{2a}{v^3}\right)}. \tag{2.11}$$

The derivative with respect to specific volume is found for constant entropy, substituting in the total derivative of temperature under constant entropy. The resulting derivative is

$$\left(\frac{\partial c}{\partial v}\right)_s = \frac{(2RTc_v^2v^4 + 3R^2Tc_vv^4 + R^3Tv^4 - 6ac_v^2v^3 + 18abc_v^2v^2 - 18ab^2c_v^2v + 6ab^3c_v^2)}{2c_v(v-b)(RTc_vv^3 + R^2Tv^3 - 2ac_vv^2 + 4abc_vv - 2ab^2c_v)}. \tag{2.12}$$

This is then substituted into equation 1.1 to find the fundamental derivative.

The above form of the fundamental derivative is used in 2.4 showing the pressure-specific density diagram for the van der Waals gas with the set of example parameters from Table 2.1, and the high pressure initial state shown by a red dot.

The van der Waals equation of state is known to be inaccurate near the inversion region (Colonna and Guardone (2006)). The output of the van der Waals equation of state is compared to the state diagram provided by the more accurate "improved Peng-Robinson with Strycek Vera modification" (iPRSV) equation of state. The iPRSV equation of state is

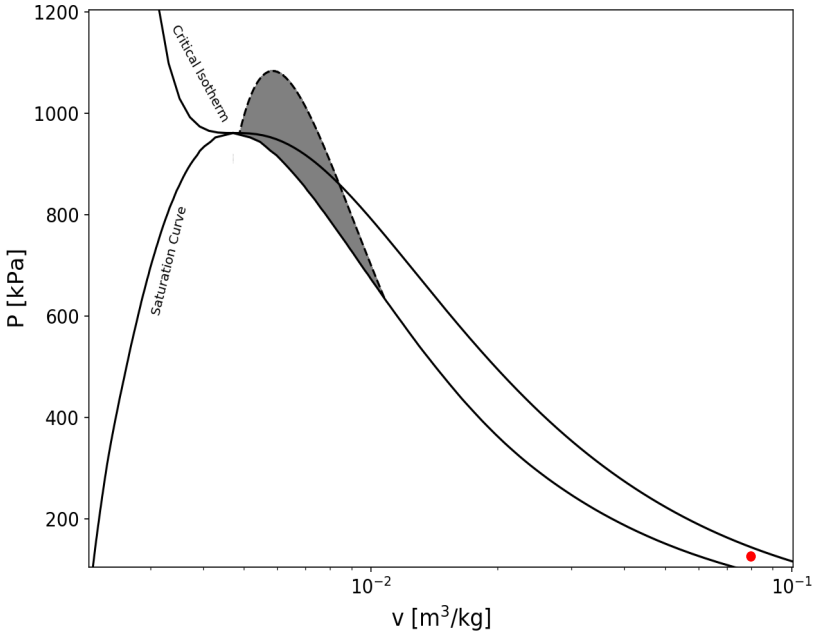

Figure 2.4: P-v diagram for the van der Waals gas, showing the saturation curve from the Maxwell construction, the isotherm for the critical temperature, the $\Gamma < 0$ region shaded grey, and the initial condition for the high pressure region in the experiment shown by the red dot.

an improved version of the PRSV cubic equation of state which removes a discontinuity in the calculated properties (Van der Stelt et al. (2012)). The thermodynamic values are computed using the FluidProp software (Colonna and Van der Stelt (2004)), and the results are shown in Figure 2.5. Figure 2.5 shows the P-v diagrams for both van der Waals and iPRSV. It is clear that the predicted regions of $\Gamma < 0$ differ greatly between the two equations of state. A comparison between the computed thermodynamic states of the two equations is made by plotting the isentrope which passes the high pressure initial state of Experiment 28, as computed by each equation. This is shown in Figure 2.6 The locations of the initial state, and the isentrope through it, are not identical between the two thermodynamic models, but the computed states do not show the higher levels of discrepancy apparent closer to the inversion region.

2.2.2 Pressure Data

The pressure data used in the subsequent calibration is now presented. The full data consists of 10 seconds of pressure-time data from the four dynamic pressure sensors. This full data is shown in Figure 2.7. The beginning of the data is the constant pressure before the experiment starts. The latter part of the data is the complicated period when reflected waves have propagated through the tube and interacted. Between these two regions is a theoretically uncomplicated region containing an expansion which passes each of the four sensors sequentially. Sensors P3 and P4 are located at the distant far end of the tube and are close enough to the end of the tube that the expansion has not fully passed when the reflection of

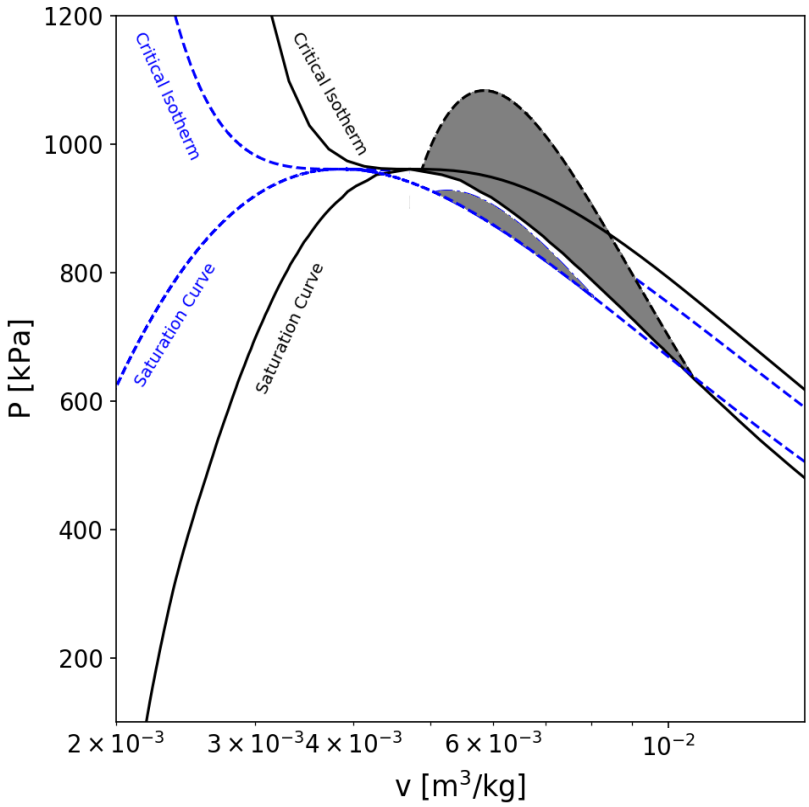

Figure 2.5: P-v diagram for the van der Waals equation of state (black), and the iPRSV equation of state (blue) and the respective inversion regions shaded.

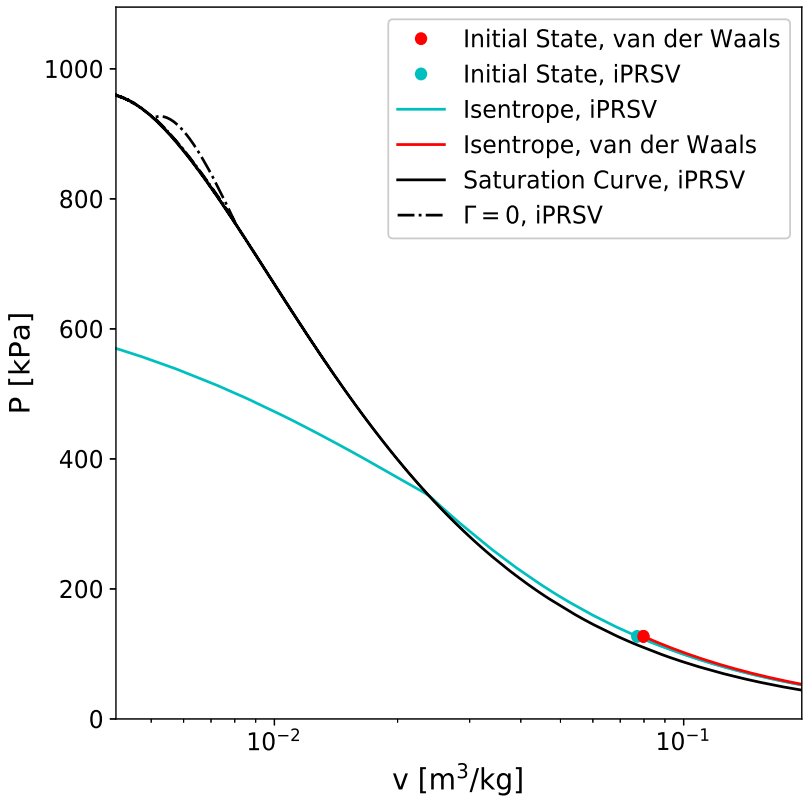

Figure 2.6: P-v diagram for the iPRSV equation of state, with the isentropes through the high pressure initial state, according to iPRSV and according to van der Waals.

the head of it has already reached the sensor. As such, the data from sensor 4 is not used. Some data from sensor 3 is used. The three rectangles in Figure 2.7 show the general region of interest. This region corresponds to the region shown in Figure 2.8. This Figure shows signals P1 and P2. The constant pressure ends with a very small pressure drop. This has been attributed to the fact that before the valve opens, there is a small gap, as the clamps are removed, which allows gas to escape (Mathijssen et al. (2015)). The flow is choked by a very narrow cross section in the valve components. This happens more than once. Finally, the valve starts to open, and the expansion waves can pass into the high pressure region. The main expansion arrives at P1 at approximately 2.91 seconds into the data. The exact way in which the processes in the nozzle and in the valve evolve to produce the expansion will be examined in detail in Chapter 3. The expansion ends because the flow at the minimum cross section becomes choked, and expansion waves can no longer pass into the high pressure region.

At the end of the approximately constant pressure after the main expansion there is a difference in the way the pressure evolves at P1 and at P2. A compression passes sensor P1 earlier than P2. This implies that the compression might be traveling from the low pressure region. Further, there is a pressure drop in the P2 data at approximately 2.92 seconds that is not obvious in the P1 data. This could be speculated to be because a reflected expansion arrives at P2 before the compression, whereas the compression arrives at P1 before the expansion passes it. However, without investigating the evolution of the flow field in a way that accounts for reflections, no solid conclusions can be drawn on exactly how the flow in the channel is behaving. Thus, the data are restricted to the region which is very likely free of reflections. Furthermore, the data are shifted, such that the 0 seconds point corresponds to the arrival of the expansion at P1. These data are shown in Figure 2.9, and this is the data that will be used in the calibration.

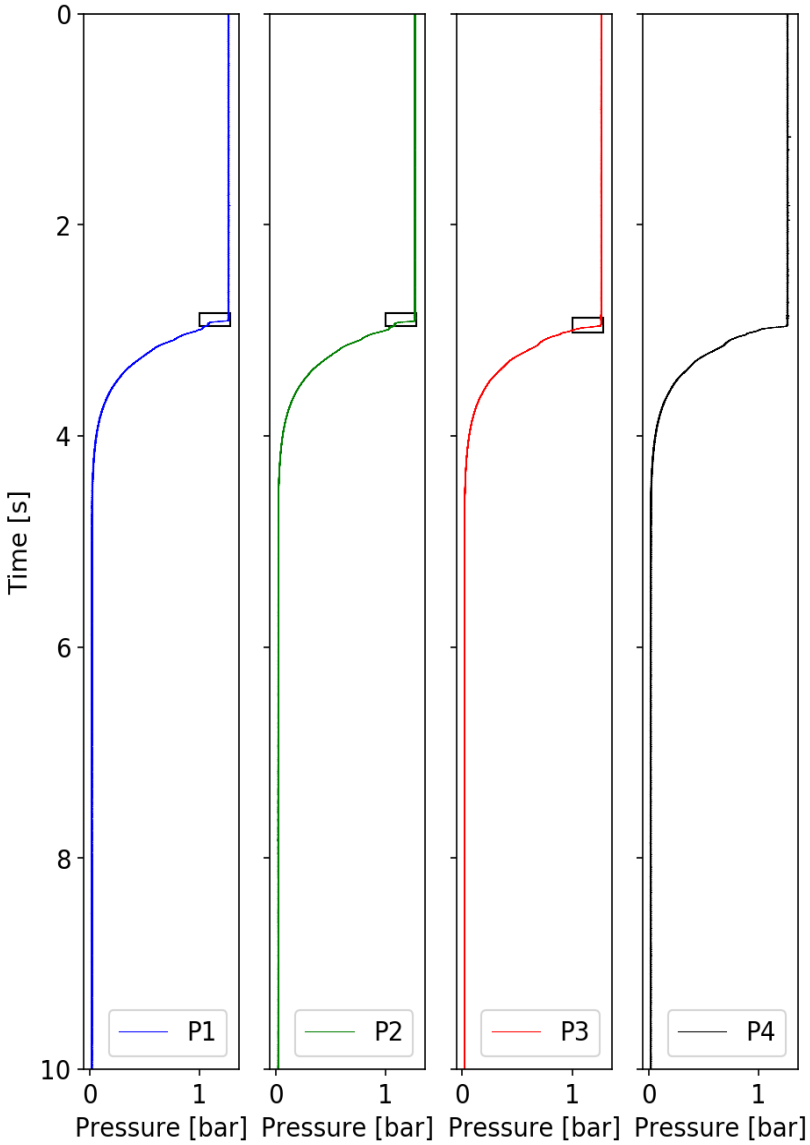

Figure 2.7: Pressure data from Experiment 28, from the four dynamic pressure sensor locations. The box indicates the region of data shown in Figure 2.8.

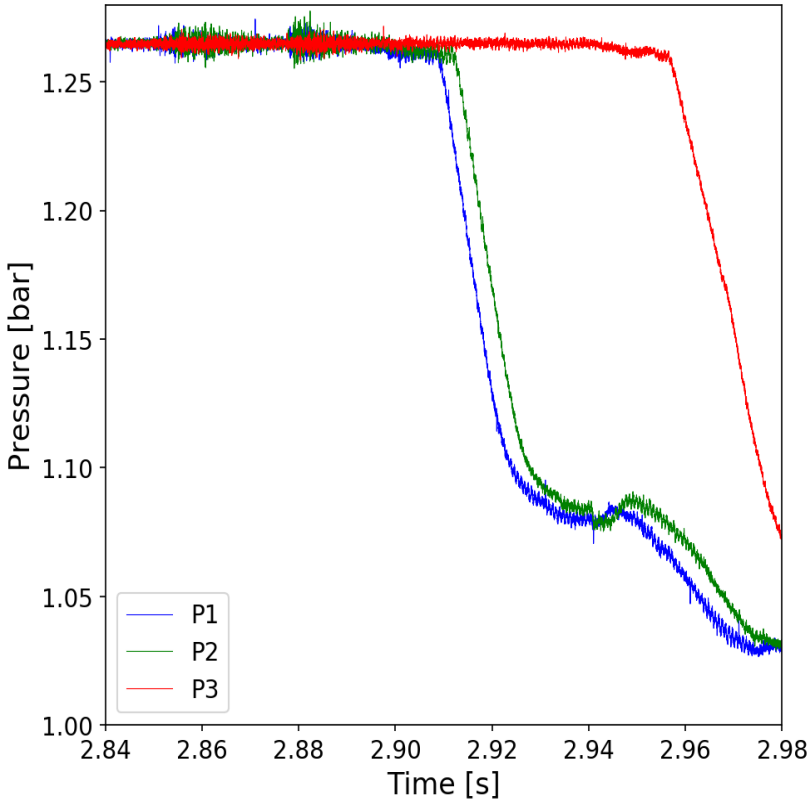

Figure 2.8: Pressure data from Experiment 28, from three of the dynamic pressure sensor locations, only showing the region from shortly before until shortly after the main expansion passes.

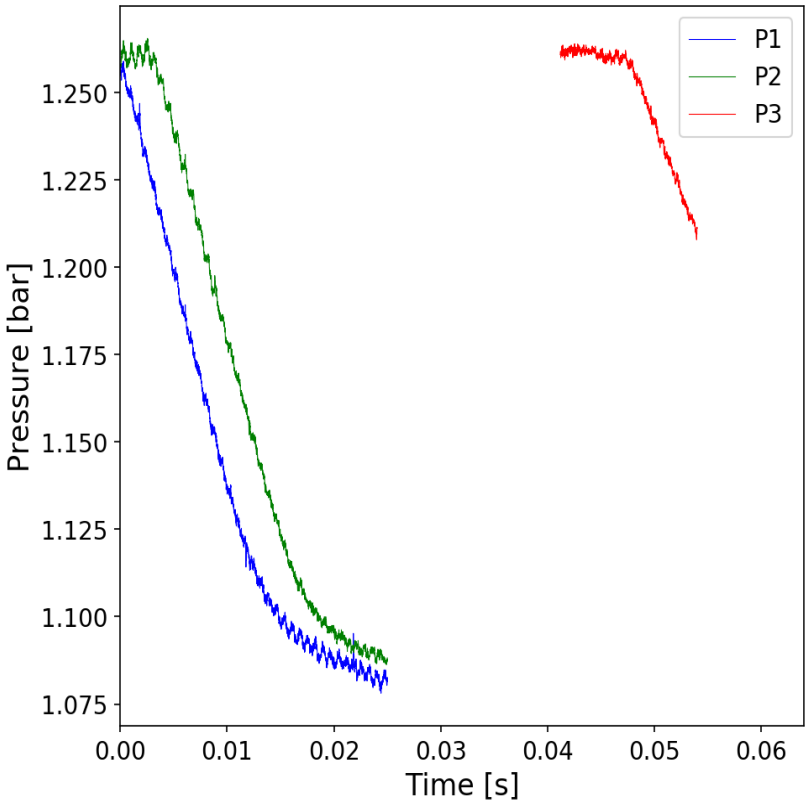

Figure 2.9: Pressure data from Experiment 28, from three of the dynamic pressure sensor locations, only showing the data to be used for the calibration procedure.

Chapter 3

Computer Model of the Shock Tube Flow

The subject of this chapter is the computer model used to simulate the real gas flow. Section 3.1 outlines the pre-existing code which is the starting point for the work done. The modifications made to the model are detailed in section 3.2. Finally, the computer model output is evaluated in section 3.3.

3.1 Existing Computer Model

The existing computer model is now described. First, the governing equations are shown. Next, the solution procedure is addressed.

3.1.1 Governing Equations

Here the quasi-one-dimensional Euler equations are derived. The derivation is from Laney (1998), but making the modification to the control volume to allow for the smooth variation of local area of the channel.

Beginning with the conservation of mass it is stated that

$$\int_a^b \left[\rho\left(x,t_2\right)A\left(x,t_2\right) - \rho\left(x,t_1\right)A\left(x,t_1\right)\right]dx = -\int_{t_2}^{t_1}\left[\rho\left(b,t\right)A\left(b,t\right)u\left(b,t\right) - \rho\left(a,t\right)A\left(a,t\right)u\left(a,t\right)\right]dt, \quad (3.1)$$

where $[a, b]$ defines the interval in x and $[t_1, t_2]$ defines the time interval, ρ is density, A is channel area and u is the flow velocity. A similar relation describes the conservation of momentum, such that

$$\begin{aligned}\int_a^b &\left[\rho\left(x,t_2\right)A\left(x,t_2\right)u\left(x,t_2\right)-\rho\left(x,t_1\right)A\left(x,t_1\right)u\left(x,t_1\right)\right]dx\\ &=-\int_{t_2}^{t_1}\left[\rho\left(b,t\right)A\left(b,t\right)u^2\left(b,t\right)-\rho\left(a,t\right)A\left(a,t\right)u^2\left(a,t\right)\right]dt\\ &\qquad\qquad-\int_{t_2}^{t_1}\left[p\left(b,t\right)A\left(b,t\right)-p\left(a,t\right)A\left(a,t\right)\right]dt,\end{aligned}\tag{3.2}$$

where p is the pressure. Finally, the integral relation describing conservation of energy,

$$\begin{aligned}\int_a^b &\left[\rho\left(x,t_2\right)A\left(x,t_2\right)E\left(x,t_2\right)-\rho\left(x,t_1\right)A\left(x,t_1\right)E\left(x,t_1\right)\right]dx\\ &=-\int_{t_2}^{t_1}\left[\rho\left(b,t\right)A\left(b,t\right)u\left(b,t\right)H\left(b,t\right)-\rho\left(a,t\right)A\left(a,t\right)u\left(a,t\right)H\left(a,t\right)\right]dt,\end{aligned}\tag{3.3}$$

where E is the total energy per unit volume and H is the total enthalpy per unit volume, is arrived at. The relation between H and E is

$$\rho H = E + p.\tag{3.4}$$

In order to complete the system of equations, a thermodynamic equation of state is required, which will be addressed later. As in Laney (1998), the equations are expressed in conservation form and the fact that the limits of integration are arbitrary is used. Omitting the dependence of the variables on x and t,

$$\frac{\partial\left(\rho A\right)}{\partial t}+\frac{\partial\left(\rho A u\right)}{\partial x}=0,\tag{3.5}$$

$$\frac{\partial\left(\rho A u\right)}{\partial t}+\frac{\partial\left(\rho A u^2+pA\right)}{\partial x}=p\frac{\partial A}{\partial x},\tag{3.6}$$

$$\frac{\partial\left(AE\right)}{\partial t}+\frac{\partial\left(\rho A u\right)}{\partial x}=-p\frac{\partial A}{\partial t}.\tag{3.7}$$

The terms on the right hand side of the momentum and energy equations appear when converting the integrals of the pressure terms at the control volume surface to integrals in the domain. By applying the product rule, and rearranging the equations, it is possible to express the above conservation forms using vectors of conserved variables. Specifically,

$$\frac{\partial \mathbf{U}}{\partial t} + \frac{\partial \mathbf{F}(\mathbf{U})}{\partial x} = \mathbf{S}(\mathbf{U}), \tag{3.8}$$

in which,

$$\mathbf{U} = \begin{bmatrix} \rho \\ \rho u \\ E \end{bmatrix}, \tag{3.9}$$

is the state vector and

$$\mathbf{F}(\mathbf{U}) = \begin{bmatrix} \rho u \\ \rho u^2 + p \\ u(E+p) \end{bmatrix}, \tag{3.10}$$

and

$$\mathbf{S}(\mathbf{U}) = -\left(u\frac{A_x}{A}\right)\begin{bmatrix} \rho \\ \rho u \\ E+p \end{bmatrix}. \tag{3.11}$$

Note that the term $\frac{A_t}{A}$ is absent from the source term. This is because the unmodified, existing, solver makes the assumption that the area at each point in space is independent of time.

Applying the chain rule to equation 3.8, yields the form showing the flux Jacobian matrix, $\frac{d(\mathbf{F})}{dx}$, where, omitting the dependence of $\mathbf{F}$ and $\mathbf{S}$ on $\mathbf{U}$,

$$\frac{\partial \mathbf{U}}{\partial t} + \frac{d\mathbf{F}}{d\mathbf{U}}\frac{\partial \mathbf{U}}{\partial x} = \mathbf{S}. \tag{3.12}$$

The polytropic van der Waals equation of state (as presented in the previous chapter) is used to complete the system of equations.

3.1.2 Solution Procedure

The solver is a high resolution upwind finite volume method, operating on a one-dimensional grid with equidistant nodes. The flux at the one-dimensional cell boundaries used to advance the state, $\mathbf{U}$, is computed using Roe's approximate method, making use of the solution at the cell boundaries. The state at the cell boundaries is reconstructed using the slope-limited value of the conservative variables which is assumed to be piecewise linear.

The flux Jacobian, $A(\mathbf{U}) = \frac{d\mathbf{F}}{d\mathbf{U}}$, can be written, as in Gallouet et al. (2002), as

$$A(\mathbf{U}) = \begin{bmatrix} 0 & 1 & 0 \\ K - u^2 & u(2-k) & k \\ (K-H)u & H - ku^2 & u(1+k), \end{bmatrix} \tag{3.13}$$

with,

$$\begin{aligned} k &= \frac{1}{\rho}\frac{\partial p}{\partial \varepsilon}\bigg|_\rho \\ K &= c^2 + k\left(u^2 - H\right) \\ c^2 &= \frac{p}{\rho^2}\frac{\partial p}{\partial \varepsilon}\bigg|_\rho + \frac{\partial p}{\partial \rho}\bigg|_\varepsilon \\ \varepsilon &= \frac{E}{\rho} - \frac{1}{2}u^2. \end{aligned} \tag{3.14}$$

The following explanation is as appears in Laney (1998). The procedure begins by replacing the system of equations in equation 3.12, with an approximation. The flux term is replaced so that

$$\mathbf{F}(\mathbf{U}) \approx A_{RL}(\mathbf{U} - \mathbf{U}_L) + \mathbf{F}(\mathbf{U}_L), \tag{3.15}$$

where $\mathbf{U}_L$ is the state immediately to the left of the cell boundary and A_{RL} is the approximation to the flux Jacobian that satisfies three conditions:

- $A_{RL}(\mathbf{U}_R, \mathbf{U}_L) \to A(\mathbf{U})$, when $\mathbf{U}_L, \mathbf{U}_R \to \mathbf{U}$
- $\mathbf{F}(\mathbf{U}_R) - \mathbf{F}(\mathbf{U}_L) = A_{RL}(\mathbf{U}_R - \mathbf{U}_L)$
- A_{RL} has only real eigenvalues and is diagonalisable.

Unlike for the ideal gas, for real equations of state, the Roe linearisation is not unique (Cinnella (2006)). As Cinnella (2006) review, there are several proposed methods to arrive at a linearisation for real gases. Their proposed simplified scheme was adopted and they show that, while it does not satisfy the above list of requirements exactly, it is advantageous from the point of view of computational efficiency.

As proposed in Cinnella (2006), the simplified Roe scheme for real gases inolves computing the Roe-averaged variables u_{RL}, ρ_{RL}, and H_{RL}. Then the derivatives of pressure with respect to ε and ρ are computed as a function of the state defined by the those three Roe-averaged variables, such that

$$\begin{aligned}\left[\left.\frac{\partial p}{\partial \varepsilon}\right|_{\rho}\right]_{RL} &= \left.\frac{\partial p}{\partial \varepsilon}\right|_{\rho}(\rho_{RL}, \varepsilon_{RL}) \\ \left[\left.\frac{\partial p}{\partial \rho}\right|_{\varepsilon}\right]_{RL} &= \left.\frac{\partial p}{\partial \rho}\right|_{\varepsilon}(\rho_{RL}, \varepsilon_{RL})\,.\end{aligned} \tag{3.16}$$

The order of accuracy of the solution is increased by computing the solution at the cell edges assuming a linear solution in each cell and the MINMOD slope limiter is applied. Time integration of the entire system is performed using the explicit Runge-Kutta 4 algorithm.

3.2 Modifications to the Computer Model

The necessary modifications that were made to the computer model to model the shock tube experiment are now discussed. These relate to the governing equations, the source term, the boundary and initial conditions and the solution procedure.

3.2.1 Changes to Governing Equations

The derivation of the source term in the modified version is exactly as for the existing solver, except the assumption, made in equation 3.11, that the area is independent of time is not made. Therefore the source term is now

$$\mathbf{S}(\mathbf{U}) = -\left(\frac{A_t}{A} + u\frac{A_x}{A}\right)\begin{bmatrix}\rho \\ \rho u \\ E + p\end{bmatrix}. \tag{3.17}$$

3.2.2 Form for the Source Term

A choice was made about the form of the source term that would attempt to model the motion of the valve.

Assumptions about the mechanical behaviour of the valve

The opening of the valve is captured in the one-dimensional model as a change in the cross section area of the channel over time. Specifically, the entire setup is assumed to be a cylindrically symmetrical channel with the area, $A(x,t)$ of the channel at each point in the x dimension and in time t. Therefore, a form for the area function must be chosen, taking into account the following assumptions about the functioning of the valve.

1. The sliding cylinder is at rest at the start of the opening.
2. The sliding cylinder is at rest at the end of the opening.
3. The sliding cylinder moves smoothly.
4. The sliding cylinder moves in one direction.
5. The sliding cylinder does not stop moving until the opening process is complete.

Assumptions 1, 2 and 3 are chosen to ensure one of the assumptions made in the derivation of the quasi-one-dimensional model is met. Specifically, it was assumed that the change in area of the channel is smooth. Assumption 4 is not expected to differ greatly from reality. Assumption 5 is made to reduce the number of potential forms for the source term. It is important to note that assumptions 1, 2, 3, and 5 may not reflect the real mechanical process. In fact, it is expected that the behaviour of the valve is unpredictable and that in reality any of those four assumptions may be invalid to different degrees in different experiments, particularly since depending on the fluid and starting conditions, there may be, according to Mathijssen et al. (2015) condensed fluid in the unheated valve when the valve opens.

Incorporating the Assumptions in the Model

The source term must capture the behaviour of the valve that can be appreciated in the one-dimensional model. The important aspects of the behaviour are stated by Mathijssen et al. (2015), and are summarised below.

1. The sliding cylinder begins moving, allowing a small area through which the gas is choked.
2. The sliding cylinder moves further, choking the gas flow at a different, larger cross section.

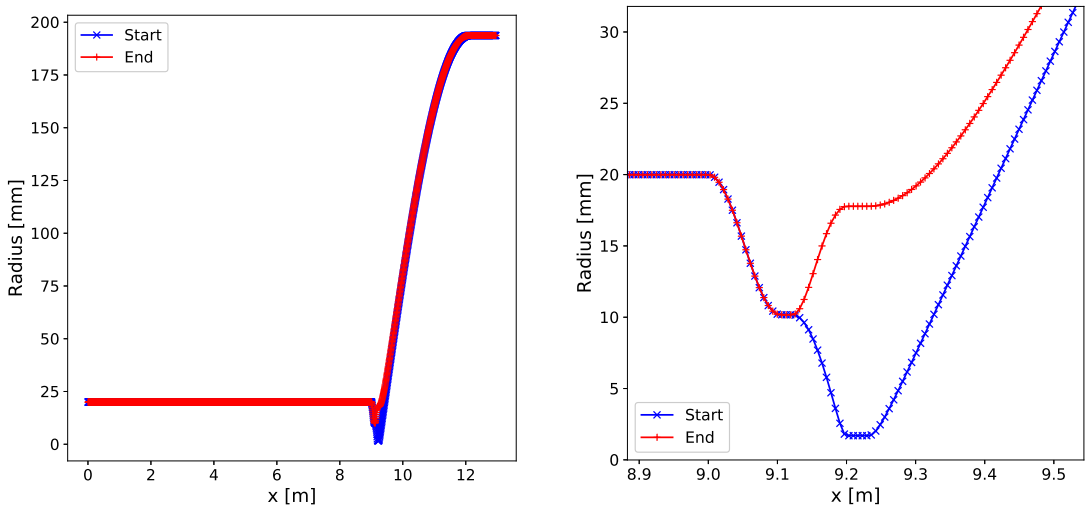

(a) (b)

Figure 3.1: Radius distribution (a) along length of domain, and (b) close to the nozzle.

3. The sliding cylinder moves past the outlet holes, meaning the flow is choked at the nozzle throat.

4. Once the cylinder has fully moved past the outlet holes the opening process is complete.

Since the quasi-one-dimensional approach does not allow for a minimum channel area of zero, the simulation must begin at the instant beginning point 2 in the above list. This means the the simulation would start with a Riemann problem featuring an area distribution with a very small minimum cross section that then smoothly widens until the opening process is complete. Figure 3.1 shows a radius distribution that matches this model at the start and the end of the opening process. The ending maximum radius of the variable part is estimated from the valve geometry.

It is then left to define an explicit form for the transient period of the source term. This is done by making sure the intermediate states are distributions similar to the starting one except for the changing minimum cross section at the varying region. To comply with the assumptions, a form for the minimum area is chosen that is a cubic function with zero first and second derivatives at the start and end time points. Figure 3.2 shows the minimum cross section area over time.

This means that there are two parameters relating to the source term which are left as unknown. One is the total duration of the main opening process depicted in Figure 3.2. The other is the throat cross section area setting of the static nozzle.

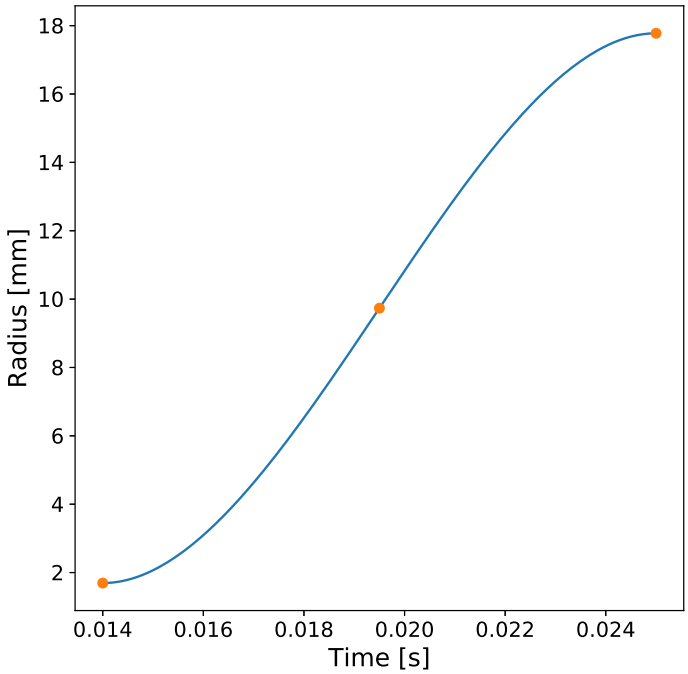

Figure 3.2: Variation of the minimum cross section during the opening process in the simulation.

3.2.3 Boundary Conditions

Using the terminology also employed by Laney (1998), the modified method adopts a solid boundary treatment of type 1. This means that the boundary is aligned with the cell border, and that the solid aspect is ensured using ghost cells in the boundary. From Laney (1998), and using two ghost cells, the left hand boundary is enforced in the conservative variables as

$$\begin{aligned} \rho^n_{i=0} &= \rho^n_{i=3}, \\ \rho^n_{i=1} &= \rho^n_{i=2}, \end{aligned} \tag{3.18}$$

$$\begin{aligned} (\rho u)^n_{i=0} &= (\rho u)^n_{i=3}\,, \\ (\rho u)^n_{i=1} &= (\rho u)^n_{i=2}\,, \end{aligned} \tag{3.19}$$

$$\begin{aligned} E^n_{i=0} &= E^n_{i=3}, \\ E^n_{i=1} &= E^n_{i=2}, \end{aligned} \tag{3.20}$$

with analogous conditions at the right hand boundary. The boundary conditions do not influence the results, however, given that the portion of the simulation that would inlude reflected waves from the boundary is not included.

3.2.4 Initial Conditions

The intial conditions are adopted are

$$T(x, t=0) = \begin{cases} 571.15 \text{ K} & \text{if} \quad 0 \leq x < 9.221 \\ 573.25 \text{ K} & \text{if} \quad 9.221 \leq x \leq 12.958 \end{cases}, \tag{3.21}$$

$$P(x, t=0) = \begin{cases} 126500 \text{ Pa} & \text{if} \quad 0 \leq x < 9.221 \\ 37950 \text{ Pa} & \text{if} \quad 9.221 \leq x \leq 12.958 \end{cases}, \tag{3.22}$$

from which the density in the intial state is computed using the equation of state. The choice is made to assume that the low pressure region and valve are at room temperature, and that there is no temperature gradient as a result of the unheated nozzle. In reality, the temperature distribution of the unheated nozzle is unknown. It is also assumed that there is a low, non-vacuum state in the low pressure chamber at the start of the experiment. In reality, the state in the low pressure chamber is close to vacuum, however this is not possible to model using the presently adopted model.

3.2.5 Solution Procedure

The modifications that were made to the solution procedure are now described.

Entropy Fix

Some solutions found using the approximate solver may violate criteria related to entropy (Toro (2013)). In order to avoid the appearance of non-physical solutions, adjustments are made to the solution procedure. Two fixes are implemented.

The entropy fixes replace the eigenvalues in the computation of the flux. The first fix of Harten and Hyman (Harten and Hyman (1983)) adjusts the eigenvalues such that

$$\lambda_{k,RL} = \begin{cases} \delta_k & \text{if} \quad |\lambda_{k,RL}| < \delta_k \\ |\lambda_{k,RL}| & \text{if} \quad |\lambda_{k,RL}| \geq \delta_k \end{cases}, \tag{3.23}$$

where

$$\delta_k = \max\{0, \lambda_{k,RL} - \lambda_k(\mathbf{U}_R), \lambda_k(\mathbf{U}_L) - \lambda_{k,RL}\}, \tag{3.24}$$

λ_k is the kth eigenvalue and the subscript RL implies the eigenvalue is computed from the Roe-average state.

The fix according to Karni and Čanić is intended to deal with the situation of slow moving shocks that can induce oscillations in the solution (Karni and Čanić (1997)), and it differs in that

$$\delta_k = \sqrt{|u_R - u_L|}. \tag{3.25}$$

This fix is used in the subsequent computations.

Handling a Source Term Depends on Time (Solving the Non-Homogeneous Problem)

The existing code solves the governing equations using Roe's approximate Riemann solver and a fourth order accurate explicit time integration, with no special treatment of the source term. The method is modified to incorporate the new source term form, and a splitting approach is applied, as suggested in Toro (2013). Thus, the Riemann solver and fourth order accurate time integration are retained for the homogeneous problem, and the non-homogeneous problem is advanced separately. Toro (2013) states that this allows the best methods to be used for each part of the problem.

The modifications to use the splitting approach are detailed in the following.

Non-Homogeneous Problem

While the existing high resolution scheme solves the problem without special treatment of the source term, in the modified solver the non-homogeneous part of the problem is updated separately and the system to be solved is

$$\frac{d}{dt}\mathbf{U} = \mathbf{S}\left(\mathbf{U}\right), \tag{3.26}$$

with the initial condition

$$\mathbf{U} = \mathbf{U_i^*}, \tag{3.27}$$

where $\mathbf{U_i^*}$ is the solution output of the Riemann solver with no source term in the ith cell.

Following the approach advised in LeVeque (2002), this system of ordinary differential equations is solved in an implicit way, with second-order accuracy in time so that

$$\mathbf{U_i^{n+1}} = \mathbf{U_i^*} + \frac{\Delta t}{2}\left[\mathbf{S}\left(\mathbf{U_i^*}\right) + \mathbf{S}\left(\mathbf{U_i^{n+1}}\right)\right], \tag{3.28}$$

where $\mathbf{U_i^{n+1}}$ is the solution at the next time step in the ith cell.

3.3 Computer Model Output

The computer model as outlined in the preceding discussion is now supplied with a nominal set of parameters and the output is discussed.

Firstly, a study of the grid convergence is performed. This is followed by the presentation of the model output.

3.3.1 Grid Convergence

Figure 3.3 shows the computer model output when run with 1000, 2000, 4000, and 8000 nodes. The use of 1000 nodes is deemed sufficient. This is after noting several features of the computer output. Firstly, the solutions exhibit most difference in the constant region before the main expansion (before $t = 0$). However, this part of the computer output is not used in the calibration. Secondly, the presence of oscillations (in the constant pressure region before the expansion) is noted in the solutions with 4000 nodes and 8000 nodes.

3.3.2 Pressure-time Output

The computer model outputs the solution state at every time step for every cell. The presentation of the computer output begins with the pressure variation over time at the cells that correspond to the pressure sensor locations in the real experiment. These values will be the output values selected to be used in the statistical analysis.

Figure 3.4 shows the pressure at the locations of sensors 1 and 2 over time, as produced by the computer model using 4000 nodes. The output is limited to the region containing no reflected waves and $t = 0$ is set to be the moment the main expansion wave arrives at sensor 1. This convention is used in all of the following analysis.

Once the expansion waves start traveling at the start of the experiment, two aspects are worth noting when explaining the shape of the expansion fan that reaches the pressure sensors. One aspect is that the flow in the nozzle accelerates up to the point at which the flow at the throat is choked, when expansion waves no longer travel into the charge tube, after which the flow through the nozzle is stationary. Another aspect is that the valve motion, simulated by the widening cross section to the right of the nozzle, means the minimum throat area is not constant until the moving cross section clears the static nozzle throat.

Figure 3.5 shows the pressure throughout the domain during the simulation. A number of features are now noted and discussed. At the start of the simulation the minimum area of the

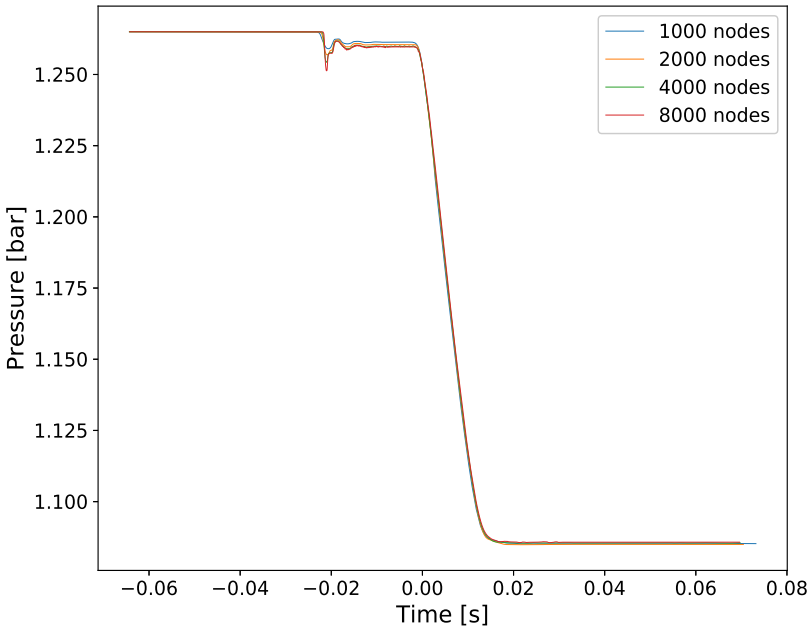

Figure 3.3: Output of pressure values from the computer model in the cell at location corresponding to pressure sensor P1 in the experiment, with 1000, 2000, 4000 and 8000 nodes.

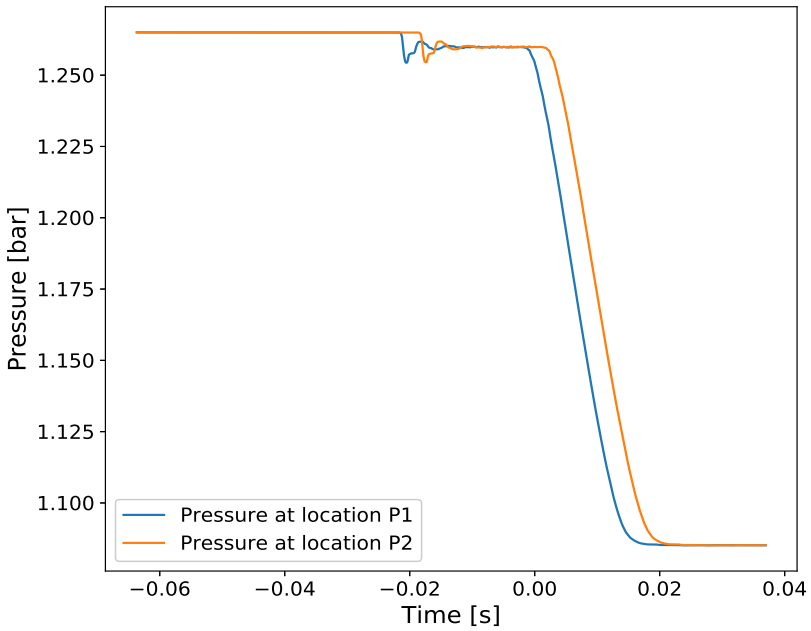

Figure 3.4: Output of pressure values from the computer model in the cells corresponding to locations of pressure sensors P1 and P2 in the experiment, with 4000 nodes.

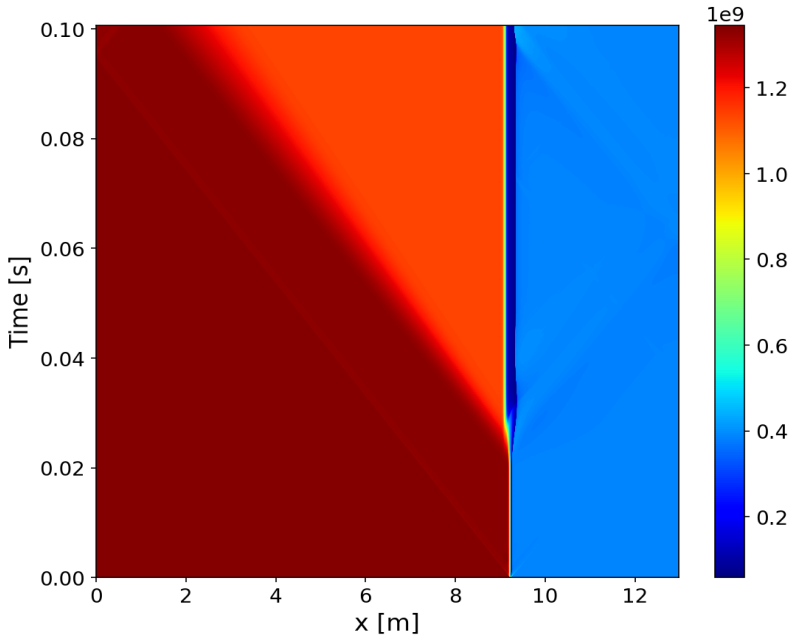

Figure 3.5: x-t diagram showing the pressure values during the experiment.

nozzle and valve is small (9 mm^2). As the waves emanate from the initial discontinuity at the minimum cross section, some interact with each other in the high radius gradient area around the nozzle and valve. Repeated reflections of the waves occur as the expansion interacts with the channel area change. As such, a pressure oscillation propagates into the charge tube at the start of the experiment. This is visible on the plot of the pressure over time at the sensor location in Figure 3.5, as an oscillation in the pressure at the foot of the very small expansion which arrives at P1 at -0.02 seconds. The oscillation itself is not visible on the x-t unless the nozzle area is viewed more closely.

Figure 3.6 shows a closer view of the nozzle area at the start of the simulation. When viewed more closely, it can be seen that the pressure after the expansion moves past is not constant. Furthermore, the pressure gradients around the nozzle are extreme.

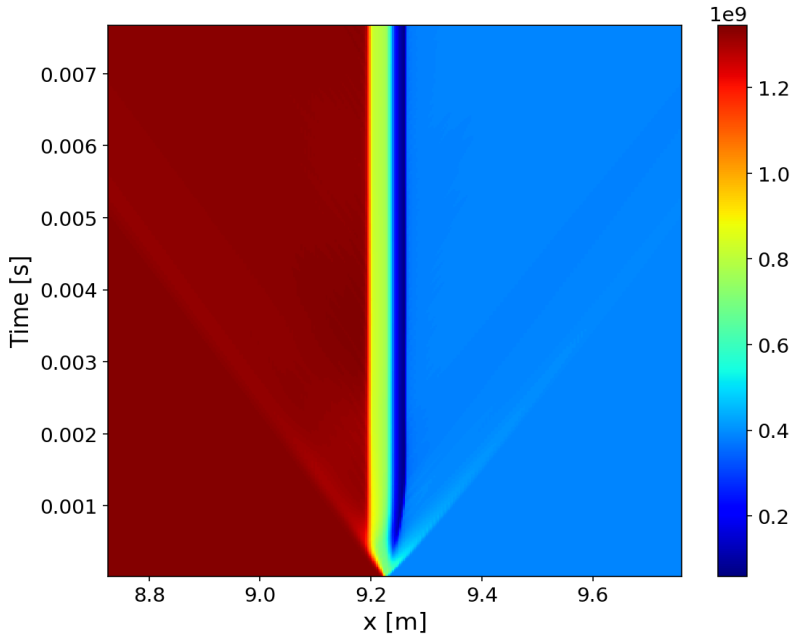

Figure 3.6: x-t diagram showing the pressure variation close to nozzle at the start of the experiment.

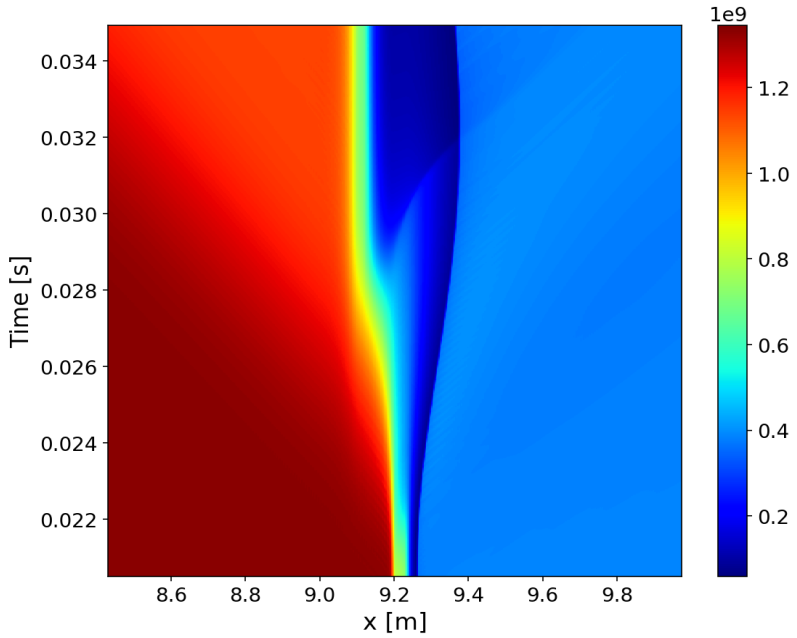

Figure 3.7: x-t diagram showing the pressure variation close to nozzle as the valve opens.

Chapter 4

Surrogate Model, Sensitivity Analysis and Statistical Model

The data used in the present investigation have been described and the computer model in use has been described and its output has been discussed. The current chapter introduces the surrogate model used, and describes the sensitivity analysis method. In addition, the statistical model which binds these two components together is presented and the Bayesian calibration approach is described.

4.1 Surrogate Model

Here the sparse grid approach is briefly overviewed, and then the application to the current project is described.

4.1.1 Sparse Grid

Given the number of parameters, a surrogate model would require a large number of dimensions, and as such, a large of sample points. The computer model is replaced with an approximation, which uses output sampled at various points. Use is made of the Sparse Grid and Sobol' Index Code (Dwight and Resmini (n.d.)). This code tackles the high dimensionality of the problem using a sparse grid approximation.

The basic approach is to construct an approximation of the computer model using a polynomial interpolation upon a sparse grid of points. A family of one-dimensional quadrature rules is chosen. Then, the Smolyak algorithm is used to construct a d-dimensional quadrature formula. This algorithm is a weighted sum of product rules, that comply with a restiction

placed on the total level of the rules in the sum (Barthelmann et al. (2000)). The total level $|\mathbf{i}|$ is the sum of the level in each dimension. The result is the quadrature formula (Barthelmann et al. (2000))

$$A(q,d) = \sum_{q-d+1 \leq |\mathbf{i}| \leq q} (-1)^{q-|\mathbf{i}|} \binom{d-1}{q-|\mathbf{i}|} \left(\mathcal{U}^{i_1} \otimes \ldots \otimes \mathcal{U}^{i_d}\right), \tag{4.1}$$

where q is the level of the complete sparse grid, d is the number of dimensions, and $\mathcal{U}^i$ is the one-dimensional quadrature formula. The one-dimensional quadrature rule used here is the Clenshaw-Curtis quadrature rule. This method consists of grid points being located at the extrema of the polynomials (Clenshaw and Curtis (1960)). The sparse grid is a so-called "classical" sparse grid, rather than a full tensor product grid. Each dimension is treated the same, regardless of the importance determined in the later sensitivity analysis.

4.1.2 Applying the Sparse Grid Approach to the Computer Model Output

An aspect of this application is that the output of the model is a series of pressure values in time. This pressure-time output is available at every point in the parameter space. As such, the output is not a single value for a given set of parameters, but rather a series of values for a given set of parameters. Two approaches are possible. Firstly, the time variable could be treated as a parameter from the point of view of the surrogate model. Thus, the scalar output would be a single pressure value for a given combination of specified parameters and also specified time point. The disadvantage of this approach is that the accuracy of the interpolation in the time dimension for a given set of parameters is poor, given that the function is only sampled at the locations in the time dimension specified by the sparse grid. Therefore, information about precise time of flight of the expansion is not well interpolated.

The second approach is to treat each point in time separately, with its own sparse grid model. In this approach, if there are 25 points selected in the time domain of the data, there would then be constructed 25 distinct sparse grids, to capture how the model output changes for each point in the time domain. There are two disadvantages to this. The first disadvantage is that the continuity in the time domain is not maintained. The second disadvantage is that, in this application the signal in the time domain is an expansion followed by constant pressure. The shape is therefore somewhat like a step. Next, consider that as the parameters change, the step in the computer model pressure output (among other changes) shifts forwards or backwards in time. Thus, a single point in the time domain with its own sparse grid that captures how that value of pressure changes with the parameters, will find itself either at the top of the step, the bottom of the step or somewhere in between, depending on the specific value of the parameters. As such, there is a step shape in the parameter space of that individual sparse grid interpolation. A polynomial interpolation may not capture such a shape well.

After considering these options, the second approach is chosen, given the need to provide a detailed interpolation in the time domain.

4.2 Sensitivity Analysis Method

As introduced by Sobol' (2001), Sobol' indices are global sensitivity indices that will be used to characterise the main effect on the computer model output of parameters and combinations of parameters. This effect is assessed at each time point, considering the entire parameter space at once. An overview of Sobol' indices is given.

4.2.1 Sobol' Indices

Sobol' indices are computed from an ANOVA-decomposition of the underlying function, according to Kucherenko et al. (2005), on which the following explanation is based. They concern a function of several variables defined on the unit hypercube in n dimensions. This is introduced as (Sobol' (2001))

$$f(x) = f_0 + \sum_{s=1}^{n} \sum_{i_1<\ldots<i_s} f_{i_1\ldots i_s}(x_{i_1}, \ldots, x_{i_s}) \tag{4.2}$$

where,

$$f_0 = \int f(x)dx, \tag{4.3}$$

and

$$\int_0^1 f_{i_1\ldots i_s} dx_{i_p} = 0, \quad \text{for} \quad 1 \leq p \leq s, \tag{4.4}$$

for which $1 \leq i_1 < i_2 < \ldots < i_s \leq n$, $1 \leq s \leq n$

The terms in the sum can be determined by applying the properties of ANOVA-decompositions. The variances from the function can be described as

$$D_{i_1\ldots i_s} = \int f^2_{i_1\ldots i_s} dx_{i_1} \ldots dx_{i_s}. \tag{4.5}$$

Further, the total variance is defined using the squared mean value and the integral of the square of the function,

$$D = \int f^2(x)dx - f_0^2. \tag{4.6}$$

From these variances, the global sensitivity indices of any combination of variables can be found as

$$S_{i_1 \ldots i_s} = \frac{D_{i_1 \ldots i_s}}{D} \tag{4.7}$$

which together sum to 1.

Finally, the total sensitivity index, S_y^{tot} for a given subset of variables, y, is defined as the sum of all sensitivity indices containing at least one index in the subset.

The sparse grid and Sobol' index code approximates the Sobol' main effect indices from the sparse grid and the associated quadrature rules as in Tang et al. (2010).

4.3 Model Incorporating Uncertainty on True Output Values

Kennedy and O'Hagan (2001) provided a sophisticated structure for incorporating many sources of uncertainty into a statistical model of measured output quantities. Kennedy and O'Hagan (2001) state that

$$y_i = \zeta(\mathbf{x}_i) + e_i = \rho\eta(\mathbf{x}_i, \boldsymbol{\theta}) + \delta(\mathbf{x}_i) + e_i. \tag{4.8}$$

The expression links the measured output quantity to an underlying true value plus some random measurement error, and further relates the true value to some uncertain model output. In this expression, y_i is the measured output quantity, ζ is the true value (which depends on some explanatory variables $\mathbf{x}_i$), and e_i is the normally distributed measurement error with zero mean. The true value is then made up of ρ, which is a constant multiplying term, $\eta(\mathbf{x}_i, \theta)$, which is the output of the computer model, and $\delta(\mathbf{x}_i)$ which is a term accounting for the inadequacy of the computer model to represent the true process.

The statistical model in the form shown in equation 4.8 is not used in this work as is. Several assumptions are made that differ from those made to arrive at equation 4.8. Firstly, the work of Kennedy and O'Hagan (2001) proceeds to construct a complex hierarchical model of the above terms, making use of Gaussian Process models for the model output and the model inadequacy terms. In this investigation, a surrogate model is used to replace the η, not a Gaussian Process model. In addition, the appropriateness, for this investigation, of the model inadequacy term is discussed.

4.3.1 Model Inadequacy Term

The above term $\delta(\mathbf{x}_i)$ is assumed to depend on the explanatory variables of the measurement, and not on the parameters, θ. The important issue to consider with this term, as is the case for the parameters θ themselves, is that of identifiability. The question is whether, upon including the term and calibrating the unknowns using data, it is actually possible to distinguish between 1) discrepancies between experiment and computer model because of uncertain model parameters, and 2) discrepancies because of model inadequacy.

With the issue of identifiability in mind, and considering the limited scope of the data used in the present calibration (many points in the time domain, but from only one experiment), it has been chosen to ignore the model inadequacy term. As such, the form of the statistical model, relating the computer model output and the experimental data is

$$y_i = \eta(x_i, t_i, \boldsymbol{\theta}) + e_i, \quad \text{for} \quad i = 1, .., 3N \tag{4.9}$$

where y_i is the measured pressure, x is the location of the pressure sensor, t is the time of the measured pressure, and N is the number of points of data used from each sensor (the choice having been made of $N = 25$). As mentioned earlier, e_i is the normally distributed measurement error,

$$e_i \sim \mathcal{N}(0, \lambda), \tag{4.10}$$

where λ is some unkown variance of the measurement error. The intention is to include this as an unknown parameter in the calibration procedure.

4.4 Bayesian Calibration Approach

The statistical model adopted earlier is very simple. Due to equation 4.9, and replacing the computer model output with the surrogate model output, $\eta_s(x_i, t_i, \boldsymbol{\theta})$,

$$e_i = y_i - \eta_s(x_i, t_i, \boldsymbol{\theta}) \sim \mathcal{N}(0, \lambda). \tag{4.11}$$

The data likelihood function can then be constructed as

$$p(\boldsymbol{y}|\boldsymbol{\theta}) \propto \prod_{i=1}^{3N} e^{\left[-\frac{1}{2}\frac{(y_i - \eta_s(x_i, t_i, \boldsymbol{\theta}))^2}{\lambda}\right]} \tag{4.12}$$

Applying Bayes' theorem yields a statement of the posterior probability (Gelman et al. (2014))

$$p\left(\boldsymbol{\theta}|\boldsymbol{y}\right) \propto p(\boldsymbol{\theta})p(\boldsymbol{y}|\boldsymbol{\theta}). \tag{4.13}$$

where $p(\boldsymbol{\theta})$ is the prior probability, which in this case is uniform on each parameter in $\boldsymbol{\theta}$.

4.4.1 Computational Method for Sampling from the Posterior Distribution

The objective is to construct a Markov chain on the parameters whose stationary distribution is the posterior probability distribution. This approximation of the posterior distribution will allow the estimation of quantities which result from integrals over the multidimensional posterior.

A Markov chain is a sequence of states (in this case, points in the parameter space), for which the transition from the current state to the subsequent state only depends on the current state. The Markov chain has a stationary distribution if the following properties are satisfied(Wakefield (2013)):

- Irreducibility (any state in the probability distribution can be reached in finite time, wherever the chain starts)
- Aperiodicity (no state is only visited at periodic increments of the chain).

4.4.2 Metropolis-Hastings Algorithm

The Metropolis-Hastings algorithm implemented in the PyMC3 software (Salvatier et al. (2016)) allows a chain to be constructed which approximates the posterior distribution. At a given state $\boldsymbol{x^{(n)}}$, the next state is chosen by sampling a proposed state from a proposal distribution. This is either added to the chain or not depending on whether a check is passed, which is based on the ratio of the posterior probability density at the current and at the proposed states. The specific steps are (Wakefield (2013)):

1. Generate a proposed new state $\boldsymbol{y}$ from the proposal distribution $q(\cdot|\boldsymbol{x^{(n)}})$. The PyMC3 software features a tuning phase for the first 500 states in the chain, in which the variance of the proposal distribution is modified to achieve the desired acceptance ratio (next step).
2. Compute the acceptance probability $\alpha(\boldsymbol{x^{(n)}}, \boldsymbol{y})$, which is

$$\alpha(\boldsymbol{x^{(n)}}, \boldsymbol{y}) = \min\left[\frac{\pi(\boldsymbol{y})}{\pi(\boldsymbol{x^{(n)}})} \times \frac{q(\boldsymbol{x^{(n)}}|\boldsymbol{y})}{q(\boldsymbol{y}|\boldsymbol{x^{(n)}})}, 1\right], \tag{4.14}$$

where $\pi(\cdot)$ is the posterior probability density evaluated at a given state.

3. Accept the proposed state as the new state $\boldsymbol{x}^{(n+1)}$ with probability $\alpha(\boldsymbol{x}^{(n)}, \boldsymbol{y})$. Otherwise, the previous state is maintained.

Once an approximation of the posterior distribution is obtained as a chain, quantities that rely on quadrature of the posterior probability can be computed by enumeration of the samples in the chain.

Chapter 5

Results

The sensitivity analysis and calibration approach described in the preceding chapters is applied to the computer model and data from Experiment 28 of Mathijssen et al. (2015). The results of the calibration procedure are presented and discussed in this chapter.

Firstly, the accuracy of the surrogate model is assessed. This will be followed by the sensitivity analysis of the surrogate model. Next the results of the Markov chain Monte Carlo simulation are presented, including an investigation of the convergence of the simulation. The resulting joint posterior distribution over the parameters, from the Markov chain Monte Carlo simulation is then discussed. Finally, the conclusions drawn from the presentation of the results are reviewed.

5.1 Surrogate Model Accuracy

The surrogate model (i.e. the sparse grid interpolation) will be used for two main tasks: assessing the sensitivity of the model output to the parameters, and for use in place of the model for the statistical analysis. The accuracy of the surrogate model is assessed before these tasks. Following the procedure of Merle and Cinnella (2015), 8 points are randomly selected from the parameter space, and then for these parameter inputs, both the actual model and the surrogate model are evaluated. The relative error at each location in the time domain is

$$\text{Relative error} = \left| \frac{\eta(\boldsymbol{\theta}) - \eta_s(\boldsymbol{\theta})}{\eta(\boldsymbol{\theta})} \right|, \tag{5.1}$$

where $\eta(\boldsymbol{\theta})$ is the computer model output and $\eta_s(\boldsymbol{\theta})$ is the surrogate model output. Two versions of the surrogate model are assessed. One version has a level 2 sparse grid (using 12

Table 5.1: Prior distributions for each of the model parameters

Parameter	Description	Prior distribution
θ_0	Critical temperature, T_c (K)	$U(581.22, 774.96)$
θ_1	Critical pressure, P_c (MPa)	$U(0.913, 1.153)$
θ_2	Molecular weight, MW (g/mol)	$U(355.936, 533.904)$
θ_3	$ln(\frac{c_v}{R})$	$U(2.303, 13.816)$
θ_4	Nozzle throat area, A_1 (mm^2)	$U(300, 350)$
θ_5	Opening duration, t_1 (ms)	$U(11, 20)$
λ	Measurement error s.d. (bar)	$U(0.0, 0.1)$

sample points) and one has a level 3 sparse grid (using 97 sample points) and one has a level 4 sparse grid (using 389 sample points). Table 5.1 restates the 7 parameters of the statistical model which will be used and the bounds of their respective uniform prior distributions.

Figure 5.1 shows the relative error for the eight randomly chosen parameter combinations at each location in the time domain, with (a) the sparse grid of level 2, (b) the sparse grid of level 3, and (c) the sparse grid of level 4.

The sparse grid of level 3 is selected for all of the subsequent analysis.

Again, following Merle and Cinnella (2015), a characterisation of the error introduced by the surrogate model is provided in Figure 5.2, which shows the actual model and surrogate model output for the set of parameters with the largest total relative error and the smallest total relative error.

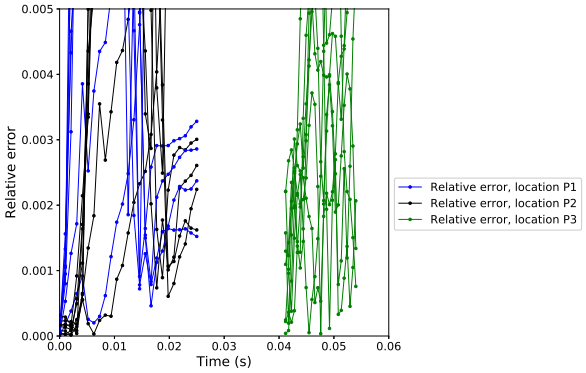

(a)

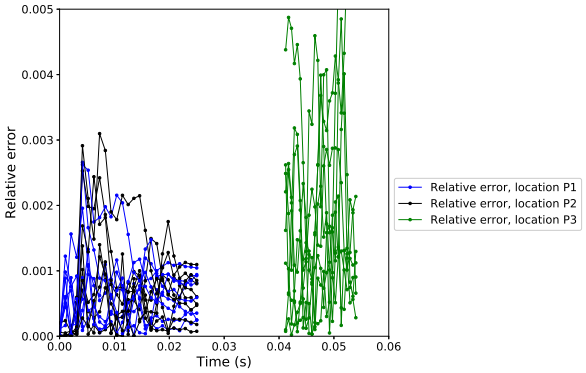

(b)

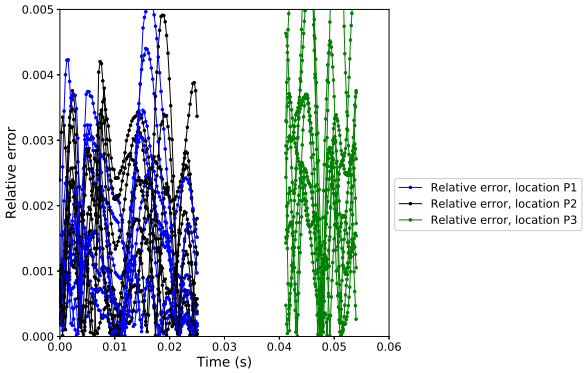

(c)

Figure 5.1: Relative error of the surrogate model compared to the actual model output at 8 random points with (a) level 2 sparse grid interpolation, (b) level 3 sparse grid interpolation, and (c) level 4 sparse grid interpolation.

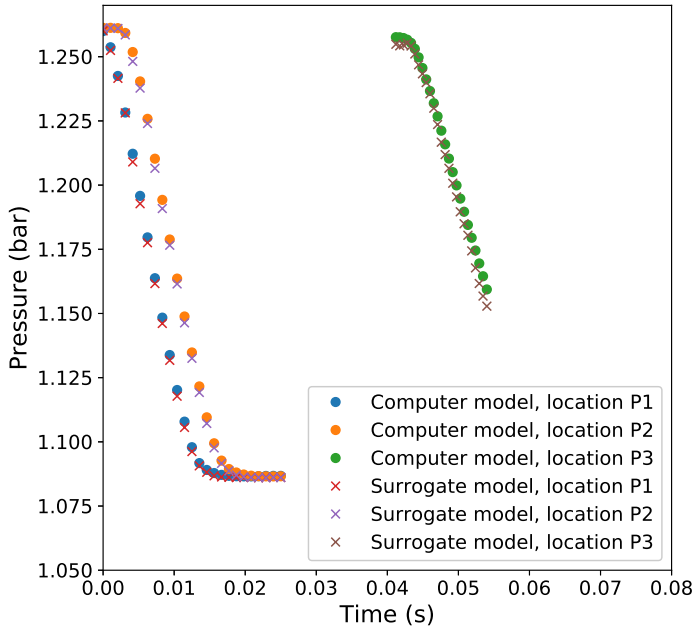

(a)

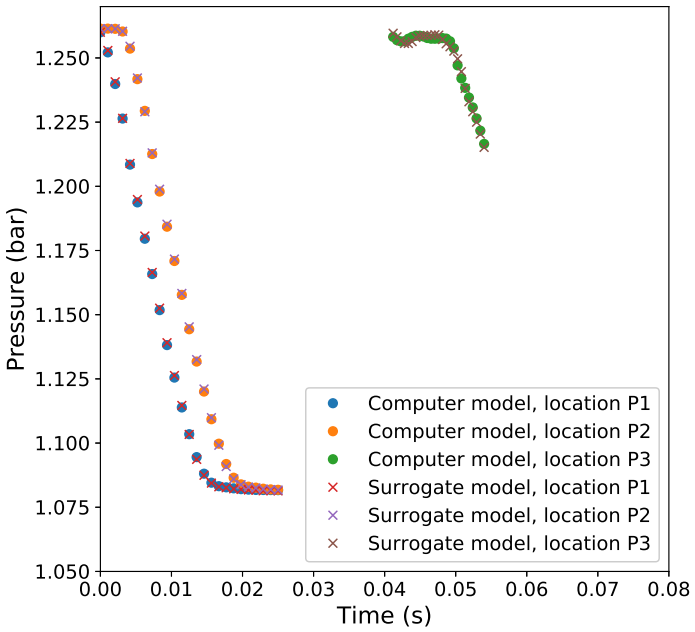

(b)

Figure 5.2: Surrogate model output and actual computer model output at points selected from the eight randomly chosen sets of parameters where (a) shows the parameter set with the highest relative error, and (b) shows the parameter set with the lowest relative error.

5.2 Sensitivity Analysis Results and Discussion

The described approach of constructing a surrogate model based on a sparse grid of points in the parameter space, followed by calculation of Sobol' indices, is applied to the one dimensional computer model.

A distinct sparse grid interpolation of the calculated pressure value is performed at each point in the time domain. This results in a value of the global sensitivity at each of the time points in question. Recalling the method described in Chapter 4, the sensitivity to the parameters of the pressure value at each point in time is found. Figure 5.3 shows the Sobol' variances calculated for each of the 25 points in the time domain for each of the two pressure sensors, respectively.

The delay before the arrival of the expansion in the second pressure sensor data is influenced by the thermodynamic properties via the wave speed. This timing information of the arrival of the expansion at the second sensor with respect to the arrival at the first sensor, means that the variances of the points at the start of the P2 expansion imply sensitivity to the thermodynamic parameters, with the opening time and nozzle diameter parameters being less important here. The expansion itself, in the case of sensor locations 1 and 2, is more strongly sensitive to the opening duration (S_5^{tot}) than the thermodynamic parameters. It can be observed that the variance in the later part of the pressure signal from sensors 1 and 2 is dominated by the area of the nozzle (S_4^{tot}), with some thermodynamic parameters also being relevant. This region of the data relates to the period when the expansion waves no longer propagate from the nozzle due to sonic conditions at the nozzle throat. Once the initial transient effects have ended, the signal is most affected by the factors of steady flow at the nozzle: the nozzle geometry and the thermodynamic model properties. The pressure output values from sensor 3 exhibit variation mostly due to the parameter corresponding to molecular weight, with the delay before arrival of the expansion also being influenced by the parameter $ln\left(\frac{c_v}{R}\right)$.

Erroneous negative or large positive values appear at points close to zero seconds because both the total variance and the total sensitivity is very small for those points in time (the pressure is still constant at pressure sensor P2 in the simulation). This means that numerically erroneous values are computed for the total sensitivity index. The value of the total variance at each time point is plotted in Figure 5.4 for all the sensor locations. This shows the very low variance at the start of the data. To further illustrate the sensitivity, Figure 5.5 shows the global variances, corresponding to the values of sensitivity index in the earlier Figure 5.3. It is worth noting at this point, that there appears to be no more than four points in the simulation (at location P2, at around 0.005 seconds) for which the thermodynamic parameters are close to the most important parameters of all. Even then, this only concerns one of the thermodynamic parameters: molecular weight (θ_2). At all other points non-thermodynamic parameters are much more important. The most important contributors to the variation at pressure sensor 3 are the thermodynamic parameters. This is explained by considering that the sensor is much further from the valve and therefore the travel time of the wave changes more as the parameters change. The Sobol' variances of the main effect and cardinality 2 are contained in the tables of Appendix A.

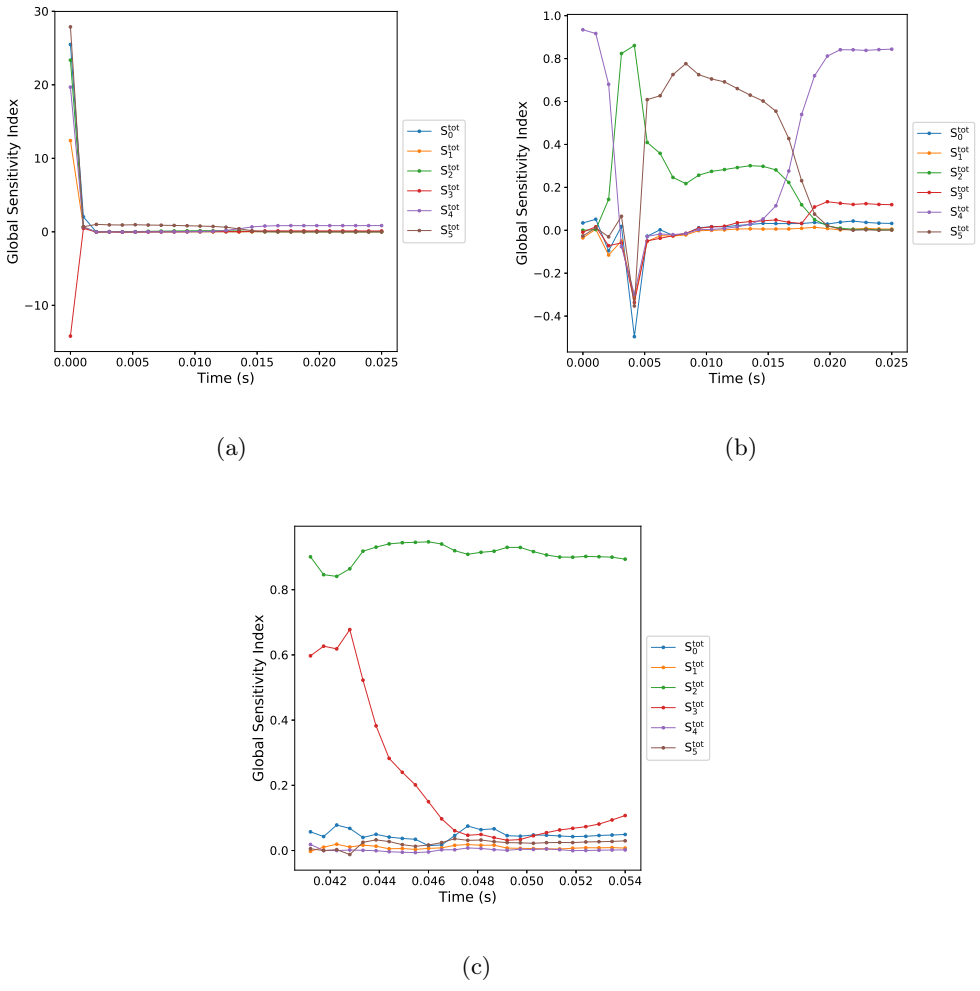

Figure 5.3: Total sensitivity indices calculated from the surrogate model at points in time from (a) simulation at pressure sensor 1, (b) simulation at pressure sensor 2, and (c) simulation at pressure sensor 3.

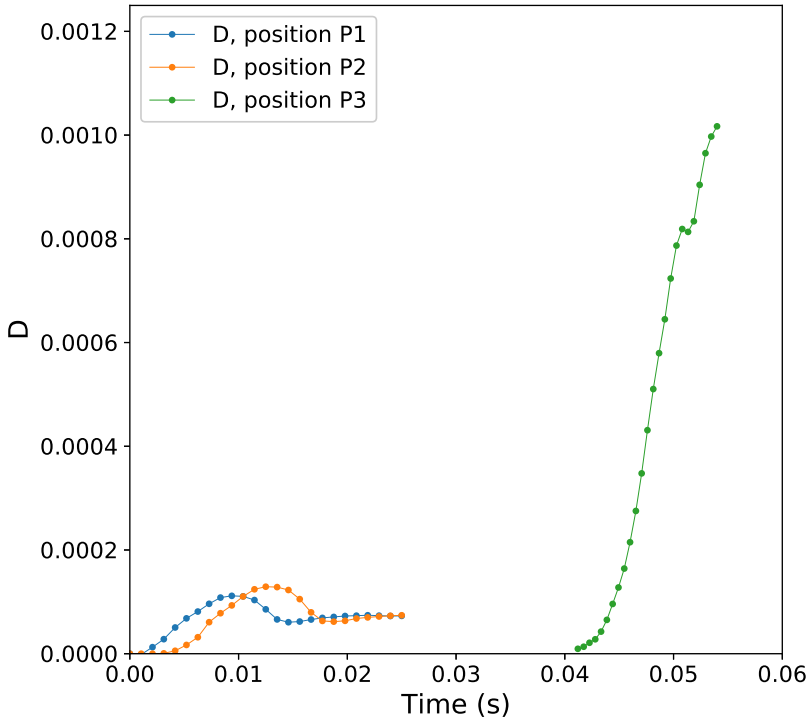

Figure 5.4: Total variance at each of the 25 time points, plotted for the two sensor locations.

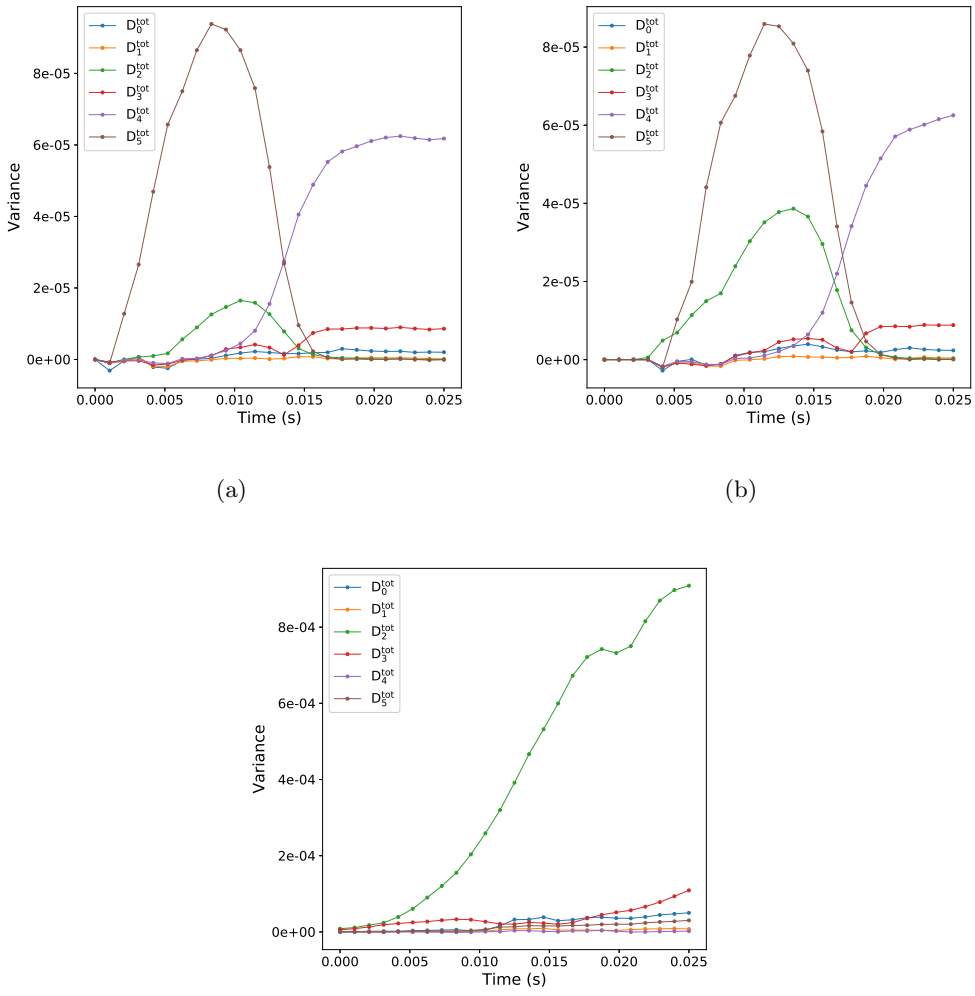

Figure 5.5: Global variances calculated from the surrogate model at points in time from (a) simulation at pressure sensor 1, (b) simulation at pressure sensor 2, and (c) simulation at pressure sensor 3.

5.3 Results of the Markov Chain Monte Carlo Simulation

The Markov chain Monte Carlo (MCMC) simulation produces an approximation to the joint posterior distribution over the parameters. The result is, specifically, the chain of samples from the parameter space. The posterior distribution for which an approximation is sought was defined in Chapter 4 to correspond to the stationary distribution of samples in the chain. The PyMC3 software of Salvatier et al. (2016) is used to sample from the posterior distribution. In this section, firstly the convergence of the chain is investigated. This is followed by the resulting approximation of the joint posterior from the MCMC simulation. After that, the results are discussed. In all of what follows, the distribution was sampled 60500 times, with the first 500 samples being immediately discarded. The remaining 60000 samples were used as the chain for the convergence investigation and as the approximation of the stationary distribution.

5.3.1 Convergence of the MCMC Simulation

The resulting chain of samples is checked for convergence. This check will use the approach of Geweke et al. (1991). The test works on each variable separately. Each chain is checked for convergence by calculating the z-score of the mean of an early part of the chain and the mean of a later part of the chain. Geweke et al. (1991) describe how the calculation of the z-score makes use of spectral density estimation. This approach allows the variance of slices of the chain to be approximated. The PyMC3 software used to produce the chains contains a function which implements this convergence check, and the expression it uses is

$$z = \frac{E[\theta_a] - E[\theta_b]}{\sqrt{V[\theta_a] + V[\theta_b]}}, \tag{5.2}$$

where θ_a refers to samples of the parameters early in the chain, and θ_b refers to samples later in the chain. The first 10% is considered to be the early part, and the final 50% is considered to be the later part. The function computes the z-score on slices of the chain that each start at positions later and later in the chain. The results of this convergence check for each of the six parameters is shown in Figure 5.6. For each parameter, the plot shows the result for the test on slices which start at iterations indicated on the horizontal axis. The plots cannot prove convergence, but for converged slices of the chains, the score should fall between 1 and -1 indicating that the computed scores distribution is standard normal, as described in Geweke et al. (1991). This check is passed for each of the parameters individually, and therefore this chain is used in the subsequent analysis. This check has been limited to a univariate check on the parameters.

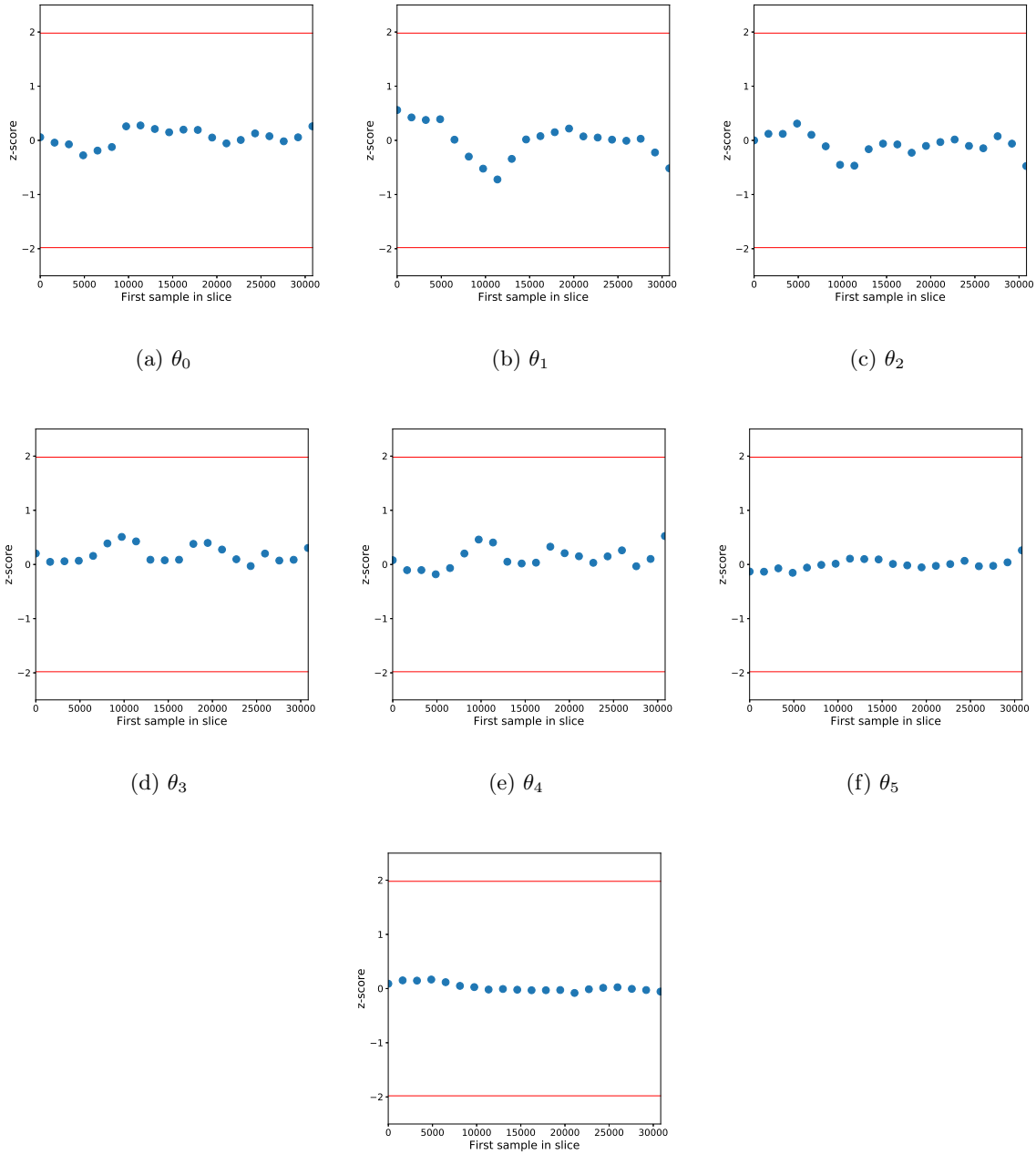

(a) θ_0 (b) θ_1 (c) θ_2

(d) θ_3 (e) θ_4 (f) θ_5

(g) λ

Figure 5.6: Geweke plots showing results on slices of the chains of each parameter and also the standard deviation of the normally distributed error term in the model.

Table 5.2: Mean values calculated from posterior distribution marginalised over all but the parameter mentioned, with the standard deviation and, where relevant, the true value.

Parameter	Mean	Standard deviation	True value
T_c (K)	656.78	19.097	645.8
P_c (MPa)	0.95355	0.023264	0.961
MW (g/mol)	472.68	5.8634	444.92
$ln(\frac{c_v}{R})$ (-)	5.4917	0.76006	-
A_1 (mm^2)	317.80	2.6311	460
t_1 (ms)	17.975	0.27204	-

5.3.2 Resulting Stationary Distribution

The results of the MCMC simulation are shown in the corner plot in Figure 5.7, plotted using the corner.py package of Foreman-Mackey (2016). There are seven parameters: six parameters from the computer model and the standard deviation, λ, of the measurement error in the statistical model. Each of the two-dimensional contour plots shows the projection of the 7-dimensional samples in the chain onto combinations of two of the variables, thereby indicating any potential correlation between parameters in the model.

The bounds for the one-dimensional histograms are the same as the uniform prior distributions, with the exception of the statistical model error standard deviation, λ, which is plotted with only part of the x axis shown, due to the very narrow posterior with respect to the prior. These histograms show the stationary distribution marginalised over all but one of the parameters. Table 5.2 shows the means and standard deviations of these distributions.

Comparing the posterior distributions to their respective priors, shows that the T_c, P_c and $ln(\frac{c_v}{R})$ (θ_0, $\theta_1$and θ_3) are not well informed by the data. Whilst the molecular weight appears more well identified, the mean is not located at the true value of 444.92 g/mol. The fact that the throat area, opening duration, and molecular weight parameters (θ_2, θ_4 and θ_5) are most narrowly specified is consistent with the observation from the sensitivity analysis that these two variables are most responsible for the total variance at most time points. The high importance in the computer model of θ_4 and θ_5, relative to the thermodynamic parameters, seems to limit the ability of the data to inform about the thermodynamic parameters.

There is some correlation observed between the molecular weight and the critical temperature in the thermodynamic model. In the sensitivity analysis, the portion of the model output which was found to be most sensitive to the molecular weight parameter was the time of the arrival of the main expansion at the second pressure sensor and the arrival and the expansion at the third sensor. Combined with the fact that this is also where the model was most sensitive to θ_3, this may imply that including the very small portion of the data from pressure sensor 3 that is not affected by reflected waves provides information about this parameter.

Comparison of all of the calibrated parameters to true values is complicated by several factors. While the critical temperature, critical pressure and molecular weight have a real meaning,

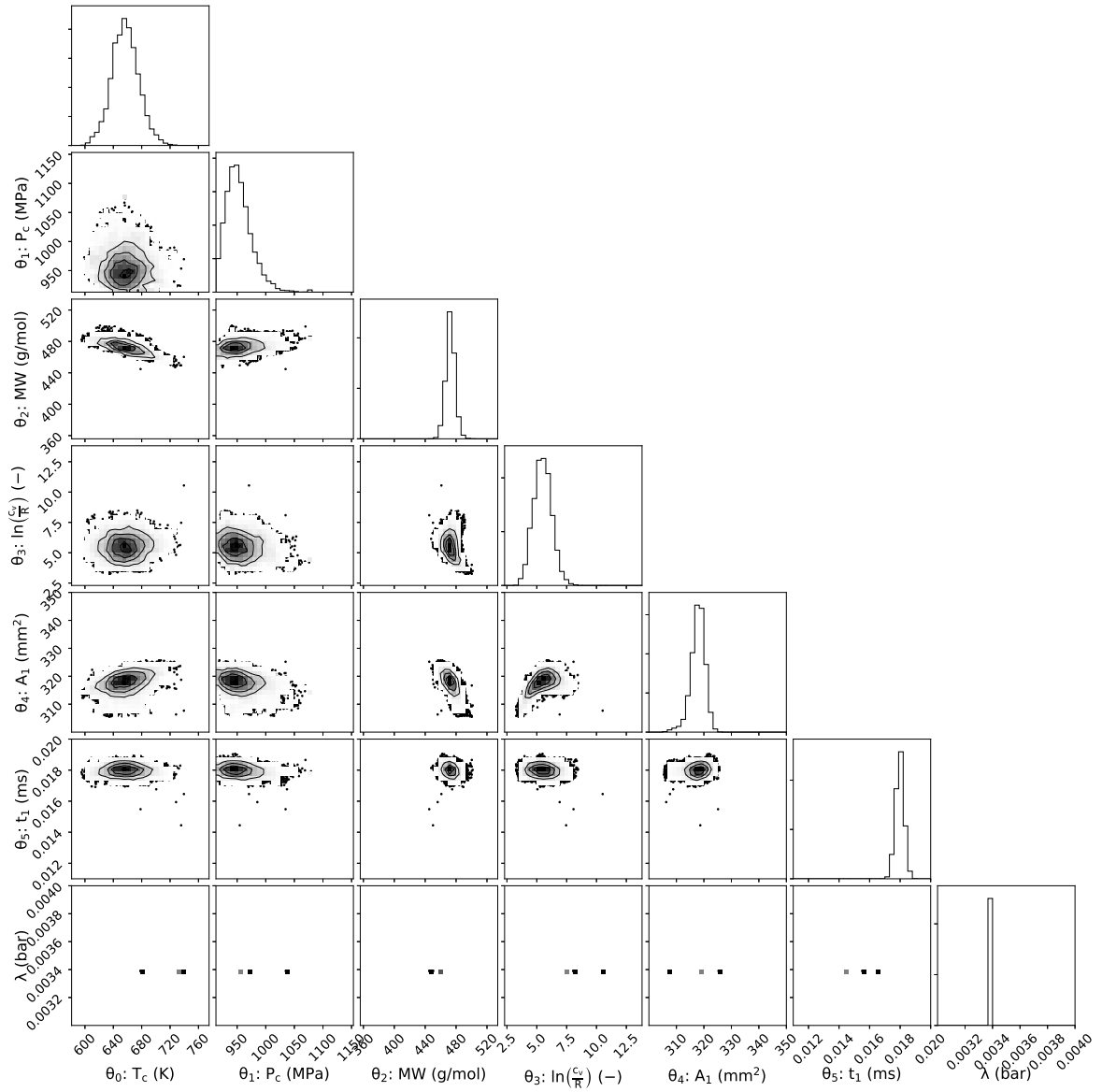

Figure 5.7: Approximation of the joint posterior distribution resulting from the MCMC simulation.

Table 5.3: Speed of sound before expansion using the computer model with van der Waals equation of state, and also using FluidProp.

Method	c at expansion start (m/s)
Computer model, van der Waals (nominal $\boldsymbol{\theta}$)	97.7
Computer model, van der Waals (calibrated $\boldsymbol{\theta}$)	94.5
Computer model, FluidProp (D6 fluid using iPRSV)	95.5
Mathijssen et al. (2015) Exp. 28 linear fit of wave speeds	96.9

the value of $\frac{c_v}{R}$ used within the polytropic van der Waals equation of state does not have an underlying true value for the dense gas in general. Furthermore, the true effective area of the throat or the true opening duration (or the reasonableness of the assumptions about the opening behaviour) are not available information by any means outside of the pressure data from each experiment. Only one set of experimental data is considered here. As mentioned earlier there is one part of the model output where one thermodynamic parameter (θ_2, the molecular weight) was expected to have an important influence, close to or more than the opening behaviour and throat area. This was the arrival time of the main expansion. The speed of sound calculated using the van der Waals model, with nominal parameters (before calibration) and with calibrated parameters, can be compared to an accurate calculation performed using the FluidProp software of Colonna and Van der Stelt (2004). Furthermore, the original analysis of the experimental data by Mathijssen et al. (2015) includes an estimation of the speed of sound in the fluid based on the experimental results. This is shown in Table 5.3.

The analysis and wave speed estimation by Mathijssen et al. (2015) was further employed by those authors to project the pressure signal of the expansion back to what its shape would theoretically have been at the nozzle exit. This allows the opening process duration to be estimated by those authors. However, before comparing that time estimation to the calibrated parameter of this work, it is worth noting that the estimate provided by Mathijssen et al. (2015) contains two parts combined:

- The unsteady process induced by the mechanical opening procedure.
- The unsteady process of the flow through the static nozzle becoming steady.

The computer model used in this work does feature idealised versions of both of these processes in the quasi-one-dimensional model with time-varying source term. However, because of the variable and unpredictable mechanical processes, the assumption made here that the valve smoothly opens without stopping and without a major change in opening speed (such as discontinuous change in opening speed or a slow starting speed that rapidly accelerates) is quite a significant one. For example, if the valve in reality opens very slowly at first and very rapidly later, then in order to capture the shape at the start of the expansion whilst assuming

Table 5.4: Calibrated opening duration parameter, compared to the start-up time computed by Mathijssen et al. (2015) from the data.

Source	Time (ms)
θ_5 (t_1) mean value	17.975
Start-up process calculated by Mathijssen et al. (2015) Exp. 28	7.5

a smooth valve opening, a much longer opening duration might be required in the simulation. In practice, however, there are other issues with these results which are more important, as can be understood when comparing the calibrated opening duration, and the value of process start-up time computed by Mathijssen et al. (2015), as shown in Table 5.4.

In Table 5.4, it is shown that the computed start-up process time is much lower than the calibrated opening duration. This means, specifically, that when projecting the pressure signal back to what it is estimated to be at the nozzle exit, Mathijssen et al. (2015) found that the signal became steady 10.475 ms faster than the time that the valve is in motion for the present calibration results. The fact that the known start-up time estimate is much lower than the calibrated opening duration parameter implies that, at the nozzle exit (i.e. before the expansion fan has spread in width as it travels along the charge tube) the experimental expansion width may be narrower than the computer model expansion width with calibrated parameter inputs. This has the further, unfortunate implication that the opening duration parameter seems to be 'correcting' the width of the expansion recorded in the simulation at P1 and P2; i.e. the expansion in the simulation exhibits insufficient spreading under any combination of thermodynamic parameters in the prior distribution, implying incorrectly simulated behaviour. The calibration then has the effect of ensuring the 'correct' expansion width by arriving at a longer opening process at the nozzle and valve than is estimated by Mathijssen et al. (2015) from the experimental data alone. This is an important weakness of this project's results, and will be returned to in the recommendations.

The "effective area" was estimated by Mathijssen et al. (2015) from the data. This value is found by looking at the constant pressure region after the expansion when the nozzle flow is steady and computing the nozzle area that would provide such a pressure value. The valve setting was $460mm^2$ and the effective area computed by Mathijssen et al. (2015) was $328mm^2$, which are somewhat comparable to the value found in this calibration. This is consistent with the fact that the effective area was calculated by Mathijssen et al. (2015) by assuming a quasi-one-dimensional isentropic flow from the state after the expansion, through the choked nozzle.

Using more than one set of experiment data would be expected to improve the identifiability of the parameters. Furthermore, a possible concern with the results relates to the use of only 25 points from the time domain of the data. It was mentioned in the sensitivity analysis that only a small region in time exhibits substantial variation due to the thermodynamic parameters, and as such it might be beneficial to ensure more points are located in these regions by including more points overall.

5.4 Conclusions

In conclusion, the computer model's replacement with a surrogate model was presented and assessed, with it being decided that a level 3 sparse grid was sufficient. The sensitivity analysis performed on the surrogate model revealed that the throat area and opening duration were by far the most important parameters, with the thermodynamic parameters of much less importance. The most important of the thermodynamic parameters is the molecular weight parameter. The samples drawn from the joint posterior distribution using the MCMC sampling technique are found to be consistent with convergence. The parameters most informed by the data were the molecular weight, opening duration, and throat area, although these do not reflect the expected true values based on the Experiment 28 definition.

Chapter 6

Conclusions and Recommendations

6.1 Conclusions

The objective of this project was to use Bayesian inference to attempt to reduce the uncertainty on thermodnyamic parameters of an equation of state for a dense gas, using shock tube data and a computer model. The van der Waals equation of state, which was used in the project, was introduced. The fundamental thermodynamic derivative was derived for the equation of state. The data used in the calibration was also introduced. The data was restricted to the region in time when the pressure signal was not affected by reflected waves from the ends of the shock tube. This restriction allowed the use of some of the data from the first 3 pressure sensors and none from sensor 4. Next, the quasi-one-dimensional computer code was introduced. This computer model solved the Euler equations using Roe's approximate Riemann solver. The changes thought necessary to allow the computer code to model the shock tube flow included changes to the governing equations, to allow for the time-varying valve geometry, changes to the boundary conditions, and changes to the solution procedure, including addition of the entropy fix. Example output from the code showed some of the issues arising, including the wave pattern resulting from the unsteady flow during the opening process. This was thought to be explained by the reflection and interaction of waves through the converging-diverging nozzle, the motion of the time-varying channel width and the evolution towards the steady nozzle flow state.

The methods of surrogate modeling and sensitivity analysis were described. The sparse grid approach available in an existing library was introduced and the manner in which this approach was applied to the problem was explained. Each point to be interpolated in time was given a separate interpolation grid in the parameter space. The global sensitivity analysis approach of Sobol' was then applied using the existing Sobol' index code. The construction of the statistical model in which the measured output pressure are related to the true values was described and justified.

The sparse grid interpolation was checked by picking several points in the parameter space and evaluating the computer code directly and also computing the interpolation using the sparse grid surrogate model. Different level sparse grids were used and compared for the error with respect to the direct evaluation of the code. The level 3 grid showed less relative error than the level 2 grid but the level 4 grid had greater relative error than the level 3 grid. The sensitivity analysis showed the importance of the non-thermodynamic parameters (nozzle area and opening duration) for much of the computer model output, but that at some time points the molecular weight parameter was important. The approximation of the posterior distribution on the parameters, from the Markov chain Monte Carlo simulation showed that the three parameters just mentioned were somewhat informed by the data, but that there was a sizable discrepancy between the mean values and the true values of the parameters.

6.2 Recommendations

A further investigation of the quasi-one-dimensional simulation may provide insight into the discrepancy between the computer model opening time and the experimentally determined opening time. Furthermore, a different modeling approach could be used. Consideration may be made of more spatial dimensions and whether the assumptions about how the expansion fan is formed are justified or whether a more complicated process is what yields the shape of the pressure drop. Investigation of the temperature distribution in the valve, the effect of condensing fluid and the rate of motion of the valve sliding cylinder may be warranted.

Adopting one of the more complex equations of state, such as iPRSV, would allow for a clearer answer to the question of whether these data inform the model in such a way as to make more precise predictions on thermodynamic states in the various applications.

An investigation might determine if a higher level sparse grid interpolation may reduce the relative error in the surrogate model. Furthermore, selecting more points in the time domain for the calibration, while computationally much more costly, would make better use of the available data.

Bibliography

P. D. Arendt, D. W. Apley, and W. Chen. Quantification of model uncertainty: Calibration, model discrepancy, and identifiability. *Journal of Mechanical Design*, 134(10):100908, 2012.

B. Argrow. Computational analysis of dense gas shock tube flow. *Shock Waves*, 6(4):241–248, 1996.

V. Barthelmann, E. Novak, and K. Ritter. High dimensional polynomial interpolation on sparse grids. *Advances in Computational Mathematics*, 12(4):273–288, 2000.

A. Bejan. *Advanced engineering thermodynamics*. John Wiley & Sons, 2016.

D. Boon, R. Dwight, J. Sterenborg, and H. Bijl. Reducing uncertainties in a wind-tunnel experiment using bayesian updating. In *53rd AIAA/ASME/ASCE/AHS/ASC Structures, Structural Dynamics and Materials Conference, Honolulu, Hawaii, 23-26 April 2012; AIAA 2012-1856*. American Institute of Aeronautics and Astronautics (AIAA), 2012.

P. Cinnella. Roe-type schemes for dense gas flow computations. *Computers & fluids*, 35(10): 1264–1281, 2006.

C. W. Clenshaw and A. R. Curtis. A method for numerical integration on an automatic computer. *Numerische Mathematik*, 2(1):197–205, Dec 1960. ISSN 0945-3245. doi: 10.1007/BF01386223. URL https://doi.org/10.1007/BF01386223.

P. Colonna and A. Guardone. Molecular interpretation of nonclassical gas dynamics of dense vapors under the van der waals model. *Physics of Fluids*, 18(5):056101, 2006.

P. Colonna and T. Van der Stelt. Fluidprop: a program for the estimation of thermo physical properties of fluids. *Energy Technology Section, Delft University of Technology, Delft, The Netherlands, http://www. FluidProp. com*, 2004.

P. Colonna, N. Nannan, A. Guardone, and E. W. Lemmon. Multiparameter equations of state for selected siloxanes. *Fluid Phase Equilibria*, 244(2):193–211, 2006.

P. Colonna, A. Guardone, and N. Nannan. Siloxanes: A new class of candidate bethe-zeldovich-thompson fluids. *Physics of Fluids*, 19(8):086102, 2007.

S. Conti and A. O'Hagan. Bayesian emulation of complex multi-output and dynamic computer models. *Journal of statistical planning and inference*, 140(3):640–651, 2010.

R. Dwight and A. Resmini. sparse grid and sobol' index code (python). https://aerodynamics.lr.tudelft.nl/~rdwight/work_sparse.html, n.d. Accessed: 2017-11-08.

B. Einfeldt, C.-D. Munz, P. L. Roe, and B. Sjögreen. On godunov-type methods near low densities. *Journal of computational physics*, 92(2):273–295, 1991.

S. Fergason, A. Guardone, and B. Argrow. Construction and validation of a dense gas shock tube. *Journal of thermophysics and heat transfer*, 17(3):326–333, 2003.

D. Foreman-Mackey. corner.py: Scatterplot matrices in python. *The Journal of Open Source Software*, 24, 2016. doi: 10.21105/joss.00024. URL http://dx.doi.org/10.5281/zenodo.45906.

T. Gallouet, J.-M. Hérard, and N. Seguin. Some recent finite volume schemes to compute euler equations using real gas eos. *International journal for numerical methods in fluids*, 39(12):1073–1138, 2002.

A. Gelman, J. B. Carlin, H. S. Stern, and D. B. Rubin. *Bayesian data analysis*, volume 2. Chapman & Hall/CRC Boca Raton, FL, USA, 2014.

T. Gerstner and M. Griebel. Dimension–adaptive tensor–product quadrature. *Computing*, 71 (1):65–87, 2003.

J. Geweke et al. *Evaluating the accuracy of sampling-based approaches to the calculation of posterior moments*, volume 196. Federal Reserve Bank of Minneapolis, Research Department Minneapolis, MN, USA, 1991.

J. Gottlieb and O. Igra. Interaction of rarefaction waves with area reductions in ducts. *Journal of Fluid Mechanics*, 137:285–305, 1983.

A. Harten and J. M. Hyman. Self adjusting grid methods for one-dimensional hyperbolic conservation laws. *Journal of computational Physics*, 50(2):235–269, 1983.

W. K. Hastings. Monte carlo sampling methods using markov chains and their applications. *Biometrika*, 57(1):97–109, 1970.

D. Higdon, J. Gattiker, B. Williams, and M. Rightley. Computer model calibration using high-dimensional output. *Journal of the American Statistical Association*, 2012.

M. E. Hubbard and P. Garcia-Navarro. Flux difference splitting and the balancing of source terms and flux gradients. *Journal of Computational Physics*, 165(1):89–125, 2000.

O. Igra, J. Gottlieb, and T. Saito. An analytical and numerical study of the interaction of rarefaction waves with area changes in ducts. part 2. area enlargements. Technical report, University of Toronto, 1984.

S. Karni and S. Čanić. Computations of slowly moving shocks. *Journal of Computational Physics*, 136(1):132–139, 1997.

M. C. Kennedy and A. O'Hagan. Bayesian calibration of computer models. *Journal of the Royal Statistical Society: Series B (Statistical Methodology)*, 63(3):425–464, 2001.

S. Kucherenko et al. Global sensitivity indices for nonlinear mathematical models. review. *Wilmott Mag*, 1:56–61, 2005.

C. B. Laney. *Computational gasdynamics*. Cambridge university press, 1998.

R. J. LeVeque. *Finite volume methods for hyperbolic problems*, volume 31. Cambridge university press, 2002.

R. J. LeVeque and H. C. Yee. A study of numerical methods for hyperbolic conservation laws with stiff source terms. *Journal of computational physics*, 86(1):187–210, 1990.

T. Mathijssen, M. Gallo, E. Casati, N. Nannan, C. Zamfirescu, A. Guardone, and P. Colonna. The flexible asymmetric shock tube (fast): a ludwieg tube facility for wave propagation measurements in high-temperature vapours of organic fluids. *Experiments in Fluids*, 56 (10):1–12, 2015.

J. McFarland, S. Mahadevan, V. Romero, and L. Swiler. Calibration and uncertainty analysis for computer simulations with multivariate output. *AIAA journal*, 46(5):1253–1265, 2008.

X. Merle and P. Cinnella. Bayesian quantification of thermodynamic uncertainties in dense gas flows. *Reliability Engineering & System Safety*, 134:305–323, 2015.

M. Pelanti, L. Quartapelle, and L. Vigevano. Low dissipation entropy fix for positivity preserving roes scheme. In *Godunov Methods*, pages 685–690. Springer, 2001.

A. Robinson, R. Berry, J. Carpenter, B. Debusschere, R. Drake, A. Mattsson, and W. Rider. Fundamental issues in the representation and propagation of uncertain equation of state information in shock hydrodynamics. *Computers & Fluids*, 83:187–193, 2013.

J. Salvatier, T. V. Wiecki, and C. Fonnesbeck. Probabilistic programming in python using pymc3. *PeerJ Computer Science*, 2:e55, 2016.

I. M. Sobol'. Global sensitivity indices for nonlinear mathematical models and their monte carlo estimates. *Mathematics and computers in simulation*, 55(1):271–280, 2001.

G. Tang, M. Eldred, and L. P. Swiler. Global sensitivity analysis for stochastic collocation expansion. *CSRI Summer Proceedings*, 2009:100, 2010.

P. A. Thompson. A fundamental derivative in gasdynamics. *The Physics of Fluids*, 14(9): 1843–1849, 1971.

E. F. Toro. *Riemann solvers and numerical methods for fluid dynamics: a practical introduction*. Springer Science & Business Media, 2013.

T. Van der Stelt, N. Nannan, and P. Colonna. The iprsv equation of state. *Fluid Phase Equilibria*, 330:24–35, 2012.

J. Wakefield. *Bayesian and frequentist regression methods*. Springer Science & Business Media, 2013.

C. Zamfirescu, A. Guardone, and P. Colonna. Numerical simulation of the fast dense gas experiment. In *Proceedings of the European conference on computational fluid dynamics, ECCOMAS CFD*, volume 2006, 2006.

Appendix A

Sobol Indices for the Computer Model Output Points

Table A.1: Sobol variances for main effect and cardinality 2, for point 1.

Property	Value for Level 2 (13 points)			Value for Level 3 (85 points)			Value for Level 4 (389 points)		
Location	P1	P2	P3	P1	P2	P3	P1	P2	P3
Mean	1.253	1.261	1.257	1.253	1.261	1.261	1.253	1.262	1.253
Variance	1.902e-08	2.479e-08	6.216e-06	1.444e-08	-1.382e-07	-0.0001644	-7.617e-09	-5.256e-07	0.0001385
D_0	1.459e-10	1.08e-08	1.424e-08	2.238e-08	3.104e-09	2.033e-06	2.132e-08	1.664e-07	1.413e-06
$D_{0,1}$	9.825e-10	1.109e-09	-7.835e-09	1.475e-08	8.056e-09	1.924e-06	7.592e-10	-2.669e-08	7.906e-07
$D_{0,2}$	-7.462e-11	4.961e-09	1.522e-07	1.614e-08	1.397e-08	-2.112e-05	8.548e-09	-1.861e-08	1.837e-07
$D_{0,3}$	-2.535e-10	-8.199e-10	-2.996e-08	1.197e-08	2.753e-09	1.405e-06	2.185e-08	-2.552e-08	8.81e-07
$D_{0,4}$	-1.808e-10	-1.385e-09	-1.014e-08	6.54e-09	8.256e-09	2.416e-06	4.066e-08	-6.529e-08	-8.76e-08
$D_{0,5}$	-1.809e-10	-2.22e-16	-1.904e-08	1.112e-08	1.191e-08	1.628e-06	2.793e-09	4.224e-09	8.165e-08
D_1	7.313e-09	3.599e-10	2.232e-08	1.852e-08	6.172e-09	1.861e-06	1.069e-08	1.871e-07	1.344e-06
$D_{1,2}$	5.03e-10	-6.439e-10	1.245e-07	1.681e-08	2.036e-08	-2.079e-05	4.064e-09	1.92e-08	2.471e-06
$D_{1,3}$	1.709e-09	1.064e-10	-2.45e-08	6.964e-09	5.117e-09	1.706e-06	2.781e-08	-2.772e-08	4.139e-07
$D_{1,4}$	1.219e-09	1.798e-10	-8.29e-09	7.699e-09	1.095e-08	2.864e-06	3.683e-08	-6.223e-08	9.776e-07
$D_{1,5}$	1.219e-09	0	-1.557e-08	1.994e-08	1.668e-08	1.718e-06	9.64e-09	-6.188e-08	6.393e-07
D_2	4.941e-10	8.214e-09	4.982e-06	1.159e-08	5.854e-09	7.453e-05	1.326e-08	3.254e-08	0.0001714
$D_{2,3}$	-1.298e-10	4.761e-10	4.76e-07	1.288e-08	-1.336e-09	-1.046e-05	4.461e-08	5.744e-09	-8.471e-06
$D_{2,4}$	-9.257e-11	8.041e-10	1.611e-07	1.276e-08	4.364e-09	-4.293e-06	6.471e-08	-2.154e-08	3.658e-06
$D_{2,5}$	-9.26e-11	0	3.025e-07	1.884e-08	2.377e-08	-2.547e-05	1.287e-08	1.083e-08	-9.779e-07
D_3	3.499e-09	2.007e-10	1.006e-07	1.025e-08	4.369e-08	1.37e-06	2.621e-09	3.32e-08	4.339e-07
$D_{3,4}$	-3.145e-10	-1.329e-10	-3.17e-08	6.46e-09	-2.138e-08	1.293e-06	-3.543e-08	-6.581e-08	6.726e-07
$D_{3,5}$	-3.146e-10	0	-5.954e-08	1.489e-08	7.431e-10	1.281e-06	1.091e-08	-1.829e-08	-1.273e-06
D_4	1.286e-09	3.465e-10	1.143e-08	3.761e-09	1.757e-08	1.563e-06	1.676e-08	9.959e-08	5.284e-07
$D_{4,5}$	-2.244e-10	0	-2.015e-08	8.916e-09	9.739e-09	2.336e-06	2.104e-08	-4.325e-08	6.885e-07
D_5	2.504e-09	2.134e-10	9.511e-08	2.202e-09	7.198e-09	2.739e-06	2.375e-08	4.174e-08	2.804e-06

Table A.2: Sobol variances for main effect and cardinality 2, for point 2.

Property	Value for Level 2 (13 points)			Value for Level 3 (85 points)			Value for Level 4 (389 points)		
Location	P1	P2	P3	P1	P2	P3	P1	P2	P3
Mean	1.24	1.261	1.256	1.241	1.261	1.261	1.24	1.262	1.252
Variance	7.253e-06	2.425e-08	2.015e-05	-1.493e-05	-1.891e-07	-0.0002218	-7.546e-07	-4.928e-07	0.0002085
D_0	1.427e-08	7.761e-09	1.355e-08	1.276e-05	3.924e-09	3.011e-06	1.413e-05	1.077e-07	7.897e-07
$D_{0,1}$	7.252e-08	-1.55e-09	-2.258e-09	2.294e-05	2.697e-08	2.497e-07	9.028e-06	-2.51e-08	8.007e-07
$D_{0,2}$	-7.634e-09	3.812e-09	-3.174e-07	9.406e-06	2.276e-08	-3.437e-05	1.946e-05	-9.016e-09	3.811e-06
$D_{0,3}$	-7.011e-08	1.063e-09	1.891e-08	1.797e-05	1.357e-08	3.438e-07	5.766e-06	-4.069e-08	1.183e-06
$D_{0,4}$	8.673e-10	7.931e-10	2.193e-09	2.424e-05	2.379e-08	1.237e-06	4.499e-06	-6.213e-08	-1.708e-07
$D_{0,5}$	-2.436e-08	7.274e-10	3.124e-08	1.287e-05	2.551e-08	-2.117e-07	1.015e-05	-2.019e-08	6.878e-07
D_1	1.729e-06	7.106e-10	4.369e-10	6.199e-06	2.239e-08	1.747e-06	1.941e-05	1.651e-07	2.09e-06
$D_{1,2}$	5.855e-08	1.588e-09	-5.903e-08	1.838e-05	4.387e-08	-3.029e-05	1.176e-05	-2.807e-08	3.553e-06
$D_{1,3}$	5.377e-07	4.43e-10	3.516e-09	2.099e-05	1.121e-08	8.825e-07	1.03e-05	-3.824e-08	1.348e-07
$D_{1,4}$	-6.652e-09	3.304e-10	4.078e-10	3.147e-05	1.757e-08	1.896e-06	1.956e-05	-6.962e-08	4.733e-07
$D_{1,5}$	1.869e-07	3.031e-10	5.809e-09	1.682e-05	4.065e-08	1.567e-06	1.118e-05	-6.754e-08	1.253e-06
D_2	6.164e-07	1.053e-08	1.891e-05	2.68e-06	3.556e-09	7.654e-05	1.292e-05	1.318e-07	0.0002326
$D_{2,3}$	-5.66e-08	-1.09e-09	4.942e-07	8.918e-06	1.083e-08	-1.614e-05	8.182e-06	-2.018e-08	-9.785e-06
$D_{2,4}$	7.003e-10	-8.128e-10	5.733e-08	1.348e-05	1.966e-08	-1.02e-05	1.529e-05	-2.195e-08	9.094e-07
$D_{2,5}$	-1.967e-08	-7.455e-10	8.165e-07	5.083e-06	3.449e-08	-3.524e-05	5.935e-06	-2.46e-08	1.666e-06
D_3	4.172e-06	5.172e-10	4.348e-08	4.786e-06	3.271e-08	1.141e-06	1.074e-05	3.885e-08	3.837e-07
$D_{3,4}$	6.43e-09	-2.267e-10	-3.415e-09	2.276e-05	-1.692e-08	7.274e-07	1.185e-05	-6.372e-08	8.108e-08
$D_{3,5}$	-1.806e-07	-2.079e-10	-4.863e-08	1.52e-05	1.123e-08	7.459e-07	6.894e-06	-3.698e-08	-1.112e-06
D_4	2.4e-09	2.587e-10	3.962e-10	3.459e-06	2.048e-08	1.603e-06	2.557e-05	7.616e-08	1.138e-06
$D_{4,5}$	2.235e-09	-1.551e-10	-5.642e-09	1.561e-05	2.552e-08	1.844e-06	1.128e-05	-3.172e-08	2.546e-07
D_5	2.197e-07	1.998e-10	1.886e-07	2.751e-05	3.239e-08	2.49e-06	5.955e-06	4.133e-08	2.194e-06

Table A.3: Sobol variances for main effect and cardinality 2, for point 3.

Property	Value for Level 2 (13 points)			Value for Level 3 (85 points)			Value for Level 4 (389 points)		
Location	P1	P2	P3	P1	P2	P3	P1	P2	P3
Mean	1.226	1.26	1.255	1.227	1.259	1.26	1.226	1.26	1.25
Variance	2.377e-05	3.638e-07	3.794e-05	-2.995e-05	-2.25e-08	-0.0002744	-5.565e-06	1.536e-06	0.0002789
D_0	1.783e-07	5.757e-08	5.048e-08	3.658e-05	6.958e-07	2.548e-06	5.169e-05	3.847e-07	7.038e-07
$D_{0,1}$	2.639e-07	5.481e-08	-5.318e-08	6.366e-05	5.271e-08	2.66e-08	1.987e-05	8.638e-07	5.288e-07
$D_{0,2}$	-4.66e-08	-2.046e-08	-7.757e-07	2.592e-05	-9.018e-08	-4.268e-05	5.492e-05	8.238e-07	6.353e-06
$D_{0,3}$	-3.432e-07	-4.802e-08	1.972e-08	4.909e-05	5.917e-08	2.774e-08	1.58e-05	3.211e-07	1.108e-06
$D_{0,4}$	-1.098e-08	-4.823e-08	-8.668e-09	6.703e-05	9.065e-08	5.189e-07	-2.453e-06	9.777e-07	-1.422e-07
$D_{0,5}$	-1.126e-07	-3.879e-08	5.75e-08	3.241e-05	1.761e-08	2.312e-07	2.878e-05	5.682e-07	1.316e-06
D_1	5.367e-06	6.664e-08	1.874e-07	1.81e-05	1.209e-06	1.711e-06	6.529e-05	6.695e-07	2.641e-06
$D_{1,2}$	1.975e-07	2.166e-08	-1.054e-06	5.049e-05	6.509e-08	-3.467e-05	3.15e-05	5.864e-07	5.776e-06
$D_{1,3}$	1.454e-06	5.085e-08	2.679e-08	5.448e-05	-7.645e-08	7.899e-07	2.645e-05	4.236e-07	-9.849e-08
$D_{1,4}$	4.653e-08	5.107e-08	-1.177e-08	8.633e-05	4.894e-08	1.525e-06	5.489e-05	1.174e-06	8.72e-07
$D_{1,5}$	4.771e-07	4.107e-08	7.81e-08	4.259e-05	1.232e-07	2.662e-06	2.963e-05	8.24e-07	1.037e-06
D_2	3.966e-06	1.931e-07	3.787e-05	6.3e-06	4.436e-08	6.662e-05	3.851e-05	3.65e-06	0.0002999
$D_{2,3}$	-2.568e-07	-1.898e-08	3.907e-07	2.504e-05	3.083e-08	-2.007e-05	1.965e-05	2.138e-07	-7.004e-06
$D_{2,4}$	-8.216e-09	-1.906e-08	-1.717e-07	3.663e-05	5.522e-08	-1.407e-05	4.61e-05	3.435e-07	4.365e-07
$D_{2,5}$	-8.425e-08	-1.533e-08	1.139e-06	9.402e-06	-1.212e-07	-3.912e-05	1.599e-05	6.429e-07	1.37e-05
D_3	1.258e-05	7.04e-08	3.915e-08	1.25e-05	4.895e-08	1.148e-06	3.796e-05	4.538e-07	3.416e-07
$D_{3,4}$	-6.051e-08	-4.474e-08	4.366e-09	6.49e-05	3.578e-09	3.985e-07	3.164e-05	3.676e-07	-1.009e-07
$D_{3,5}$	-6.205e-07	-3.598e-08	-2.896e-08	4.025e-05	-6.398e-10	8.583e-07	2.085e-05	1.425e-07	-3.379e-07
D_4	3.348e-08	4.546e-08	2.489e-09	1.066e-05	5.73e-08	1.797e-06	7.641e-05	1.278e-06	1.496e-06
$D_{4,5}$	-1.985e-08	-3.614e-08	1.273e-08	3.984e-05	6.164e-08	1.594e-06	2.961e-05	4.619e-07	5.592e-07
D_5	7.783e-07	3.69e-08	1.641e-07	7.316e-05	1e-06	1.721e-06	1.607e-05	2.26e-07	1.54e-06

Table A.4: Sobol variances for main effect and cardinality 2, for point 4.

Property	Value for Level 2 (13 points)			Value for Level 3 (85 points)			Value for Level 4 (389 points)		
Location	P1	P2	P3	P1	P2	P3	P1	P2	P3
Mean	1.207	1.253	1.253	1.212	1.253	1.258	1.205	1.251	1.248
Variance	4.974e-05	3.453e-06	6.069e-05	-8.935e-05	1.309e-06	-0.0003124	-3.241e-05	1.309e-05	0.0003508
D_0	6.806e-07	3.792e-07	1.105e-07	8.554e-05	7.743e-07	2.04e-06	8.555e-05	4.978e-07	1.138e-06
$D_{0,1}$	1.215e-06	3.166e-08	-2.396e-07	0.0001095	4.976e-07	9.11e-07	6.762e-05	1.865e-07	7.12e-07
$D_{0,2}$	-4.945e-07	4.863e-08	-1.503e-06	3.67e-05	4.664e-08	-4.563e-05	0.0001148	8.951e-07	4.365e-06
$D_{0,3}$	-1.104e-06	-3.169e-07	-1.982e-08	8.079e-05	1.591e-07	-1.804e-07	4.022e-05	3.963e-07	8.792e-07
$D_{0,4}$	-1.487e-07	-3.34e-07	-3.297e-08	0.0001158	3.083e-07	7.153e-08	2.911e-05	5.081e-07	5.814e-07
$D_{0,5}$	-3.973e-07	-2.79e-07	4.149e-08	6.805e-05	2.467e-07	1.542e-06	6.534e-05	1.734e-06	4.242e-06
D_1	1.246e-05	2.69e-07	1.655e-06	4.557e-05	3.033e-07	2.642e-06	0.0001087	5.278e-07	1.843e-06
$D_{1,2}$	1.797e-06	-4.211e-09	-3.799e-06	8.548e-05	7.835e-07	-3.39e-05	6.225e-05	1.232e-06	9.018e-06
$D_{1,3}$	4.011e-06	2.744e-08	-5.01e-08	0.0001001	3.827e-07	1.316e-06	6.521e-05	1.193e-07	4.439e-07
$D_{1,4}$	5.405e-07	2.892e-08	-8.334e-08	0.0001634	-2.288e-08	1.553e-06	0.0001193	4.474e-07	2.582e-06
$D_{1,5}$	1.444e-06	2.416e-08	1.049e-07	8.977e-05	9.321e-08	3.341e-06	6.604e-05	1.176e-06	1.038e-06
D_2	8.14e-06	3.427e-06	6.461e-05	9.602e-06	1.503e-06	5.012e-05	9.486e-05	1.739e-05	0.0003748
$D_{2,3}$	-1.633e-06	4.215e-08	-3.143e-07	3.925e-05	8.32e-08	-2.275e-05	4.095e-05	-1.398e-08	-3.088e-06
$D_{2,4}$	-2.201e-07	4.443e-08	-5.229e-07	6.536e-05	6.346e-07	-1.623e-05	9.933e-05	-1.225e-08	-4.137e-06
$D_{2,5}$	-5.879e-07	3.711e-08	6.58e-07	2.249e-05	3.245e-07	-3.941e-05	2.801e-05	5.112e-07	2.706e-05
D_3	2.362e-05	2.808e-07	2.143e-08	2.729e-05	1.455e-07	1.584e-06	6.068e-05	7.279e-07	7.331e-07
$D_{3,4}$	-4.912e-07	-2.895e-07	-6.894e-09	0.0001112	4.333e-07	7.998e-08	8.054e-05	1.536e-07	-1.307e-07
$D_{3,5}$	-1.312e-06	-2.418e-07	8.676e-09	8.197e-05	1.028e-07	1.042e-06	3.71e-05	-1.576e-07	1.855e-06
D_4	7.74e-08	3.057e-07	1.396e-08	1.839e-05	8.19e-08	2.698e-06	0.0001779	8.908e-07	1.747e-06
$D_{4,5}$	-1.768e-07	-2.549e-07	1.443e-08	8.587e-05	5.648e-08	1.206e-06	7.263e-05	8.053e-07	2.675e-06
D_5	2.317e-06	2.274e-07	2.273e-08	0.0001661	6.101e-07	1.593e-06	3.819e-05	4.439e-07	2.706e-06

Table A.5: Sobol variances for main effect and cardinality 2, for point 5.

Property	Value for Level 2 (13 points)			Value for Level 3 (85 points)			Value for Level 4 (389 points)		
Location	P1	P2	P3	P1	P2	P3	P1	P2	P3
Mean	1.193	1.241	1.252	1.196	1.241	1.255	1.189	1.238	1.245
Variance	6.931e-05	1.492e-05	9.239e-05	-0.0001236	-2.728e-05	-0.0003457	-1.616e-05	1.821e-05	0.0004328
D_0	3.746e-07	1.821e-07	1.127e-07	0.0001034	8.38e-06	1.349e-06	0.0001082	1.661e-05	5.563e-06
$D_{0,1}$	-2.912e-07	-1.842e-07	-4.407e-07	0.0001545	2.432e-05	1.986e-06	8.841e-05	5.247e-06	3.507e-06
$D_{0,2}$	1.722e-08	6.209e-08	-1.684e-06	4.706e-05	9.604e-06	-4.608e-05	0.0001765	1.789e-05	-5.302e-06
$D_{0,3}$	1.681e-07	1.024e-07	-4.647e-08	0.0001122	1.757e-05	9.063e-08	4.09e-05	3.996e-06	1.554e-06
$D_{0,4}$	-3.757e-08	-1.116e-07	-2.184e-08	0.0001572	2.381e-05	2.877e-07	9.243e-06	-7.741e-07	2.034e-06
$D_{0,5}$	5.95e-08	-1.501e-08	-2.274e-08	8.421e-05	1.375e-05	3.248e-06	9.407e-05	1.656e-05	1.368e-05
D_1	1.981e-05	3.376e-06	6.268e-06	5.798e-05	4.43e-06	6.565e-06	0.0001308	1.738e-05	2.267e-06
$D_{1,2}$	3.907e-07	1.236e-07	-9.579e-06	0.0001115	1.984e-05	-3.509e-05	7.068e-05	9.807e-06	9.062e-06
$D_{1,3}$	3.813e-06	2.038e-07	-2.644e-07	0.0001409	2.177e-05	2.406e-06	7.624e-05	7.669e-06	3.985e-06
$D_{1,4}$	-8.522e-07	-2.221e-07	-1.242e-07	0.0002157	2.948e-05	1.256e-06	0.0001384	1.14e-05	8.093e-06
$D_{1,5}$	1.35e-06	-2.988e-08	-1.294e-07	0.0001102	1.4e-05	2.613e-06	7.904e-05	8.218e-06	2.423e-06
D_2	1.283e-05	7.493e-06	0.0001003	1.574e-05	2.942e-06	3.782e-05	0.0001466	2.905e-05	0.0004991
$D_{2,3}$	-2.255e-07	-6.868e-08	-1.01e-06	5.082e-05	7.273e-06	-2.404e-05	5.917e-05	5.898e-06	-1.067e-06
$D_{2,4}$	5.04e-08	7.486e-08	-4.747e-07	8.431e-05	1.609e-05	-1.617e-05	0.000143	1.879e-05	-2.256e-05
$D_{2,5}$	-7.983e-08	1.007e-08	-4.944e-07	2.845e-05	8.758e-06	-4.012e-05	3.57e-05	-1.695e-06	3.018e-05
D_3	3.028e-05	3.543e-06	3.265e-08	3.134e-05	4.417e-06	2.095e-06	9.454e-05	9.986e-06	2.665e-06
$D_{3,4}$	4.919e-07	1.235e-07	-1.31e-08	0.0001511	2.405e-05	2.499e-07	9.734e-05	1.072e-05	1.049e-06
$D_{3,5}$	-7.79e-07	1.661e-08	-1.364e-08	9.774e-05	1.581e-05	1.853e-06	5.237e-05	8.206e-06	7.712e-06
D_4	1.144e-07	1.376e-07	1.575e-08	2.408e-05	3.963e-06	4.145e-06	0.0002062	1.95e-05	5.893e-06
$D_{4,5}$	1.741e-07	-1.81e-08	-6.412e-09	0.0001037	1.471e-05	1.424e-07	0.0001027	1.525e-05	8.154e-06
D_5	1.653e-06	1.2e-07	2.156e-08	0.0001876	1.96e-05	4.312e-06	4.947e-05	7.137e-06	5.112e-06

Table A.6: Sobol variances for main effect and cardinality 2, for point 6.

Property	Value for Level 2 (13 points)			Value for Level 3 (85 points)			Value for Level 4 (389 points)		
Location	P1	P2	P3	P1	P2	P3	P1	P2	P3
Mean	1.178	1.227	1.251	1.18	1.227	1.25	1.171	1.225	1.242
Variance	8.196e-05	4.188e-05	0.0001384	-0.0001597	-4.505e-05	-0.0003771	-5.777e-05	2.264e-05	0.0005382
D_0	7.271e-07	3.973e-07	4.088e-08	0.0001151	2.642e-05	1.877e-06	0.0001367	5.698e-05	1.776e-05
$D_{0,1}$	-6.2e-07	-2.376e-07	-3.074e-07	0.0001894	6.459e-05	2.125e-06	8.796e-05	9.889e-06	1.058e-05
$D_{0,2}$	1.446e-07	1.447e-07	-9.005e-07	5.449e-05	2.777e-05	-4.717e-05	0.0002066	5.016e-05	-6.911e-06
$D_{0,3}$	5.991e-07	2.531e-07	-1.173e-08	0.0001332	4.78e-05	6.86e-07	3.362e-05	1.139e-05	3.191e-06
$D_{0,4}$	-4.52e-08	-1.126e-07	3.048e-09	0.0001902	6.52e-05	5.04e-07	-1.5e-05	-1.456e-05	5.869e-06
$D_{0,5}$	2.092e-07	1.967e-08	-1.874e-08	9.733e-05	3.299e-05	3.968e-06	0.0001185	3.915e-05	3.763e-05
D_1	2.325e-05	8.582e-06	1.55e-05	5.257e-05	1.284e-05	1.576e-05	0.0001391	5.609e-05	5.632e-06
$D_{1,2}$	9.591e-07	4.045e-07	-1.806e-05	0.00013	5.134e-05	-3.985e-05	6.123e-05	2.675e-05	8.204e-06
$D_{1,3}$	3.975e-06	7.075e-07	-2.352e-07	0.0001675	5.393e-05	2.745e-06	6.831e-05	1.948e-05	1.194e-05
$D_{1,4}$	-2.999e-07	-3.146e-07	6.113e-08	0.000255	7.866e-05	-3.348e-07	0.0001383	3.393e-05	2.024e-05
$D_{1,5}$	1.388e-06	5.498e-08	-3.758e-07	0.0001279	3.488e-05	-1.88e-06	7e-05	2.111e-05	5.747e-06
D_2	1.745e-05	2.055e-05	0.0001443	2.072e-05	8.505e-06	2.915e-05	0.0001853	5.302e-05	0.0006479
$D_{2,3}$	-9.267e-07	-4.308e-07	-6.892e-07	5.594e-05	2.554e-05	-2.511e-05	6.05e-05	1.683e-05	4.46e-06
$D_{2,4}$	6.991e-08	1.916e-07	1.791e-07	0.0001027	4.136e-05	-1.658e-05	0.0001677	4.893e-05	-5.222e-05
$D_{2,5}$	-3.235e-07	-3.348e-08	-1.101e-06	3.596e-05	1.378e-05	-4.428e-05	1.593e-05	1.382e-06	2.902e-05
D_3	3.418e-05	1.075e-05	1.099e-08	3.391e-05	1.126e-05	1.721e-06	0.00011	3.173e-05	6.509e-06
$D_{3,4}$	2.897e-07	3.351e-07	2.333e-09	0.0001865	6.561e-05	1.186e-06	0.0001003	2.767e-05	4.711e-06
$D_{3,5}$	-1.341e-06	-5.856e-08	-1.434e-08	0.0001198	4.127e-05	2.561e-06	5.453e-05	2.212e-05	2.027e-05
D_4	6.138e-08	1.764e-07	1.086e-09	3.109e-05	1.137e-05	5.77e-06	0.0002337	6.166e-05	1.985e-05
$D_{4,5}$	1.012e-07	2.604e-08	3.727e-09	0.0001228	3.687e-05	-2.633e-06	0.0001194	3.721e-05	2.144e-05
D_5	2.116e-06	4.724e-07	4.155e-08	0.0002045	5.71e-05	1.388e-05	5.648e-05	1.784e-05	1.007e-05

Table A.7: Sobol variances for main effect and cardinality 2, for point 7.

Property	Value for Level 2 (13 points)			Value for Level 3 (85 points)			Value for Level 4 (389 points)		
Location	P1	P2	P3	P1	P2	P3	P1	P2	P3
Mean	1.163	1.209	1.249	1.165	1.212	1.246	1.155	1.205	1.24
Variance	0.0001035	7.13e-05	0.0001984	-0.0002015	-0.0001008	-0.0004133	-8.919e-05	5.831e-06	0.0006797
D_0	1.06e-06	4.496e-07	9.24e-09	0.0001276	6.796e-05	4.402e-06	0.000179	8.959e-05	4.138e-05
$D_{0,1}$	-5.863e-07	3.527e-07	1.929e-07	0.0002265	0.0001045	-2.743e-07	0.0001016	5.021e-05	2.438e-05
$D_{0,2}$	2.099e-07	-9.673e-08	4.803e-07	6.024e-05	2.822e-05	-5.073e-05	0.0002416	9.416e-05	7.599e-06
$D_{0,3}$	7.147e-07	-3.226e-07	-1.923e-09	0.000155	7.256e-05	8.514e-07	3.167e-05	3.286e-05	7.115e-06
$D_{0,4}$	-6.182e-08	-3.054e-09	-7.226e-09	0.0002224	0.0001051	-2.269e-07	-3.752e-05	7.335e-06	1.428e-05
$D_{0,5}$	2.478e-07	-8.479e-08	8.494e-09	0.0001095	5.866e-05	2.128e-06	0.0001623	7.468e-05	8.323e-05
D_1	3.142e-05	1.51e-05	2.974e-05	5.796e-05	3.289e-05	3.202e-05	0.0001519	9.392e-05	1.257e-05
$D_{1,2}$	1.136e-06	8.026e-07	-2.889e-05	0.000151	7.572e-05	-5.061e-05	5.695e-05	4.791e-05	1.777e-05
$D_{1,3}$	3.869e-06	2.677e-06	1.157e-07	0.0001999	9.801e-05	5.65e-07	7.583e-05	5.308e-05	2.588e-05
$D_{1,4}$	-3.346e-07	2.534e-08	4.347e-07	0.0002974	0.0001458	-5.523e-06	0.0001506	8.746e-05	4.17e-05
$D_{1,5}$	1.342e-06	7.035e-07	-5.11e-07	0.0001425	7.258e-05	-1.222e-05	7.399e-05	5.345e-05	1.126e-05
D_2	2.453e-05	3.202e-05	0.0001966	2.816e-05	9.865e-06	2.706e-05	0.0002257	0.0001065	0.0008037
$D_{2,3}$	-1.385e-06	-7.34e-07	2.879e-07	6.236e-05	3.052e-05	-2.71e-05	7.241e-05	3.281e-05	2.203e-05
$D_{2,4}$	1.198e-07	-6.95e-09	1.082e-06	0.0001209	5.94e-05	-1.878e-05	0.0001958	9.388e-05	-7.991e-05
$D_{2,5}$	-4.803e-07	-1.929e-07	-1.272e-06	4.293e-05	2.22e-05	-5.405e-05	7.877e-06	9.427e-06	4.38e-05
D_3	4.042e-05	1.937e-05	1.562e-08	3.808e-05	2.388e-05	1.133e-06	0.0001354	6.088e-05	1.333e-05
$D_{3,4}$	4.079e-07	-2.318e-08	-4.332e-09	0.0002222	0.000108	2.496e-06	0.0001132	7.026e-05	1.22e-05
$D_{3,5}$	-1.635e-06	-6.434e-07	5.092e-09	0.0001431	7.62e-05	1.388e-06	7.216e-05	4.019e-05	4.078e-05
D_4	7.356e-08	2.485e-09	1.639e-08	3.873e-05	1.922e-05	8.598e-06	0.0002678	0.0001496	4.441e-05
$D_{4,5}$	1.415e-07	-6.092e-09	1.914e-08	0.0001437	7.494e-05	-9.023e-06	0.0001517	7.418e-05	4.488e-05
D_5	2.257e-06	1.909e-06	2.256e-08	0.0002281	0.0001347	3.422e-05	7.257e-05	3.757e-05	1.888e-05

Table A.8: Sobol variances for main effect and cardinality 2, for point 8.

Property	Value for Level 2 (13 points)			Value for Level 3 (85 points)			Value for Level 4 (389 points)		
Location	P1	P2	P3	P1	P2	P3	P1	P2	P3
Mean	1.148	1.194	1.247	1.15	1.195	1.24	1.139	1.19	1.238
Variance	0.000126	8.86e-05	0.0002862	-0.0002491	-0.000142	-0.0004628	-0.0001152	2.301e-05	0.0008519
D_0	1.207e-06	5.359e-07	2.107e-07	0.0001457	8.414e-05	1.069e-05	0.0002136	0.0001163	7.303e-05
$D_{0,1}$	-7.003e-07	-5.189e-07	1.891e-06	0.0002575	0.0001442	-6.266e-06	0.0001208	6.819e-05	4.787e-05
$D_{0,2}$	2.886e-07	8.9e-08	4.442e-06	6.208e-05	3.87e-05	-5.495e-05	0.0002716	0.00016	3.989e-05
$D_{0,3}$	8.487e-07	3.404e-07	-1.393e-07	0.000174	0.0001004	-7.279e-08	2.971e-05	2.9e-05	1.518e-05
$D_{0,4}$	-5.905e-08	-1.045e-07	-2.131e-07	0.0002464	0.000142	-2.959e-06	-5.401e-05	-1.674e-05	3.129e-05
$D_{0,5}$	3.2e-07	1.259e-07	7.766e-09	0.0001186	7.048e-05	-2.084e-06	0.0002011	0.0001072	0.0001503
D_1	4.133e-05	2.289e-05	4.568e-05	6.545e-05	4.202e-05	5.353e-05	0.0001574	0.0001111	2.138e-05
$D_{1,2}$	1.266e-06	6.748e-07	-4.002e-05	0.0001638	9.81e-05	-6.168e-05	5.099e-05	5.275e-05	3.954e-05
$D_{1,3}$	3.723e-06	2.581e-06	1.255e-06	0.0002261	0.0001316	-6.483e-06	8.446e-05	5.962e-05	4.32e-05
$D_{1,4}$	-2.591e-07	-7.925e-07	1.92e-06	0.0003279	0.0001912	-1.629e-05	0.0001596	0.0001038	7.096e-05
$D_{1,5}$	1.404e-06	9.548e-07	-6.997e-08	0.000153	8.942e-05	-2.756e-05	7.979e-05	5.971e-05	1.503e-05
D_2	3.295e-05	3.47e-05	0.0002636	3.134e-05	1.477e-05	3.208e-05	0.0002602	0.0001635	0.0009792
$D_{2,3}$	-1.535e-06	-4.427e-07	2.949e-06	6.436e-05	4.213e-05	-2.994e-05	8.32e-05	5.399e-05	5.027e-05
$D_{2,4}$	1.068e-07	1.359e-07	4.51e-06	0.0001297	7.81e-05	-2.229e-05	0.0002115	0.0001362	-0.000101
$D_{2,5}$	-5.788e-07	-1.638e-07	-1.644e-07	4.685e-05	2.576e-05	-6.449e-05	1.053e-05	1.71e-05	7.477e-05
D_3	4.443e-05	2.605e-05	1.197e-07	4.208e-05	2.745e-05	8.25e-07	0.0001618	9.256e-05	2.22e-05
$D_{3,4}$	3.14e-07	5.199e-07	-1.414e-07	0.0002442	0.0001436	2.82e-06	0.0001272	8.011e-05	2.181e-05
$D_{3,5}$	-1.702e-06	-6.264e-07	5.155e-09	0.0001599	8.824e-05	-3.228e-06	8.911e-05	5.656e-05	6.631e-05
D_4	5.973e-08	1.652e-07	2.273e-07	4.441e-05	2.385e-05	1.277e-05	0.0002921	0.0001765	7.68e-05
$D_{4,5}$	1.184e-07	1.923e-07	7.885e-09	0.0001613	8.935e-05	-2.033e-05	0.0001783	0.0001034	7.353e-05
D_5	2.438e-06	1.304e-06	1.236e-07	0.0002476	0.0001488	6.48e-05	8.858e-05	4.961e-05	3.14e-05

Table A.9: Sobol variances for main effect and cardinality 2, for point 9.

Property	Value for Level 2 (13 points)			Value for Level 3 (85 points)			Value for Level 4 (389 points)		
Location	P1	P2	P3	P1	P2	P3	P1	P2	P3
Mean	1.134	1.179	1.245	1.135	1.181	1.235	1.122	1.173	1.237
Variance	0.0001369	0.000106	0.0003749	-0.0002878	-0.0001802	-0.0005052	-0.0001662	-6.586e-06	0.001044
D_0	1.637e-06	1.029e-06	1.104e-06	0.0001567	9.703e-05	1.826e-05	0.0002303	0.0001479	0.0001027
$D_{0,1}$	-8.893e-07	-5.956e-07	4.445e-06	0.0002723	0.0001762	-1.249e-05	0.0001353	7.045e-05	7.67e-05
$D_{0,2}$	4.643e-07	2.676e-07	9.905e-06	6.238e-05	4.419e-05	-5.5e-05	0.0002821	0.0001889	7.933e-05
$D_{0,3}$	1.198e-06	7.627e-07	-6.517e-07	0.0001813	0.0001194	-2.151e-06	2.143e-05	2.213e-05	2.312e-05
$D_{0,4}$	-6.342e-08	-8.95e-08	-8.498e-07	0.0002573	0.0001705	-6.728e-06	-6.771e-05	-3.722e-05	5.302e-05
$D_{0,5}$	4.799e-07	2.902e-07	-1.942e-07	0.0001194	8.158e-05	-4.508e-06	0.0002215	0.0001366	0.0002239
D_1	4.842e-05	2.696e-05	5.954e-05	6.42e-05	3.866e-05	8.062e-05	0.0001404	0.0001206	3.022e-05
$D_{1,2}$	1.296e-06	8.658e-07	-4.608e-05	0.000169	0.0001138	-6.874e-05	3.48e-05	4.677e-05	6.664e-05
$D_{1,3}$	3.345e-06	2.468e-06	3.031e-06	0.0002403	0.0001547	-1.994e-05	8.198e-05	5.408e-05	5.682e-05
$D_{1,4}$	-1.771e-07	-2.896e-07	3.953e-06	0.0003414	0.0002236	-3.317e-05	0.0001511	0.0001056	0.0001037
$D_{1,5}$	1.34e-06	9.392e-07	9.032e-07	0.0001549	0.0001023	-4.406e-05	7.088e-05	5.145e-05	1.502e-05
D_2	3.69e-05	4.337e-05	0.0003211	3.337e-05	1.923e-05	4.31e-05	0.0002804	0.0002054	0.001155
$D_{2,3}$	-1.747e-06	-1.109e-06	6.755e-06	6.359e-05	4.47e-05	-3.263e-05	8.364e-05	5.776e-05	7.294e-05
$D_{2,4}$	9.246e-08	1.301e-07	8.809e-06	0.000134	9.285e-05	-2.611e-05	0.0002045	0.0001548	-0.0001134
$D_{2,5}$	-6.996e-07	-4.219e-07	2.013e-06	5.174e-05	3.2e-05	-7.062e-05	6.567e-06	2.097e-06	9.169e-05
D_3	4.426e-05	3.026e-05	4.928e-07	4.139e-05	2.982e-05	1.588e-06	0.0001739	0.0001066	2.864e-05
$D_{3,4}$	2.386e-07	3.709e-07	-5.795e-07	0.0002525	0.000173	2.973e-08	0.0001315	8.431e-05	2.998e-05
$D_{3,5}$	-1.805e-06	-1.203e-06	-1.324e-07	0.0001682	0.0001072	-1.122e-05	9.396e-05	6.149e-05	8.945e-05
D_4	2.249e-08	5.568e-08	8.079e-07	4.741e-05	3.027e-05	1.72e-05	0.0002997	0.0002025	0.000112
$D_{4,5}$	9.555e-08	1.411e-07	-1.727e-07	0.0001715	0.0001047	-3.324e-05	0.0001867	0.0001221	0.0001052
D_5	2.503e-06	1.792e-06	6.862e-07	0.0002509	0.0001622	9.693e-05	9.706e-05	5.772e-05	4.566e-05

Table A.10: Sobol variances for main effect and cardinality 2, for point 10.

Property	Value for Level 2 (13 points)			Value for Level 3 (85 points)			Value for Level 4 (389 points)		
Location	P1	P2	P3	P1	P2	P3	P1	P2	P3
Mean	1.121	1.165	1.243	1.123	1.166	1.23	1.107	1.157	1.234
Variance	0.0001396	0.0001295	0.0004422	-0.000325	-0.0002152	-0.0004767	-0.0002389	-3.163e-05	0.001203
D_0	2.811e-06	1.422e-06	2.989e-06	0.0001531	0.0001051	2.553e-05	0.0002343	0.0001883	0.0001244
$D_{0,1}$	-1.224e-06	-5.37e-07	6.944e-06	0.0002738	0.0002072	-1.379e-05	0.0001545	8.38e-05	0.0001039
$D_{0,2}$	7.716e-07	4.117e-07	1.43e-05	6.203e-05	4.752e-05	-4.85e-05	0.0002659	0.0002193	9.729e-05
$D_{0,3}$	1.764e-06	9.47e-07	-1.262e-06	0.0001796	0.0001358	-3.31e-06	3.411e-06	1.966e-05	3.175e-05
$D_{0,4}$	-2.001e-07	-1.236e-07	-1.855e-06	0.0002565	0.0001971	-8.263e-06	-8.567e-05	-5.824e-05	6.677e-05
$D_{0,5}$	7.597e-07	3.57e-07	-4.617e-07	0.00012	8.953e-05	-3.536e-06	0.0002305	0.0001806	0.0002816
D_1	5.306e-05	3.556e-05	6.788e-05	5.665e-05	4.244e-05	0.0001024	0.0001022	0.0001322	3.531e-05
$D_{1,2}$	1.128e-06	9.72e-07	-4.585e-05	0.0001637	0.000131	-6.5e-05	1.041e-06	4.368e-05	8.713e-05
$D_{1,3}$	2.578e-06	2.236e-06	4.045e-06	0.0002418	0.0001815	-3.096e-05	6.977e-05	6.104e-05	6.143e-05
$D_{1,4}$	-2.925e-07	-2.918e-07	5.947e-06	0.0003362	0.0002587	-4.81e-05	0.0001287	0.0001159	0.0001251
$D_{1,5}$	1.11e-06	8.429e-07	1.48e-06	0.0001529	0.0001104	-5.549e-05	3.989e-05	5.403e-05	8.591e-06
D_2	3.688e-05	5.326e-05	0.0003624	3.708e-05	2.432e-05	5.942e-05	0.000276	0.000246	0.001306
$D_{2,3}$	-1.626e-06	-1.714e-06	8.33e-06	5.933e-05	4.81e-05	-3.035e-05	7.354e-05	6.923e-05	7.478e-05
$D_{2,4}$	1.845e-07	2.237e-07	1.225e-05	0.0001331	0.0001079	-2.475e-05	0.0001682	0.0001757	-0.0001204
$D_{2,5}$	-7.003e-07	-6.462e-07	3.048e-06	6.163e-05	3.815e-05	-6.599e-05	-8.387e-06	-3.186e-06	9.503e-05
D_3	4.115e-05	3.536e-05	8.01e-07	3.959e-05	3.275e-05	2.673e-06	0.0001677	0.0001292	3.075e-05
$D_{3,4}$	4.216e-07	5.145e-07	-1.08e-06	0.0002453	0.0002037	-2.855e-06	0.0001186	9.484e-05	3.277e-05
$D_{3,5}$	-1.601e-06	-1.486e-06	-2.689e-07	0.0001728	0.0001259	-1.685e-05	8.895e-05	7.938e-05	0.000102
D_4	4.834e-08	7.743e-08	1.738e-06	4.807e-05	3.699e-05	2.164e-05	0.0002856	0.0002335	0.0001351
$D_{4,5}$	1.816e-07	1.94e-07	-3.954e-07	0.0001779	0.0001197	-4.093e-05	0.0001799	0.0001528	0.0001307
D_5	2.353e-06	1.89e-06	1.225e-06	0.0002342	0.0001835	0.0001232	9.816e-05	7.363e-05	5.78e-05

Table A.11: Sobol variances for main effect and cardinality 2, for point 11.

Property	Value for Level 2 (13 points)			Value for Level 3 (85 points)			Value for Level 4 (389 points)		
Location	P1	P2	P3	P1	P2	P3	P1	P2	P3
Mean	1.109	1.151	1.239	1.112	1.151	1.228	1.091	1.141	1.23
Variance	0.0001305	0.0001557	0.0004884	-0.000358	-0.000261	-0.000337	-0.0003659	-5.274e-05	0.00132
D_0	4.479e-06	1.669e-06	5.804e-06	0.0001384	0.0001193	2.395e-05	0.000226	0.0002235	0.0001504
$D_{0,1}$	-1.071e-06	-6.06e-07	6.696e-06	0.0002601	0.0002385	-1.314e-06	0.0001836	0.0001014	0.0001052
$D_{0,2}$	8.827e-07	4.708e-07	1.296e-05	5.836e-05	5.118e-05	-3.818e-05	0.0002238	0.0002473	6.673e-05
$D_{0,3}$	1.874e-06	1.077e-06	-1.455e-06	0.0001655	0.0001552	-4.342e-07	-2.718e-05	1.627e-05	2.279e-05
$D_{0,4}$	-3.534e-07	-1.426e-07	-2.059e-06	0.0002401	0.0002228	-3.239e-06	-0.0001046	-7.644e-05	4.583e-05
$D_{0,5}$	1.059e-06	4.179e-07	-6.505e-07	0.0001165	0.0001006	2.264e-06	0.0002275	0.0002227	0.0003099
D_1	5.528e-05	4.592e-05	7.285e-05	4.609e-05	4.962e-05	8.747e-05	6.509e-05	0.0001393	3.394e-05
$D_{1,2}$	6.528e-07	9.574e-07	-3.849e-05	0.0001464	0.0001454	-4.257e-05	-4.141e-05	3.999e-05	7.841e-05
$D_{1,3}$	1.386e-06	2.19e-06	4.323e-06	0.0002283	0.000208	-2.099e-05	5.381e-05	6.931e-05	5.681e-05
$D_{1,4}$	-2.613e-07	-2.9e-07	6.117e-06	0.0003067	0.0002898	-4.247e-05	8.653e-05	0.0001256	0.0001166
$D_{1,5}$	7.833e-07	8.498e-07	1.932e-06	0.0001467	0.000121	-4.831e-05	-1.115e-05	5.816e-05	4.725e-07
D_2	3.232e-05	6.431e-05	0.0003944	3.965e-05	2.775e-05	8.177e-05	0.0002509	0.000281	0.001451
$D_{2,3}$	-1.142e-06	-1.701e-06	8.366e-06	4.927e-05	5.324e-05	-2.283e-05	5.348e-05	8.145e-05	5.234e-05
$D_{2,4}$	2.154e-07	2.253e-07	1.184e-05	0.0001198	0.0001183	-1.439e-05	9.903e-05	0.0001898	-0.000132
$D_{2,5}$	-6.455e-07	-6.601e-07	3.739e-06	7.178e-05	4.237e-05	-4.811e-05	-2.126e-05	1.176e-06	7.741e-05
D_3	3.339e-05	3.977e-05	9.629e-07	3.674e-05	3.662e-05	1.468e-06	0.0001438	0.0001531	3.765e-05
$D_{3,4}$	4.572e-07	5.153e-07	-1.33e-06	0.0002127	0.0002285	3.15e-06	8.757e-05	0.0001059	2.725e-05
$D_{3,5}$	-1.37e-06	-1.51e-06	-4.2e-07	0.0001683	0.0001441	-9.035e-06	7.692e-05	9.841e-05	0.0001144
D_4	9.558e-08	9.108e-08	2.191e-06	4.613e-05	4.334e-05	1.855e-05	0.0002444	0.0002574	0.0001264
$D_{4,5}$	2.584e-07	2e-07	-5.943e-07	0.0001799	0.0001378	-3.604e-05	0.000149	0.0001809	0.0001486
D_5	2.224e-06	1.977e-06	1.197e-06	0.0001885	0.0002003	0.0001179	9.436e-05	8.982e-05	6.85e-05

Table A.12: Sobol variances for main effect and cardinality 2, for point 12.

Property	Value for Level 2 (13 points)			Value for Level 3 (85 points)			Value for Level 4 (389 points)		
Location	P1	P2	P3	P1	P2	P3	P1	P2	P3
Mean	1.1	1.137	1.234	1.103	1.137	1.226	1.076	1.126	1.226
Variance	0.0001067	0.0001688	0.0005213	-0.0003478	-0.0002937	-0.0002181	-0.0006199	-0.0001024	0.001447
D_0	7.545e-06	1.877e-06	5.695e-06	0.0001071	0.0001324	1.364e-05	0.0002043	0.0002458	0.000186
$D_{0,1}$	-3.412e-07	-6.604e-07	5.259e-06	0.0002185	0.0002532	8.143e-06	0.0002162	0.000117	8.73e-05
$D_{0,2}$	8.027e-07	5.504e-07	9.128e-06	5.025e-05	5.106e-05	-3.167e-05	0.0001632	0.0002605	3.518e-05
$D_{0,3}$	1.602e-06	1.301e-06	-5.937e-07	0.0001342	0.0001636	1.424e-07	-5.263e-05	1.117e-05	4.599e-06
$D_{0,4}$	-5.926e-07	-1.493e-07	-8.193e-07	0.0001982	0.000234	-1.054e-06	-0.0001145	-8.788e-05	1.752e-05
$D_{0,5}$	1.518e-06	5.323e-07	6.125e-08	9.992e-05	0.000101	1.634e-06	0.0002191	0.0002463	0.000329
D_1	5.465e-05	5.378e-05	8.44e-05	3.3e-05	5.107e-05	8.608e-05	7.677e-05	0.0001314	3.114e-05
$D_{1,2}$	8.823e-08	8.43e-07	-3.566e-05	0.0001163	0.0001503	-1.69e-05	-6.246e-05	3.01e-05	5.856e-05
$D_{1,3}$	1.761e-07	1.992e-06	2.32e-06	0.0001897	0.0002226	-1.042e-05	3.716e-05	7.144e-05	5.515e-05
$D_{1,4}$	-6.514e-08	-2.287e-07	3.201e-06	0.0002453	0.0003039	-3.782e-05	1.918e-05	0.0001237	9.134e-05
$D_{1,5}$	1.668e-07	8.153e-07	-2.393e-07	0.0001241	0.0001217	-5.031e-05	-7.752e-05	5.573e-05	-3.018e-06
D_2	2.067e-05	6.887e-05	0.0004383	3.925e-05	2.95e-05	0.0001118	0.0002158	0.0002977	0.001594
$D_{2,3}$	-4.142e-07	-1.66e-06	4.026e-06	2.985e-05	5.205e-05	-1.558e-05	3.004e-05	8.513e-05	4.027e-05
$D_{2,4}$	1.532e-07	1.906e-07	5.556e-06	8.738e-05	0.0001209	5.847e-07	1.162e-06	0.0001856	-0.0001394
$D_{2,5}$	-3.925e-07	-6.795e-07	-4.154e-07	7.923e-05	4.62e-05	-2.901e-05	-2.381e-05	2.867e-06	7.545e-05
D_3	1.962e-05	4.03e-05	6.046e-07	2.87e-05	3.674e-05	2.648e-07	0.0001087	0.0001687	5.098e-05
$D_{3,4}$	3.058e-07	4.504e-07	-3.614e-07	0.0001483	0.0002374	1.33e-05	4.377e-05	0.0001135	2.524e-05
$D_{3,5}$	-7.832e-07	-1.606e-06	2.702e-08	0.0001437	0.0001519	-1.547e-06	5.145e-05	0.0001064	0.0001348
D_4	1.361e-07	5.626e-08	5.155e-07	4.444e-05	4.636e-05	2.016e-05	0.0002133	0.0002719	0.0001058
$D_{4,5}$	2.897e-07	1.844e-07	3.728e-08	0.0001667	0.0001472	-3.248e-05	8.453e-05	0.000193	0.0001509
D_5	1.561e-06	2.062e-06	2.491e-07	0.0001187	0.0002098	9.64e-05	8.572e-05	0.0001003	7.661e-05

Table A.13: Sobol variances for main effect and cardinality 2, for point 13.

Property	Value for Level 2 (13 points)			Value for Level 3 (85 points)			Value for Level 4 (389 points)		
Location	P1	P2	P3	P1	P2	P3	P1	P2	P3
Mean	1.093	1.124	1.23	1.097	1.124	1.222	1.063	1.111	1.223
Variance	8.332e-05	0.0001722	0.0005752	-0.0002745	-0.0003217	-0.0001989	-0.001002	-0.0001707	0.001577
D_0	1.358e-05	2.892e-06	4.504e-06	6.495e-05	0.0001335	7.915e-06	0.0001919	0.0002539	0.0002236
$D_{0,1}$	1.911e-06	-7.529e-07	5.294e-06	0.0001539	0.0002582	1.413e-05	0.0002224	0.0001349	7.662e-05
$D_{0,2}$	5.149e-07	7.519e-07	8.035e-06	4.409e-05	5.147e-05	-2.349e-05	9.532e-05	0.0002523	3.059e-05
$D_{0,3}$	5.409e-07	1.728e-06	-2.811e-07	9.554e-05	0.0001655	1.775e-06	-5.503e-05	-1.331e-06	-1.764e-06
$D_{0,4}$	-7.799e-07	-2.46e-07	-6.892e-07	0.0001437	0.0002377	1.612e-06	-0.0001166	-0.0001013	-1.755e-06
$D_{0,5}$	1.378e-06	7.455e-07	3.786e-07	7.018e-05	0.0001022	-4.298e-06	0.0002149	0.0002578	0.0003714
D_1	5.137e-05	5.865e-05	9.6e-05	2.115e-05	4.739e-05	9.661e-05	0.0001594	0.0001027	3.652e-05
$D_{1,2}$	-1.555e-07	6.712e-07	-3.255e-05	8.975e-05	0.0001484	4.786e-06	-4.222e-05	6.883e-06	5.023e-05
$D_{1,3}$	-1.634e-07	1.542e-06	1.139e-06	0.0001418	0.0002279	-7.358e-06	2.27e-05	6.446e-05	5.249e-05
$D_{1,4}$	2.356e-07	-2.196e-07	2.792e-06	0.0001768	0.000306	-4.047e-05	-5.138e-05	0.0001104	6.918e-05
$D_{1,5}$	-4.161e-07	6.656e-07	-1.534e-06	8.924e-05	0.0001216	-7.01e-05	-0.0001347	3.43e-05	-2.076e-06
D_2	7.091e-06	6.751e-05	0.0004866	3.761e-05	3.223e-05	0.0001423	0.0001845	0.0002918	0.001712
$D_{2,3}$	-4.403e-08	-1.54e-06	1.729e-06	7.092e-06	5.013e-05	-1.014e-05	5.328e-06	7.919e-05	3.497e-05
$D_{2,4}$	6.349e-08	2.193e-07	4.237e-06	4.385e-05	0.0001223	1.537e-05	-9.607e-05	0.0001579	-0.0001452
$D_{2,5}$	-1.121e-07	-6.646e-07	-2.328e-06	8.213e-05	5.433e-05	-1.265e-05	-7.788e-06	-5.172e-06	9.483e-05
D_3	7.589e-06	3.896e-05	1.236e-06	2.626e-05	3.556e-05	1.103e-06	7.428e-05	0.0001669	6.748e-05
$D_{3,4}$	6.669e-08	5.038e-07	-1.483e-07	7.229e-05	0.0002372	2.248e-05	-8.004e-06	0.0001074	2.436e-05
$D_{3,5}$	-1.178e-07	-1.527e-06	8.144e-08	0.0001073	0.0001584	-8.244e-07	1.679e-05	0.000105	0.0001557
D_4	1.093e-07	7.413e-08	3.636e-07	4.547e-05	4.756e-05	2.43e-05	0.0002241	0.0002709	9.86e-05
$D_{4,5}$	1.698e-07	2.174e-07	1.996e-07	0.0001375	0.0001544	-3.896e-05	6.89e-06	0.0001902	0.0001635
D_5	4.886e-07	2.032e-06	1.782e-07	5.57e-05	0.0002038	8.411e-05	8.379e-05	0.0001029	8.519e-05

Table A.14: Sobol variances for main effect and cardinality 2, for point 14.

Property	Value for Level 2 (13 points)			Value for Level 3 (85 points)			Value for Level 4 (389 points)		
Location	P1	P2	P3	P1	P2	P3	P1	P2	P3
Mean	1.088	1.113	1.226	1.094	1.113	1.216	1.052	1.096	1.219
Variance	7.358e-05	0.0001649	0.0006455	-0.0001774	-0.0003467	-0.0002173	-0.001424	-0.0002796	0.001704
D_0	2.051e-05	4.266e-06	4.941e-06	2.721e-05	0.0001264	7.65e-06	0.0002231	0.0002516	0.0002573
$D_{0,1}$	6.062e-06	-6.23e-07	6.592e-06	9.591e-05	0.0002537	2.206e-05	0.0001941	0.0001673	7.731e-05
$D_{0,2}$	1.628e-06	8.17e-07	8.638e-06	4.095e-05	5.13e-05	-1.52e-05	3.79e-05	0.0002211	3.129e-05
$D_{0,3}$	-6.051e-07	1.922e-06	-2.265e-07	6.222e-05	0.0001597	5.238e-06	-4.39e-05	-2.364e-05	-6.548e-06
$D_{0,4}$	-1.179e-06	-4.111e-07	-1.253e-06	9.849e-05	0.0002319	6.89e-06	-0.0001206	-0.0001155	-1.472e-05
$D_{0,5}$	7.418e-07	1e-06	3.878e-07	4.554e-05	0.0001032	-1.374e-05	0.000213	0.0002598	0.0004164
D_1	4.393e-05	6.17e-05	0.0001053	2.265e-05	4.148e-05	0.0001097	0.0002697	6.709e-05	4.401e-05
$D_{1,2}$	-9.29e-07	3.532e-07	-2.804e-05	7.364e-05	0.0001372	2.677e-05	3.079e-06	-2.575e-05	6.558e-05
$D_{1,3}$	3.453e-07	8.309e-07	7.35e-07	9.994e-05	0.0002234	-4.768e-06	8.702e-06	5.503e-05	5.073e-05
$D_{1,4}$	6.729e-07	-1.777e-07	4.066e-06	0.000126	0.0002923	-4.546e-05	-9.203e-05	8.739e-05	6.465e-05
$D_{1,5}$	-4.234e-07	4.323e-07	-1.259e-06	5.674e-05	0.0001203	-9.988e-05	-0.0001712	-3.86e-06	-3.258e-06
D_2	4.226e-07	6.045e-05	0.0005376	3.746e-05	3.398e-05	0.0001687	0.0001635	0.0002613	0.001831
$D_{2,3}$	9.272e-08	-1.09e-06	9.631e-07	-9.964e-06	4.488e-05	-4.739e-06	-8.643e-06	6.527e-05	3.385e-05
$D_{2,4}$	1.807e-07	2.331e-07	5.327e-06	8.556e-06	0.0001146	3.205e-05	-0.0001688	0.0001046	-0.0001561
$D_{2,5}$	-1.137e-07	-5.67e-07	-1.649e-06	7.769e-05	6.48e-05	4.412e-06	2.678e-05	-1.135e-05	0.0001291
D_3	1.985e-06	3.412e-05	2.226e-06	4.497e-05	3.393e-05	2.128e-06	5.12e-05	0.0001512	8.042e-05
$D_{3,4}$	-6.716e-08	5.483e-07	-1.397e-07	1.133e-05	0.0002186	3.384e-05	-6.419e-05	8.768e-05	2.232e-05
$D_{3,5}$	4.226e-08	-1.334e-06	4.324e-08	7.457e-05	0.0001604	-3.296e-06	-1.221e-05	9.781e-05	0.0001784
D_4	1.574e-07	1.301e-07	7.922e-07	4.776e-05	4.63e-05	2.977e-05	0.0002758	0.0002477	0.0001086
$D_{4,5}$	8.234e-08	2.853e-07	2.392e-07	0.0001035	0.0001605	-5.036e-05	-5.594e-05	0.0001701	0.0001956
D_5	5.236e-08	1.997e-06	1.439e-07	2.306e-05	0.000178	8.447e-05	0.0001012	0.0001015	9.421e-05

Table A.15: Sobol variances for main effect and cardinality 2, for point 15.

Property	Value for Level 2 (13 points)			Value for Level 3 (85 points)			Value for Level 4 (389 points)		
Location	P1	P2	P3	P1	P2	P3	P1	P2	P3
Mean	1.086	1.103	1.223	1.094	1.104	1.212	1.045	1.082	1.216
Variance	7.72e-05	0.00014	0.0007122	-0.0001321	-0.000338	-0.0002224	-0.001729	-0.0004771	0.001833
D_0	2.532e-05	6.492e-06	5.156e-06	7.144e-06	0.0001064	7.976e-06	0.0002968	0.0002323	0.0002876
$D_{0,1}$	9.678e-06	-1.262e-08	6.858e-06	6.264e-05	0.000226	3.437e-05	0.0001636	0.0002089	7.739e-05
$D_{0,2}$	4.783e-06	3.872e-07	7.561e-06	3.447e-05	4.623e-05	-1.133e-05	-4.674e-06	0.0001768	3.826e-05
$D_{0,3}$	-1.368e-06	1.768e-06	5.814e-08	3.821e-05	0.0001382	1.015e-05	-3.437e-05	-4.843e-05	-9.472e-06
$D_{0,4}$	-2.197e-06	-6.525e-07	-1.533e-06	6.515e-05	0.0002047	1.501e-05	-0.0001265	-0.0001218	-2.078e-05
$D_{0,5}$	2.673e-07	1.388e-06	2.982e-07	3.432e-05	9.409e-05	-1.425e-05	0.0002211	0.0002537	0.0004512
D_1	3.562e-05	6.186e-05	0.0001125	4.019e-05	3.356e-05	0.0001187	0.0003703	6.145e-05	5.015e-05
$D_{1,2}$	-3.284e-06	2.024e-09	-2.399e-05	6.505e-05	0.0001143	4.573e-05	5.286e-05	-4.71e-05	8.481e-05
$D_{1,3}$	9.392e-07	9.245e-09	-1.845e-07	7.351e-05	0.0001979	1.84e-06	1.83e-06	4.606e-05	5.054e-05
$D_{1,4}$	1.508e-06	-3.411e-09	4.865e-06	9.777e-05	0.0002508	-4.553e-05	-0.0001002	4.176e-05	6.613e-05
$D_{1,5}$	-1.835e-07	7.257e-09	-9.464e-07	3.511e-05	0.0001088	-0.0001111	-0.0001869	-5.757e-05	-6.434e-06
D_2	4.138e-06	4.354e-05	0.0005926	4.625e-05	3.33e-05	0.0001829	0.0001617	0.0002236	0.001955
$D_{2,3}$	4.642e-07	-2.836e-07	-2.034e-07	-2.228e-05	3.027e-05	-3.516e-06	-3.609e-06	4.762e-05	3.552e-05
$D_{2,4}$	7.454e-07	1.046e-07	5.364e-06	-1.309e-05	8.907e-05	4.553e-05	-0.0002027	2.603e-05	-0.0001642
$D_{2,5}$	-9.072e-08	-2.226e-07	-1.043e-06	7.126e-05	7.27e-05	1.948e-05	7.405e-05	-9.855e-06	0.0001699
D_3	4.855e-07	2.386e-05	3.392e-06	7.131e-05	2.855e-05	2.65e-06	5.061e-05	0.000121	9.167e-05
$D_{3,4}$	-2.132e-07	4.779e-07	4.124e-08	-2.327e-05	0.000169	4.492e-05	-0.0001042	5.413e-05	2.411e-05
$D_{3,5}$	2.594e-08	-1.017e-06	-8.023e-09	5.461e-05	0.0001463	-1.508e-06	-2.633e-05	8.054e-05	0.0001959
D_4	4.358e-07	2.075e-07	1.184e-06	4.993e-05	4.425e-05	3.516e-05	0.0003307	0.0002218	0.000121
$D_{4,5}$	4.166e-08	3.751e-07	2.115e-07	8.026e-05	0.0001575	-5.555e-05	-8.572e-05	0.0001199	0.0002284
D_5	7.57e-08	1.746e-06	1.415e-07	1.174e-05	0.000129	8.72e-05	0.0001285	9.505e-05	0.0001055

Table A.16: Sobol variances for main effect and cardinality 2, for point 16.

Property	Value for Level 2 (13 points)			Value for Level 3 (85 points)			Value for Level 4 (389 points)		
Location	P1	P2	P3	P1	P2	P3	P1	P2	P3
Mean	1.085	1.096	1.218	1.093	1.098	1.208	1.042	1.069	1.212
Variance	8.695e-05	0.0001074	0.0007721	-0.0001195	-0.0002754	-0.0002919	-0.001896	-0.00081	0.001951
D_0	2.717e-05	1.106e-05	5.916e-06	4.546e-06	7.427e-05	8.901e-06	0.0003648	0.0002112	0.000304
$D_{0,1}$	1.164e-05	1.594e-06	7.466e-06	4.766e-05	0.0001743	4.139e-05	0.0001487	0.0002309	7.712e-05
$D_{0,2}$	8.163e-06	-6.111e-07	6.712e-06	2.618e-05	4.134e-05	-1.536e-05	-2.764e-05	0.000123	5.81e-05
$D_{0,3}$	-1.408e-06	1.028e-06	3.776e-07	2.298e-05	0.0001074	1.338e-05	-2.539e-05	-5.822e-05	-3.556e-06
$D_{0,4}$	-2.891e-06	-9.07e-07	-1.891e-06	4.17e-05	0.0001609	1.93e-05	-0.0001261	-0.0001172	-1.986e-05
$D_{0,5}$	7.563e-08	1.473e-06	3.442e-07	3.019e-05	7.45e-05	-1.263e-05	0.000237	0.0002415	0.0004667
D_1	3.212e-05	5.925e-05	0.0001155	5.755e-05	2.552e-05	0.0001238	0.0004457	0.0001174	5.394e-05
$D_{1,2}$	-5.996e-06	1.899e-07	-1.895e-05	5.994e-05	9.029e-05	5.249e-05	9.68e-05	-3.929e-05	0.0001007
$D_{1,3}$	1.035e-06	-3.194e-07	-1.066e-06	5.965e-05	0.0001585	4.715e-06	-9.576e-07	3.494e-05	4.78e-05
$D_{1,4}$	2.124e-06	2.818e-07	5.339e-06	8.3e-05	0.000194	-4.916e-05	-0.0001029	-2.269e-05	6.692e-05
$D_{1,5}$	-5.556e-08	-4.578e-07	-9.72e-07	2.368e-05	8.585e-05	-0.0001102	-0.0001962	-0.0001147	-1.267e-05
D_2	1.204e-05	2.207e-05	0.0006441	5.753e-05	3.15e-05	0.0001758	0.0001708	0.0001916	0.002072
$D_{2,3}$	7.256e-07	1.225e-07	-9.587e-07	-2.52e-05	1.298e-05	-6.8e-06	1.279e-05	2.467e-05	3.782e-05
$D_{2,4}$	1.489e-06	-1.08e-07	4.8e-06	-2.154e-05	5.355e-05	5.246e-05	-0.0002109	-6.316e-05	-0.0001614
$D_{2,5}$	-3.896e-08	1.755e-07	-8.739e-07	6.893e-05	7.797e-05	2.457e-05	0.0001157	1.261e-06	0.0001949
D_3	1.962e-07	1.152e-05	4.185e-06	8.909e-05	2.326e-05	2.881e-06	5.746e-05	8.666e-05	9.662e-05
$D_{3,4}$	-2.57e-07	1.818e-07	2.7e-07	-3.941e-05	0.0001016	4.975e-05	-0.0001218	1.183e-05	2.666e-05
$D_{3,5}$	6.722e-09	-2.952e-07	-4.916e-08	4.668e-05	0.0001185	-1.509e-06	-3.466e-05	4.643e-05	0.0001974
D_4	6.334e-07	1.735e-07	1.514e-06	5.272e-05	4.383e-05	4.656e-05	0.0003674	0.0002278	0.0001359
$D_{4,5}$	1.38e-08	2.605e-07	2.462e-07	7.091e-05	0.0001425	-6.223e-05	-0.0001018	4.461e-05	0.0002424
D_5	1.739e-07	7.461e-07	1.28e-07	9.078e-06	7.244e-05	8.843e-05	0.0001492	8.743e-05	0.0001085

Table A.17: Sobol variances for main effect and cardinality 2, for point 17.

Property	Value for Level 2 (13 points)			Value for Level 3 (85 points)			Value for Level 4 (389 points)		
Location	P1	P2	P3	P1	P2	P3	P1	P2	P3
Mean	1.084	1.09	1.213	1.093	1.094	1.203	1.04	1.057	1.206
Variance	9.355e-05	8.242e-05	0.0008165	-0.000116	-0.0001859	-0.0004093	-0.001961	-0.001225	0.002036
D_0	2.716e-05	1.782e-05	7.419e-06	8.046e-06	4.056e-05	8.465e-06	0.0003875	0.0002109	0.0002992
$D_{0,1}$	1.221e-05	4.684e-06	7.517e-06	4.443e-05	0.0001166	4.154e-05	0.0001409	0.0002133	8.199e-05
$D_{0,2}$	9.934e-06	-9.2e-07	5.186e-06	2.239e-05	3.969e-05	-3.075e-05	-4.059e-05	6.738e-05	9.356e-05
$D_{0,3}$	-1.286e-06	-1.283e-07	8.325e-07	1.642e-05	7.485e-05	1.093e-05	-2.53e-05	-4.984e-05	7.877e-06
$D_{0,4}$	-2.548e-06	-1.068e-06	-1.91e-06	3.152e-05	0.0001168	1.99e-05	-0.0001277	-0.0001134	-3.036e-05
$D_{0,5}$	3.542e-08	1.059e-06	4.27e-07	2.954e-05	5.261e-05	-9.597e-06	0.0002373	0.0002311	0.000476
D_1	3.238e-05	5.082e-05	0.0001139	6.521e-05	2.453e-05	0.0001235	0.0004757	0.0002174	5.409e-05
$D_{1,2}$	-7.732e-06	4.914e-07	-1.365e-05	5.967e-05	7.538e-05	4.6e-05	0.0001211	-9.214e-06	0.000108
$D_{1,3}$	1.001e-06	6.851e-08	-2.19e-06	5.632e-05	0.0001179	-4.039e-07	-3.213e-06	2.036e-05	4.313e-05
$D_{1,4}$	1.983e-06	5.706e-07	5.025e-06	7.957e-05	0.0001452	-4.996e-05	-0.0001073	-7.509e-05	6.83e-05
$D_{1,5}$	-2.757e-08	-5.658e-07	-1.123e-06	1.982e-05	6.14e-05	-0.0001032	-0.0002017	-0.000155	-1.645e-05
D_2	1.744e-05	5.478e-06	0.0006871	6.556e-05	3.158e-05	0.0001577	0.0001727	0.0001682	0.00215
$D_{2,3}$	8.147e-07	-1.346e-08	-1.511e-06	-2.322e-05	-2.186e-06	-1.421e-05	2.114e-05	1.996e-06	3.802e-05
$D_{2,4}$	1.614e-06	-1.121e-07	3.467e-06	-2.075e-05	2.072e-05	5.137e-05	-0.0002132	-0.0001437	-0.0001454
$D_{2,5}$	-2.244e-08	1.111e-07	-7.751e-07	6.809e-05	7.791e-05	2.27e-05	0.0001306	2.566e-05	0.0001955
D_3	1.217e-07	3.698e-06	4.266e-06	9.973e-05	3.197e-05	2.58e-06	6.081e-05	5.741e-05	9.823e-05
$D_{3,4}$	-2.09e-07	-1.562e-08	5.565e-07	-4.535e-05	3.782e-05	4.636e-05	-0.0001304	-3.933e-05	2.883e-05
$D_{3,5}$	2.905e-09	1.549e-08	-1.244e-07	4.462e-05	8.611e-05	-6.319e-06	-4.098e-05	1.036e-05	0.0001872
D_4	4.871e-07	1.376e-07	1.495e-06	5.474e-05	4.612e-05	5.386e-05	0.0003813	0.0002679	0.0001471
$D_{4,5}$	5.756e-09	1.29e-07	2.854e-07	6.848e-05	0.0001157	-6.445e-05	-0.0001131	-2.795e-05	0.0002587
D_5	1.953e-07	1.605e-07	2.516e-07	8.613e-06	3.28e-05	8.613e-05	0.0001539	9.6e-05	0.000111

Table A.18: Sobol variances for main effect and cardinality 2, for point 18.

Property	Value for Level 2 (13 points)			Value for Level 3 (85 points)			Value for Level 4 (389 points)		
Location	P1	P2	P3	P1	P2	P3	P1	P2	P3
Mean	1.083	1.087	1.209	1.093	1.094	1.199	1.04	1.048	1.2
Variance	9.617e-05	7.307e-05	0.0008436	-0.0001112	-0.0001314	-0.0005758	-0.001969	-0.001581	0.002095
D_0	2.684e-05	2.354e-05	8.616e-06	9.233e-06	1.449e-05	7.611e-06	0.0003936	0.0002643	0.0002962
$D_{0,1}$	1.222e-05	8.345e-06	7.567e-06	4.305e-05	7.415e-05	4.521e-05	0.0001379	0.0001785	8.221e-05
$D_{0,2}$	1.044e-05	1.148e-06	3.813e-06	2.136e-05	3.596e-05	-5.681e-05	-4.545e-05	2.144e-05	0.0001105
$D_{0,3}$	-1.116e-06	-1.133e-06	3.494e-07	1.393e-05	4.847e-05	1.085e-05	-2.696e-05	-3.826e-05	-6.303e-06
$D_{0,4}$	-2.175e-06	-1.691e-06	-2.244e-06	2.764e-05	8.039e-05	2.33e-05	-0.0001278	-0.000118	-4.809e-05
$D_{0,5}$	5.8e-08	4.398e-07	3.327e-07	2.869e-05	3.78e-05	-4.517e-06	0.0002296	0.0002282	0.0004685
D_1	3.312e-05	4.007e-05	0.0001089	6.929e-05	3.662e-05	0.0001124	0.0004882	0.0003244	4.78e-05
$D_{1,2}$	-8.431e-06	-7.682e-07	-8.113e-06	5.906e-05	6.496e-05	3.59e-05	0.0001296	3.234e-05	0.0001001
$D_{1,3}$	9.009e-07	7.584e-07	-7.433e-07	5.478e-05	8.549e-05	5.919e-06	-1.795e-06	8.439e-06	4.044e-05
$D_{1,4}$	1.756e-06	1.132e-06	4.774e-06	7.781e-05	0.0001099	-4.266e-05	-0.0001083	-9.336e-05	6.289e-05
$D_{1,5}$	-4.682e-08	-2.943e-07	-7.077e-07	1.764e-05	3.987e-05	-0.0001023	-0.0002044	-0.0001771	-1.493e-05
D_2	1.987e-05	1.056e-07	0.000712	6.781e-05	3.824e-05	0.000137	0.0001728	0.0001588	0.002219
$D_{2,3}$	7.701e-07	1.043e-07	-3.746e-07	-2.386e-05	-1.932e-05	-3.1e-05	2.396e-05	-4.938e-06	3.143e-05
$D_{2,4}$	1.501e-06	1.557e-07	2.406e-06	-2.18e-05	-7.11e-06	4.48e-05	-0.000214	-0.0001893	-0.0001302
$D_{2,5}$	-4.002e-08	-4.048e-08	-3.567e-07	6.71e-05	7.228e-05	1.972e-05	0.0001322	6.335e-05	0.0001748
D_3	8.61e-08	9.115e-07	5.039e-06	0.0001043	5.76e-05	3.727e-06	6.106e-05	4.724e-05	0.0001006
$D_{3,4}$	-1.604e-07	-1.537e-07	2.204e-07	-4.921e-05	-8.605e-06	5.083e-05	-0.0001319	-8.658e-05	2.1e-05
$D_{3,5}$	4.277e-09	3.996e-08	-3.268e-08	4.338e-05	6.188e-05	1.297e-07	-4.199e-05	-1.268e-05	0.0001973
D_4	3.885e-07	2.973e-07	1.739e-06	5.642e-05	4.877e-05	4.814e-05	0.0003838	0.0003184	0.0001417
$D_{4,5}$	8.334e-09	5.965e-08	2.099e-07	6.654e-05	8.821e-05	-5.789e-05	-0.000118	-7.05e-05	0.0002709
D_5	1.705e-07	4.604e-08	2.359e-07	8.345e-06	1.489e-05	7.342e-05	0.0001513	0.0001186	0.0001123

Table A.19: Sobol variances for main effect and cardinality 2, for point 19.

Property	Value for Level 2 (13 points)			Value for Level 3 (85 points)			Value for Level 4 (389 points)		
Location	P1	P2	P3	P1	P2	P3	P1	P2	P3
Mean	1.083	1.085	1.204	1.093	1.094	1.195	1.039	1.043	1.193
Variance	9.766e-05	7.824e-05	0.0008565	-0.000108	-0.0001185	-0.0007327	-0.001984	-0.001824	0.002219
D_0	2.695e-05	2.668e-05	6.868e-06	9.081e-06	3.964e-06	6.16e-06	0.0004001	0.00034	0.0003098
$D_{0,1}$	1.264e-05	1.088e-05	6.418e-06	4.189e-05	5.189e-05	4.919e-05	0.0001356	0.0001563	8.69e-05
$D_{0,2}$	1.086e-05	5.117e-06	2.964e-06	2.158e-05	2.765e-05	-7.5e-05	-5.069e-05	-9.719e-06	0.0001194
$D_{0,3}$	-1.081e-06	-1.445e-06	2.301e-09	1.365e-05	2.888e-05	1.383e-05	-2.754e-05	-2.7e-05	-1.599e-05
$D_{0,4}$	-1.996e-06	-2.771e-06	-2.24e-06	2.686e-05	5.127e-05	2.722e-05	-0.0001291	-0.0001205	-5.692e-05
$D_{0,5}$	9.416e-08	1.357e-07	2.181e-07	2.798e-05	3.092e-05	-3.081e-06	0.0002236	0.0002375	0.000475
D_1	3.263e-05	3.341e-05	0.0001112	7.001e-05	5.359e-05	0.000106	0.0004932	0.0004127	4.471e-05
$D_{1,2}$	-9.066e-06	-3.632e-06	-6.483e-06	5.803e-05	5.854e-05	3.343e-05	0.0001307	7.73e-05	9.1e-05
$D_{1,3}$	9.024e-07	1.025e-06	-5.033e-09	5.368e-05	6.462e-05	1.674e-05	-1.773e-06	3.382e-06	4.222e-05
$D_{1,4}$	1.666e-06	1.967e-06	4.901e-06	7.672e-05	8.807e-05	-3.276e-05	-0.0001096	-9.812e-05	5.954e-05
$D_{1,5}$	-7.858e-08	-9.63e-08	-4.77e-07	1.653e-05	2.606e-05	-9.942e-05	-0.0002062	-0.0001895	-1.827e-05
D_2	2.156e-05	4.792e-06	0.0007226	6.777e-05	4.896e-05	0.000134	0.0001728	0.000167	0.002381
$D_{2,3}$	7.755e-07	4.824e-07	-2.324e-09	-2.48e-05	-2.803e-05	-4.428e-05	2.389e-05	6.694e-06	2.965e-05
$D_{2,4}$	1.432e-06	9.253e-07	2.263e-06	-2.335e-05	-2.271e-05	4.315e-05	-0.000216	-0.0002069	-0.000131
$D_{2,5}$	-6.753e-08	-4.531e-08	-2.203e-07	6.694e-05	6.848e-05	1.739e-05	0.0001322	0.0001028	0.0001593
D_3	8.097e-08	2.888e-07	6.183e-06	0.000107	7.942e-05	5.337e-06	6.16e-05	5.363e-05	0.000109
$D_{3,4}$	-1.425e-07	-2.613e-07	1.757e-09	-5.119e-05	-3.39e-05	5.959e-05	-0.0001335	-0.0001131	1.844e-05
$D_{3,5}$	6.722e-09	1.279e-08	-1.71e-10	4.294e-05	4.901e-05	8.441e-06	-4.401e-05	-2.665e-05	0.0002114
D_4	3.322e-07	6.161e-07	1.967e-06	5.721e-05	5.124e-05	4.598e-05	0.0003812	0.0003637	0.0001364
$D_{4,5}$	1.241e-08	2.454e-08	1.665e-07	6.62e-05	7.293e-05	-4.966e-05	-0.0001218	-9.356e-05	0.0002747
D_5	1.509e-07	1.405e-07	1.279e-07	8.27e-06	9.691e-06	6.376e-05	0.0001498	0.0001413	0.0001177

Table A.20: Sobol variances for main effect and cardinality 2, for point 20.

Property	Value for Level 2 (13 points)			Value for Level 3 (85 points)			Value for Level 4 (389 points)		
Location	P1	P2	P3	P1	P2	P3	P1	P2	P3
Mean	1.083	1.084	1.199	1.093	1.093	1.191	1.039	1.041	1.186
Variance	9.837e-05	8.818e-05	0.0008829	-0.000112	-0.0001179	-0.000863	-0.002003	-0.001942	0.002405
D_0	2.681e-05	2.708e-05	6.347e-06	9.545e-06	6.187e-06	5.568e-06	0.0004059	0.0003801	0.0003325
$D_{0,1}$	1.298e-05	1.219e-05	6.062e-06	4.192e-05	4.553e-05	5.147e-05	0.0001329	0.0001445	9.068e-05
$D_{0,2}$	1.115e-05	8.485e-06	3.112e-06	2.132e-05	2.259e-05	-8.65e-05	-5.282e-05	-3.128e-05	0.0001236
$D_{0,3}$	-1.041e-06	-1.237e-06	-3.161e-08	1.316e-05	1.895e-05	1.629e-05	-2.929e-05	-2.439e-05	-2.158e-05
$D_{0,4}$	-1.96e-06	-2.757e-06	-2.233e-06	2.618e-05	3.546e-05	3.024e-05	-0.0001319	-0.0001254	-6.373e-05
$D_{0,5}$	1.197e-07	7.86e-08	2.642e-07	2.835e-05	2.956e-05	-5.644e-06	0.0002221	0.0002417	0.0004994
D_1	3.23e-05	3.255e-05	0.000117	7.075e-05	6.362e-05	0.0001038	0.0004988	0.0004644	4.182e-05
$D_{1,2}$	-9.613e-06	-6.561e-06	-6.887e-06	5.764e-05	5.818e-05	3.281e-05	0.0001297	0.000109	9.015e-05
$D_{1,3}$	8.977e-07	9.561e-07	6.995e-08	5.367e-05	5.744e-05	2.38e-05	-1.539e-06	-1.623e-06	4.47e-05
$D_{1,4}$	1.69e-06	2.132e-06	4.942e-06	7.671e-05	8.077e-05	-2.639e-05	-0.0001097	-0.000105	5.939e-05
$D_{1,5}$	-1.032e-07	-6.078e-08	-5.848e-07	1.681e-05	2.052e-05	-9.961e-05	-0.0002062	-0.0001983	-2.312e-05
D_2	2.256e-05	1.253e-05	0.0007427	6.838e-05	5.914e-05	0.0001458	0.0001729	0.0001706	0.002631
$D_{2,3}$	7.711e-07	6.654e-07	3.591e-08	-2.492e-05	-2.685e-05	-5.484e-05	2.294e-05	1.777e-05	2.506e-05
$D_{2,4}$	1.452e-06	1.484e-06	2.537e-06	-2.377e-05	-2.434e-05	4.624e-05	-0.0002176	-0.0002131	-0.0001396
$D_{2,5}$	-8.864e-08	-4.23e-08	-3.002e-07	6.723e-05	6.819e-05	2.093e-05	0.0001324	0.0001258	0.0001584
D_3	7.393e-08	1.299e-07	7.521e-06	0.0001093	9.405e-05	7.218e-06	6.288e-05	5.952e-05	0.0001176
$D_{3,4}$	-1.356e-07	-2.162e-07	-2.577e-08	-5.188e-05	-4.364e-05	6.661e-05	-0.0001352	-0.0001275	1.77e-05
$D_{3,5}$	8.278e-09	6.164e-09	3.049e-09	4.264e-05	4.542e-05	1.311e-05	-4.419e-05	-3.769e-05	0.0002257
D_4	3.31e-07	5.606e-07	2.069e-06	5.754e-05	5.407e-05	4.658e-05	0.0003785	0.000383	0.0001391
$D_{4,5}$	1.558e-08	1.374e-08	2.154e-07	6.616e-05	6.94e-05	-4.717e-05	-0.000123	-0.0001092	0.0002828
D_5	1.613e-07	1.905e-07	8.971e-08	8.155e-06	8.859e-06	6.134e-05	0.0001526	0.0001534	0.0001237

Table A.21: Sobol variances for main effect and cardinality 2, for point 21.

Property	Value for Level 2 (13 points)			Value for Level 3 (85 points)			Value for Level 4 (389 points)		
Location	P1	P2	P3	P1	P2	P3	P1	P2	P3
Mean	1.083	1.084	1.194	1.093	1.093	1.186	1.039	1.04	1.179
Variance	9.906e-05	9.366e-05	0.0009408	-0.0001142	-0.000113	-0.0009959	-0.002009	-0.001971	0.002591
D_0	2.69e-05	2.684e-05	6.27e-06	1.015e-05	8.887e-06	5.463e-06	0.0004064	0.0003906	0.0003616
$D_{0,1}$	1.3e-05	1.218e-05	6.03e-06	4.149e-05	4.38e-05	5.477e-05	0.0001319	0.000139	9.925e-05
$D_{0,2}$	1.129e-05	9.877e-06	3.758e-06	2.028e-05	2.127e-05	-0.0001039	-5.544e-05	-4.095e-05	0.0001316
$D_{0,3}$	-1.124e-06	-1.136e-06	6.353e-08	1.201e-05	1.483e-05	1.79e-05	-3.01e-05	-2.678e-05	-2.336e-05
$D_{0,4}$	-1.948e-06	-2.313e-06	-2.233e-06	2.449e-05	2.919e-05	3.315e-05	-0.000133	-0.0001272	-6.501e-05
$D_{0,5}$	1.855e-07	6.028e-08	3.951e-07	2.81e-05	2.895e-05	-6.163e-06	0.0002205	0.0002336	0.000528
D_1	3.204e-05	3.302e-05	0.0001231	7.098e-05	6.886e-05	0.0001067	0.0005018	0.0004828	3.964e-05
$D_{1,2}$	-9.704e-06	-7.911e-06	-8.422e-06	5.717e-05	5.901e-05	2.146e-05	0.0001309	0.0001252	9.682e-05
$D_{1,3}$	9.667e-07	9.102e-07	-1.424e-07	5.334e-05	5.577e-05	2.752e-05	-5.158e-07	-1.153e-06	4.679e-05
$D_{1,4}$	1.674e-06	1.853e-06	5.005e-06	7.621e-05	7.909e-05	-2.255e-05	-0.0001099	-0.0001075	6.323e-05
$D_{1,5}$	-1.595e-07	-4.828e-08	-8.855e-07	1.675e-05	1.824e-05	-9.875e-05	-0.0002061	-0.0002027	-3.19e-05
D_2	2.335e-05	1.758e-05	0.0007941	6.838e-05	6.563e-05	0.0001578	0.0001727	0.0001725	0.002894
$D_{2,3}$	8.397e-07	7.382e-07	-8.874e-08	-2.524e-05	-2.444e-05	-6.567e-05	2.266e-05	2.232e-05	2.771e-05
$D_{2,4}$	1.454e-06	1.503e-06	3.119e-06	-2.439e-05	-2.203e-05	4.55e-05	-0.0002178	-0.0002146	-0.0001462
$D_{2,5}$	-1.385e-07	-3.915e-08	-5.519e-07	6.643e-05	6.702e-05	1.316e-05	0.0001321	0.0001305	0.0001656
D_3	8.473e-08	9.275e-08	8.617e-06	0.0001093	0.0001021	8.383e-06	6.303e-05	6.091e-05	0.0001221
$D_{3,4}$	-1.449e-07	-1.729e-07	5.273e-08	-5.307e-05	-4.784e-05	7.089e-05	-0.000136	-0.000131	1.911e-05
$D_{3,5}$	1.38e-08	4.505e-09	-9.33e-09	4.196e-05	4.364e-05	1.54e-05	-4.412e-05	-4.042e-05	0.000235
D_4	3.2e-07	4.239e-07	2.105e-06	5.798e-05	5.577e-05	4.771e-05	0.0003802	0.0003866	0.0001481
$D_{4,5}$	2.39e-08	9.171e-09	3.28e-07	6.49e-05	6.693e-05	-4.578e-05	-0.0001246	-0.0001162	0.0002934
D_5	1.465e-07	1.883e-07	9.159e-08	7.874e-06	8.379e-06	6.097e-05	0.0001529	0.0001523	0.0001266

Table A.22: Sobol variances for main effect and cardinality 2, for point 22.

Property	Value for Level 2 (13 points)			Value for Level 3 (85 points)			Value for Level 4 (389 points)		
Location	P1	P2	P3	P1	P2	P3	P1	P2	P3
Mean	1.083	1.083	1.188	1.093	1.093	1.181	1.039	1.039	1.172
Variance	9.983e-05	9.61e-05	0.001039	-0.0001103	-0.0001075	-0.001136	-0.002002	-0.001973	0.002774
D_0	2.728e-05	2.676e-05	6.429e-06	1.032e-05	9.059e-06	5.575e-06	0.0004054	0.0003971	0.0003847
$D_{0,1}$	1.303e-05	1.239e-05	6.2e-06	4.078e-05	4.238e-05	5.901e-05	0.0001327	0.0001376	0.0001064
$D_{0,2}$	1.136e-05	1.047e-05	5.024e-06	2.052e-05	2.138e-05	-0.0001276	-5.52e-05	-4.654e-05	0.000152
$D_{0,3}$	-1.252e-06	-1.014e-06	2.202e-07	1.236e-05	1.385e-05	1.943e-05	-2.904e-05	-2.658e-05	-2.45e-05
$D_{0,4}$	-1.895e-06	-1.983e-06	-2.188e-06	2.46e-05	2.736e-05	3.619e-05	-0.0001316	-0.0001272	-6.464e-05
$D_{0,5}$	1.053e-07	1.148e-07	5.101e-07	2.759e-05	2.821e-05	-5.85e-06	0.0002201	0.0002267	0.0005506
D_1	3.194e-05	3.314e-05	0.000129	7.146e-05	7.064e-05	0.0001122	0.000504	0.000491	3.869e-05
$D_{1,2}$	-9.612e-06	-8.677e-06	-1.141e-05	5.714e-05	5.81e-05	1.251e-06	0.0001333	0.0001312	0.0001065
$D_{1,3}$	1.059e-06	8.408e-07	-5.003e-07	5.318e-05	5.422e-05	3.099e-05	-8.474e-08	-1.337e-06	4.94e-05
$D_{1,4}$	1.604e-06	1.643e-06	4.971e-06	7.631e-05	7.722e-05	-1.929e-05	-0.0001093	-0.0001086	6.689e-05
$D_{1,5}$	-8.909e-08	-9.518e-08	-1.159e-06	1.666e-05	1.67e-05	-9.972e-05	-0.0002054	-0.0002051	-4.131e-05
D_2	2.362e-05	2.004e-05	0.0008876	6.848e-05	6.738e-05	0.0001689	0.0001727	0.0001728	0.003119
$D_{2,3}$	9.237e-07	7.105e-07	-4.054e-07	-2.483e-05	-2.452e-05	-7.751e-05	2.405e-05	2.478e-05	2.941e-05
$D_{2,4}$	1.398e-06	1.389e-06	4.028e-06	-2.473e-05	-2.242e-05	4.071e-05	-0.0002163	-0.000214	-0.0001499
$D_{2,5}$	-7.769e-08	-8.042e-08	-9.392e-07	6.583e-05	6.682e-05	-2.821e-06	0.0001333	0.0001324	0.0001789
D_3	1.021e-07	7.317e-08	9.39e-06	0.0001086	0.0001053	8.8e-06	6.292e-05	6.118e-05	0.0001239
$D_{3,4}$	-1.541e-07	-1.346e-07	1.766e-07	-5.312e-05	-5.018e-05	7.531e-05	-0.0001365	-0.0001324	2.077e-05
$D_{3,5}$	8.561e-09	7.793e-09	-4.117e-08	4.145e-05	4.322e-05	1.775e-05	-4.476e-05	-4.281e-05	0.0002424
D_4	3.024e-07	3.321e-07	2.014e-06	5.865e-05	5.676e-05	5.02e-05	0.0003819	0.0003835	0.0001608
$D_{4,5}$	1.296e-08	1.523e-08	4.09e-07	6.394e-05	6.637e-05	-4.481e-05	-0.0001259	-0.0001201	0.0003028
D_5	1.65e-07	1.563e-07	1.107e-07	7.731e-06	8.349e-06	6.2e-05	0.000152	0.0001496	0.0001288

Table A.23: Sobol variances for main effect and cardinality 2, for point 23.

Property	Value for Level 2 (13 points)			Value for Level 3 (85 points)			Value for Level 4 (389 points)		
Location	P1	P2	P3	P1	P2	P3	P1	P2	P3
Mean	1.083	1.083	1.183	1.093	1.093	1.176	1.039	1.039	1.166
Variance	0.0001001	9.745e-05	0.001154	-0.0001072	-0.0001088	-0.00128	-0.002005	-0.001994	0.002947
D_0	2.747e-05	2.685e-05	6.715e-06	1.045e-05	9.216e-06	5.986e-06	0.0004064	0.0004032	0.000396
$D_{0,1}$	1.315e-05	1.287e-05	6.595e-06	3.995e-05	4.188e-05	6.473e-05	0.0001309	0.0001348	0.0001121
$D_{0,2}$	1.135e-05	1.093e-05	6.816e-06	2.024e-05	2.157e-05	-0.0001537	-5.536e-05	-5.2e-05	0.0001778
$D_{0,3}$	-1.281e-06	-1.043e-06	3.843e-07	1.204e-05	1.36e-05	2.13e-05	-2.927e-05	-2.839e-05	-2.252e-05
$D_{0,4}$	-1.974e-06	-1.97e-06	-2.003e-06	2.405e-05	2.68e-05	3.997e-05	-0.0001325	-0.0001303	-6.544e-05
$D_{0,5}$	5.876e-08	1.159e-07	6.631e-07	2.695e-05	2.809e-05	-5.246e-06	0.0002191	0.0002236	0.0005721
D_1	3.18e-05	3.245e-05	0.0001346	7.081e-05	7.061e-05	0.0001195	0.0005045	0.0004959	3.902e-05
$D_{1,2}$	-9.61e-06	-9.314e-06	-1.612e-05	5.649e-05	5.777e-05	-2.141e-05	0.0001332	0.0001304	0.0001214
$D_{1,3}$	1.084e-06	8.889e-07	-9.088e-07	5.223e-05	5.36e-05	3.472e-05	3.33e-07	-1.511e-06	5.2e-05
$D_{1,4}$	1.671e-06	1.679e-06	4.737e-06	7.554e-05	7.672e-05	-1.708e-05	-0.0001098	-0.00011	7.028e-05
$D_{1,5}$	-4.974e-08	-9.876e-08	-1.568e-06	1.62e-05	1.651e-05	-0.0001032	-0.0002046	-0.0002062	-4.685e-05
D_2	2.368e-05	2.154e-05	0.0009994	6.788e-05	6.784e-05	0.0001785	0.0001724	0.0001729	0.003296
$D_{2,3}$	9.361e-07	7.546e-07	-9.393e-07	-2.55e-05	-2.502e-05	-8.872e-05	2.482e-05	2.305e-05	3.833e-05
$D_{2,4}$	1.443e-06	1.425e-06	4.896e-06	-2.549e-05	-2.373e-05	3.603e-05	-0.0002166	-0.0002173	-0.0001555
$D_{2,5}$	-4.294e-08	-8.384e-08	-1.621e-06	6.51e-05	6.703e-05	-2.491e-05	0.0001332	0.0001326	0.0002047
D_3	1.06e-07	7.462e-08	1.002e-05	0.0001104	0.0001081	9.17e-06	6.351e-05	6.228e-05	0.0001267
$D_{3,4}$	-1.628e-07	-1.36e-07	2.76e-07	-5.382e-05	-5.141e-05	8.077e-05	-0.0001375	-0.0001345	2.35e-05
$D_{3,5}$	4.845e-09	8.001e-09	-9.138e-08	4.063e-05	4.271e-05	2.003e-05	-4.492e-05	-4.375e-05	0.0002484
D_4	3.2e-07	3.299e-07	1.656e-06	5.862e-05	5.731e-05	5.287e-05	0.0003808	0.00038	0.000171
$D_{4,5}$	7.468e-09	1.511e-08	4.763e-07	6.299e-05	6.608e-05	-4.49e-05	-0.0001279	-0.0001226	0.0003137
D_5	1.705e-07	1.622e-07	1.622e-07	7.704e-06	8.217e-06	6.364e-05	0.0001531	0.0001518	0.000134

Table A.24: Sobol variances for main effect and cardinality 2, for point 24.

Property	Value for Level 2 (13 points)			Value for Level 3 (85 points)			Value for Level 4 (389 points)		
Location	P1	P2	P3	P1	P2	P3	P1	P2	P3
Mean	1.083	1.083	1.177	1.093	1.093	1.17	1.039	1.039	1.159
Variance	9.989e-05	9.823e-05	0.001259	-0.0001083	-0.000114	-0.001397	-0.002006	-0.00201	0.0031
D_0	2.727e-05	2.675e-05	7.021e-06	1.078e-05	9.707e-06	6.676e-06	0.0004092	0.0004062	0.0004023
$D_{0,1}$	1.324e-05	1.302e-05	7.118e-06	3.992e-05	4.187e-05	7.093e-05	0.0001317	0.0001319	0.0001197
$D_{0,2}$	1.129e-05	1.116e-05	8.525e-06	1.99e-05	2.068e-05	-0.000173	-5.562e-05	-5.428e-05	0.0001987
$D_{0,3}$	-1.304e-06	-1.03e-06	6.079e-07	1.167e-05	1.25e-05	2.367e-05	-2.895e-05	-3.047e-05	-1.947e-05
$D_{0,4}$	-1.949e-06	-1.945e-06	-1.883e-06	2.352e-05	2.529e-05	4.371e-05	-0.0001315	-0.0001333	-6.505e-05
$D_{0,5}$	5.872e-08	2.025e-07	7.674e-07	2.7e-05	2.828e-05	-5.748e-06	0.0002215	0.0002207	0.0005986
D_1	3.163e-05	3.219e-05	0.0001419	7.115e-05	7.099e-05	0.0001279	0.0005055	0.0005006	4.027e-05
$D_{1,2}$	-9.628e-06	-9.64e-06	-2.147e-05	5.635e-05	5.721e-05	-4.209e-05	0.0001334	0.0001301	0.0001385
$D_{1,3}$	1.112e-06	8.901e-07	-1.531e-06	5.198e-05	5.352e-05	3.834e-05	8.302e-07	-1.129e-06	5.481e-05
$D_{1,4}$	1.663e-06	1.68e-06	4.743e-06	7.496e-05	7.63e-05	-1.664e-05	-0.0001087	-0.0001097	7.403e-05
$D_{1,5}$	-5.01e-08	-1.75e-07	-1.933e-06	1.603e-05	1.693e-05	-0.0001093	-0.0002043	-0.0002062	-4.951e-05
D_2	2.379e-05	2.262e-05	0.001101	6.746e-05	6.793e-05	0.0001855	0.0001729	0.0001727	0.003444
$D_{2,3}$	9.483e-07	7.626e-07	-1.834e-06	-2.572e-05	-2.528e-05	-9.636e-05	2.477e-05	2.223e-05	5.806e-05
$D_{2,4}$	1.418e-06	1.44e-06	5.68e-06	-2.592e-05	-2.404e-05	3.055e-05	-0.0002163	-0.0002184	-0.0001581
$D_{2,5}$	-4.272e-08	-1.499e-07	-2.315e-06	6.518e-05	6.679e-05	-4.993e-05	0.0001349	0.000132	0.0002422
D_3	1.102e-07	7.203e-08	1.036e-05	0.0001104	0.0001095	9.52e-06	6.383e-05	6.296e-05	0.0001303
$D_{3,4}$	-1.638e-07	-1.329e-07	4.051e-07	-5.38e-05	-5.256e-05	8.594e-05	-0.0001376	-0.000136	2.729e-05
$D_{3,5}$	4.934e-09	1.384e-08	-1.651e-07	4.062e-05	4.227e-05	2.232e-05	-4.428e-05	-4.434e-05	0.0002551
D_4	3.066e-07	3.239e-07	1.429e-06	5.833e-05	5.78e-05	5.605e-05	0.0003797	0.0003795	0.0001836
$D_{4,5}$	7.379e-09	2.613e-08	5.114e-07	6.291e-05	6.551e-05	-4.588e-05	-0.0001265	-0.000124	0.0003284
D_5	1.766e-07	1.484e-07	2.094e-07	7.727e-06	7.978e-06	6.66e-05	0.000154	0.0001532	0.0001421

Table A.25: Sobol variances for main effect and cardinality 2, for point 25.

Property	Value for Level 2 (13 points)			Value for Level 3 (85 points)			Value for Level 4 (389 points)		
Location	P1	P2	P3	P1	P2	P3	P1	P2	P3
Mean	1.083	1.083	1.171	1.093	1.093	1.164	1.039	1.039	1.152
Variance	0.0001	9.927e-05	0.001354	-0.0001113	-0.0001099	-0.001475	-0.002005	-0.002002	0.003228
D_0	2.718e-05	2.719e-05	7.356e-06	1.145e-05	1.029e-05	7.807e-06	0.0004104	0.0004054	0.0004193
$D_{0,1}$	1.323e-05	1.298e-05	7.907e-06	3.988e-05	4.073e-05	7.842e-05	0.000131	0.0001331	0.0001306
$D_{0,2}$	1.135e-05	1.127e-05	1.061e-05	1.961e-05	2.026e-05	-0.0001811	-5.532e-05	-5.499e-05	0.0002234
$D_{0,3}$	-1.306e-06	-1.236e-06	7.748e-07	1.118e-05	1.215e-05	2.643e-05	-2.87e-05	-2.913e-05	-1.478e-05
$D_{0,4}$	-2.001e-06	-1.927e-06	-1.872e-06	2.315e-05	2.437e-05	4.773e-05	-0.0001315	-0.0001315	-6.627e-05
$D_{0,5}$	2.353e-08	1.283e-07	7.761e-07	2.723e-05	2.748e-05	-7.584e-06	0.0002224	0.0002216	0.000637
D_1	3.146e-05	3.195e-05	0.0001544	7.259e-05	7.152e-05	0.0001422	0.0005077	0.0005034	4.437e-05
$D_{1,2}$	-9.651e-06	-9.557e-06	-2.804e-05	5.661e-05	5.691e-05	-5.029e-05	0.0001335	0.0001331	0.0001545
$D_{1,3}$	1.11e-06	1.049e-06	-2.048e-06	5.209e-05	5.311e-05	4.263e-05	3.185e-07	1.825e-07	6.013e-05
$D_{1,4}$	1.701e-06	1.635e-06	4.948e-06	7.492e-05	7.615e-05	-1.805e-05	-0.0001078	-0.0001094	7.937e-05
$D_{1,5}$	-2e-08	-1.088e-07	-2.051e-06	1.572e-05	1.626e-05	-0.0001222	-0.0002041	-0.0002061	-5.167e-05
D_2	2.409e-05	2.322e-05	0.001187	6.865e-05	6.777e-05	0.0001898	0.0001736	0.0001726	0.003563
$D_{2,3}$	9.523e-07	9.103e-07	-2.748e-06	-2.584e-05	-2.513e-05	-9.66e-05	2.498e-05	2.402e-05	8.232e-05
$D_{2,4}$	1.459e-06	1.419e-06	6.64e-06	-2.593e-05	-2.484e-05	2.758e-05	-0.0002156	-0.0002164	-0.0001655
$D_{2,5}$	-1.716e-08	-9.447e-08	-2.752e-06	6.543e-05	6.571e-05	-7.128e-05	0.0001363	0.0001339	0.0002749
D_3	1.099e-07	1.012e-07	1.057e-05	0.0001105	0.0001089	9.674e-06	6.387e-05	6.284e-05	0.0001356
$D_{3,4}$	-1.678e-07	-1.557e-07	4.849e-07	-5.332e-05	-5.334e-05	9.263e-05	-0.0001374	-0.0001358	3.207e-05
$D_{3,5}$	1.974e-09	1.037e-08	-2.01e-07	4.043e-05	4.152e-05	2.473e-05	-4.476e-05	-4.418e-05	0.0002662
D_4	3.187e-07	3.104e-07	1.319e-06	5.803e-05	5.839e-05	5.97e-05	0.0003815	0.0003813	0.0001987
$D_{4,5}$	3.024e-09	1.616e-08	4.857e-07	6.268e-05	6.407e-05	-4.838e-05	-0.0001247	-0.0001252	0.0003479
D_5	1.857e-07	1.595e-07	2.025e-07	7.619e-06	7.782e-06	7.284e-05	0.0001543	0.000152	0.0001547